# The roles of *modB* and *rpoC* mutations in quinolone-resistant *Escherichia coli*

An der Universität Hamburg eingereichte Dissertation

Zur Erlangung des naturwissenschaftlichen Doktorgrades

Der Universität Hamburg

Fakultät für Mathematik, Informatik und Naturwissenschaften

Institut für Biochemie und Molekularbiologie

Vorgelegt von

Philip Bienert

Hamburg, 2022

1. Gutachter: Prof. Dr. Peter Heisig

2. Gutachter: Prof. Dr. Zoya Ignatova

Namen der Prüfungskommissionsmitglieder:

1. Prof. Dr. Peter Heisig
2. Prof. Dr. Daniel Wilson
3. Prof. Dr. Bernward Bisping

Disputationstermin: 30.10.22

Die vorliegende Arbeit wurde in der Zeit von April 2017 bis Juli 2022 unter der Leitung von Herrn Prof. Dr. Peter Heisig in der Abteilung für Pharmazeutische Biologie und Mikrobiologie im Institut für Biochemie und Molekularbiologie am Fachbereich Chemie der Universität Hamburg angefertigt.

Für Frank Dohler (✝2020)

# Index

# Abbreviations

| | |
|---|---|
| *ABC* | *ATP-binding casette* |
| *APS* | *Adenosine 5′-phosphosulfate* |
| *ARMS* | *Amplification-refractory mutation system* |
| *aTet* | *Anhydro tetracylcline* |
| *ATP* | *Adenosine triphosphate* |
| *BCA* | *Background corrected absorption* |
| *cDNA* | *Complementary DNA* |
| *CFP* | *Cerulean fluorescence protein* |
| *CFU* | *Colony forming units* |
| *CIP* | *Ciprofloxacin, Ciprofloxacin* |
| *Clm* | *Chloramphenicol* |
| *CRISPR* | *Clustered Regularly Interspaced Short Palindromic Repeats* |
| *Ct* | *Threshold cycle* |
| *CTP* | *Cytosine triphosphate* |
| *DAEC* | *Diffusely adherent E. coli* |
| *dATP-α-S* | *Deoxyadenosine α-thio triphosphate* |
| *DMSO* | *Dimethyl sulfoxide* |
| *DNA* | *Desoxyribonucleic acid* |
| *dNTP* | *Nucleoside triphosphate* |
| *DSB* | *Double-strand breaks* |
| *EAEC* | *Enteroaggregative E. coli* |
| *EDTA* | *Ethylenediaminetetraacetate* |
| *EHEC* | *Enterohaemorrhagic E. coli* |
| *EIEC* | *Enterinvasive E. coli* |
| *EPEC* | *Enteropathogenic E. coli* |
| *EtBr* | *Ethidium bromide* |
| *ETEC* | *Enterotoxigenic E. coli* |
| *FADH* | *Flavin adenine dinucleotide* |
| *FQ* | *Fluoroquinolones* |
| *FRET* | *Förster-resonance energy transfer* |
| *gDNA* | *Genomic DNA* |
| *GTP* | *Guanine-triphosphate, Guanine triphosphate* |
| *kDa* | *Kilodalton* |
| *MATE* | *Multi-drug and toxic compound extrusion* |
| *MFS* | *Major facilitator superfamily* |
| *MHK* | *Minimale Hemmkonzentration* |
| *MoCo* | *Molybdenum-cofactor* |
| *mRNA* | *Messenger RNA* |
| *NADPH* | *Nicotinamide adenine dinucleotide phosphate* |
| *NGS* | *Next-generation sequencing* |
| *OD* | *Optical density* |
| *PAM* | *Protospacer adjacent motif* |
| *PCR* | *Polymerase chain reaction* |
| $PP_i$ | *Pyrophosphate* |

| | |
|---|---|
| *PSQ* | *Pyrosequencing* |
| *qRT-PCR* | *Quantitative real-time PCR* |
| *RNA* | *Ribonucleic acid* |
| *RNAP* | *RNA Polymerase* |
| *RND* | *Resistance nodulation division* |
| *rNTPs* | *Ribonucleotide* |
| *ROS* | *Reactive oxygen species* |
| *RT* | *Reverse transcriptase* |
| *SDS* | *Sodium dodecylsulfate* |
| *SMR* | *Small multidrug resistance* |
| *SNP* | *Single nucleotide polymorphism* |
| *Spec* | *Spectinomycin* |
| *ssDNA* | *Single stranded DNA* |
| *Tat* | *Twin-arginine-translocation* |
| *TCA* | *Tricarboxylic acid cycle* |
| *TMAO* | *Trimethylamine-N-oxide* |
| *TTP* | *Thymine triphosphate* |
| *UPEC* | *Uropathogenic E. coli* |
| *UTI* | *Urinary tracts infections* |
| *UV* | *Ultraviolet* |
| *YFP* | *Yellow fluorescence protein* |

# 1. Zusammenfassung

Als Antibiotika werden heutzutage Wirkstoffe biologischen oder rein synthetischen Ursprungs bezeichnet, die eine reversibel wachstumshemmende (d.h. bakteriostatische) oder irreversibel abtötende (d.h. bakterizide) Wirkung gegen Bakterien aufweisen und vor allem zur Bekämpfung von Infektionen durch pathogene Erreger bei Mensch und Tier eingesetzt werden. Durch den verstärkten Selektionsdruck seit Einführung von Antibiotika in die Therapie haben sich Bakterien durch Erwerb einer Vielzahl von genetischen Veränderungen angepasst und binnen kurzer Zeit Resistenzen auch gegen neueste Antibiotika entwickelt. Gründe dafür sind der nicht sachgemäße Einsatz von Antibiotika zur Behandlung viraler Infektionen sowie der präventive Einsatz in nicht hemmenden Konzentrationen in der Tierzucht als Wachstumsförderer. Resistente pathogene Bakterien stellen jedoch weiterhin weltweit eine der häufigsten Ursachen für Todesfälle dar. Die stetig zunehmende Zahl antibiotikaresistenter Erreger und damit die Verkürzung des klinischen Anwendungszeitraums nach Markteinführung, hat das Interesse der Pharmaunternehmen an der Erforschung neuer Antibiotika genommen. Daher gewinnt die Erforschung von Resistenzmechanismen und neuen Zielstrukturen immer mehr an Bedeutung.

Zur Untersuchung der Resistenzmechanismen gegen Chinolone, die im Gegensatz zu den meisten bereits vor vielen Jahrmillionen in der Umwelt vorhandenen Antibiotika biologischen Ursprungs (z.B. Benzyl-Penicillin produziert von Pilzen der Gattung *Penicillum*) rein chemisch synthetisiert und erst seit ca. 40 Jahren eingesetzt werden, wurden von einem *E. coli* Wildtyp (WT)-Stamm als klinischem Isolat ohne bekannte Resistenz gegen Antibiotika aus der Stuhlflora einer gesunden Person durch schrittweise Selektion mit steigenden Konzentrationen von Chinolonen, wie Ciprofloxacin (CIP) erhalten. Die Sequenzierung des gesamten Genoms hat ergeben, dass sich bei diesen Mutanten neben bekannten Resistenzmutationen, auch Veränderungen in Genen ohne direkten Einfluss auf Resistenz gegen Fluorchinolone fanden.

Am Beispiel der Mutante, *Escherichia coli* MIVb mit der höchsten Fluorchinolonresistenz aller isolierten Mutanten wurden im Vergleich zum direkten Vorgänger MIII zwei neue Mutationen in den Genen *modB* und *rpoC* identifiziert und im Hinblick auf ihre Rolle bei der Entstehung und/oder Stabilisierung extrem hoher Fluorchinolon-resistenter Isolate analysiert. Das Gen *modB* kodiert für die Transmembrandomäne eines ABC-Transporters, der für die

Aufnahme des Spurenelements Molybdän verantwortlich ist. Das Gen *rpoC* kodiert für die β'-Untereinheit der RNA-Polymerase, die für den Transkriptionsvorgang essentiell ist. Keines der Gene besitzt eine Funktion, die mit der Fluorchinolonresistenz in Verbindung gebracht werden kann. Dennoch zeigt *E. coli* MIVb eine minimale Hemmkonzentration (MHK) von Ciprofloxacin von 256 µg/ml, während sein direkter Vorgängerstamm, *E. coli* MIII, 64 µg/ml aufweist.

Daher war es Ziel dieser Arbeit, die Rolle dieser Mutationen für die hohe Fluorchinolonresistenz in *E. coli* zu analysieren.

Für Untersuchungen zur Rolle von *modB* wurde ein auf dem Förster-Resonanz-Energie-Transfer basierendes Molybdat-Sensorsystem verwendet, um die Molybdat-Aufnahme in *E. coli* WT und in definierte, von diesen mittels CRISPR-cas9-Technologie erzeugte Mutanten mit Mutationen aus *E. coli* MIVb zu analysieren. Der Molybdat Influx in *E. coli* WT/ModB-L106M war im Vergleich zu *E. coli* WT, und *E. coli* WT/ModB-L106M/RpoC-P246Q reduziert.

Eine mögliche Rolle der *rpoC*-Mutation könnte das Zusammenspiel zwischen Mutationen zur Resistenz gegen Fluorchinolone und solchen zur Abschwächung/Neutralisierung bakterizider Mechanismen durch reaktive Sauerstoffspezies (ROS) betreffen. Diese Hypothese fußt darauf, dass die Mutation in *rpoC* mit einer Erhöhung der MHK von Ciprofloxacin einhergeht und Transkriptomanalysen (die nicht im Rahmen dieser Arbeit generiert wurden) eine veränderte Expression solcher Gene bei *E. coli* MIVb zeigten, welche mit Reaktionen auf oxidativen Stress assoziiert sind. Um die Rolle dieser Gene zu untersuchen, wurden CRISPR-Cas9-generierte Varianten von *E. coli* WT mit *rpoC*-Mutation mittels quantitativer realtime-PCR (qRT-PCR) analysiert. Dabei zeigte sich ein Anstieg in der Genexpression von ROS-assoziierten Genen, wenn sie oxidativem Stress ausgesetzt waren. Ein wichtiger Teil dieser Arbeit ist die Untersuchung, ob eine veränderte Genregulierung als Reaktion auf ROS infolge der Exposition gegenüber Chinolonen durch RpoC stattfindet.

In weiteren Experimenten wurden die Wachstumsrate und die Persistenz dieser Mutanten bestimmt, indem *E. coli* MIVb über 300 Generationen ohne Antibiotikum kultiviert wurde. Es zeigte sich, dass nach 300 Generationen alle direkt mit hoher Fluorchinolonesistenz assoziierten Mutationen erhalten blieben, aber bereits nach 25 Generationen *E. coli* MIVb eine neue Mutation erworben hatte, die dessen Wachstumsgeschwindigkeit deutlich erhöhte. Dies zeigt, dass die *E. coli* Mutante MIVb-300 ihre erhöhte Verdopplungsrate auf Kosten der hohen Fluorchinolonresistenz ausprägt, auf die in diesem Experiment nicht selektiert wurde.

Dennoch blieb die MHK des Fluorchinolons Ciprofloxacin für diese Mutante mit 32 µg/ml immer noch auf einem aus klinischer Sicht sehr hohen Niveau. Weiterhin deuten die Daten darauf hin, dass die nach 25 Generationen erhöhte Wachstumsrate selbst zu der Abnahme der Fluorchinolonresistenz beitragen könnte.

# 2. Abstract

Nowadays, antibiotics are active substances of biological or purely synthetic origin that have a reversible growth-inhibiting (i.e., bacteriostatic) or irreversible killing (i.e., bactericidal) effect against bacteria. Antibioticsare used primarily to combat infections caused by pathogenic b in humans and animals. Due to increased selection pressure since the introduction of antibiotics into therapy, bacteria have adapted within a short period of time to even the newest antibiotics by acquisition of various genetic modifications resulting in resistance . One reason for this is the inappropriate use of antibiotics to treat viral infections, as well as their preventive use as growth promoters in sub-inhibitory concentrations for stockbreeding. However, resistant pathogenic bacteria continue to be one of the leading causes of death worldwide. The steadily increasing number of antibiotic-resistant pathogens, resulting in the shortening of the period of clinical antibiotic use after the introduction into market, has led pharmaceutical companies to stop research for new antibiotics. Therefore, research on resistance mechanisms and new targets is becoming increasingly important.

In contrast to most antibiotics of biological origin (e.g., benzyl penicillin produced by fungi of the genus *Penicillum*) present in the environment many millions of years ago, quinolones, are synthesized chemically and have only been used clinically for about 40 years. To study mechanisms of resistance to quinolones,mutants were obtained from an *E. coli* wild-type (WT) strain as an antibiotic-susceptible clinical isolate without known resistance to antibiotics obtained from the fecal flora of a healthy individual by subsequent stepwise selection with increasing concentrations of ciprofloxacin (CIP). Whole genome sequencing showed that in these mutants, in addition to known resistance mutations, there were also changes in genes with no known role in resistance to fluoroquinolones.

*Escherichia coli* MIVb, with the highest fluoroquinolone resistance, two mutations in the genes *modB* and *rpoC* were identified and analyzed with regard to their role in the development and/or stabilization of extremely highly fluoroquinolone-resistant isolates. The gene *modB*

encodes the transmembrane domain of an ABC transporter responsible for the uptake of the trace element molybdenum. The gene *rpoC* encodes the β'-subunit of RNA polymerase. Both genes have very different functions within the bacterium, neither of which can be linked to fluoroquinolone resistance. Nevertheless, *E. coli* MIVb has a minimum inhibitory concentration (MIC) of ciprofloxacin of 256 µg/ml, while its direct progenitor, mutant *E. coli* MIII, has 64 µg/ml.

Therefore, the aim of this work was to analyze the role of these mutations in the high fluoroquinolone resistance in *E. coli*.

For studies on the role of *modB*, a Förster resonance energy transfer-based molybdate sensing system was used to determine molybdate uptake in *E. coli* WT as well as in defined mutants generated by CRISPR-cas9 technology to establish mutations from *E. coli* MIVb in different genetic background. Molybdate influx in *E. coli* WT/ModB-L106M was reduced compared with *E. coli* WT, and *E. coli* WT/ModB-L106M/RpoC-P246Q.

A possible role of this *rpoC* mutation could be that it plays a role in the interplay between mutations for resistance to fluoroquinolones and those for attenuation/neutralization of bactericidal mechanisms by reactive oxygen species (ROS). This hypothesis is based on the finding that the *rpoC* mutation is associated with an increase in the MIC of ciprofloxacin and transcriptome analyses (not generated as part of this work) showed altered expression of those genes in *E. coli* MIVb, which are associated with responses to oxidative stress. To investigate the role of these genes, CRISPR-Cas9-generated derivatives of *E. coli* WT carrying a *rpoC* mutation were analyzed by quantitative real-time PCR (qRT-PCR). This showed an increase in gene expression of ROS-associated genes when exposed to oxidative stress. An important part of this work is to investigate whether altered gene regulation in response to ROS occurs as a result of exposure to quinolones by *rpoC*.

In further experiments, the growth rate and persistence of these mutants were determined by growing *E. coli* MIVb for 300 generations without antibiotic. After 300 generations, all mutations directly associated with high fluoroquinolone resistance were maintained, but after only 25 generations, *E. coli* MIVb had acquired a new mutation that significantly increased its growth rate. This indicates that the *E. coli* mutant MIVb-300 increased its doubling rate at the cost of high fluoroquinolone resistance. Nevertheless, the MIC of ciprofloxacin of this mutant still remained at a high level from a clinical perspective with 32 µg/ml. Furthermore, the data

suggest that the increased growth rate after 25 generations may contribute to the reduction in fluoroquinolone resistance.

# 3. Introduction

## *3.1 Escherichia coli*

*Escherichia coli* Gram-negative bacteria, which belong to the family of *Enterobacteriaceae*, remains one of the most common causative agents of infections such as urinary tracts infections (UTIs), septicaemia, enterititis, neonatal meningitis and other clinically relevant infections. Apathogenic *Escherichia coli* cells are a main part of the facultative aerobic intestinal microflora in humans and several animals. It benefits from non-absorbed nutrients in the lower gastrointestinal tract, while the host, mutually benefits from the presence of *Escherichia coli* cells attached to the mucosal surface thereby preventing pathogenic bacteria from colonizing (Allocati et al., 2013).

These bacteria including virulent variants of *Escherichia coli*, however, are highly adaptive and promote an increased ability to cause a broad spectrum of diseases. The most successful persisting combinations of virulence factors are designated as PATHOTYPES, that enable these strains to cause those diseases described above. These intestinal pathogens are categorized in six groups: enteropathogenic *E. coli* (EPEC), enterohaemorrhagic *E. coli* (EHEC), enterotoxigenic *E. coli* (ETEC), enteroaggregative *E. coli* (EAEC), enteroinvasive *E. coli* (EIEC) and diffusely adherent *E. coli* (DAEC). The most common extraintestinal infections are UTIs and are caused by uropathogenic *E. coli* (UPEC) (Kaper et al., 2004; Nataro and Kaper, 1998).

The *E. coli* pathotypes are generally characterized by shared O (lipopolysaccharide, LPS) and H (flagellar) antigens that define the SEROGROUPS (only the O antigen) or SEROTYPES (O and H antigens) (Nataro and Kaper, 1998; Schaechter and The View From Here Group, 2001).

However, when pathogenic *E. coli* are found in other intestinal habitats, factors are required that enable a strain to colonize these habitats. One way to enable *E. coli* strains to colonize these environments, like the urethra, is promoted by adhesins or adherence factors. *E. coli* adhesins form fimbriae, which are not to be mistaken with flagella, and facilitate the attachment of the organism to intestinal receptor molecules (Cassels and Wolf, 1995).

But it is not just the capability of pathogenic *E. coli* to invade other human habitats that makes pathogenic strains harmful to the host. Pathogenic *E. coli* harbors the ability to produce a vast variety of toxins that are harmful to the host cell and affect many eukaryotic processes. For instance, the pathogenic strains ExPEC and APEC secrete the hemoglobin-binding protease (Tsh) that degrades hemoglobin. The toxins HlyA (UPEC) and Ehx (EHEC) target erythrocytes

and leukocytes and trigger their cell lysis. EHECs shiga toxin alone has a variety of pathogenic functions, including the depurination of rRNA, the inhibition of protein synthesis as well as the induction of apoptosis (Kaper et al., 2004).

*Escherichia coli* is a facultative anaerobic organism, which means that providing energy by the respiratory chain, as well as the formation of redox compounds can be achieved with and without the usage of oxygen. Also the fact, that the complete genomes of many strains of *E. coli* are fully sequenced makes it one of the most favorable bacterial strains in biotechnology and the most frequently used microorganism in the field of recombinant DNA technology (Allocati et al., 2013).

## 3.2 *Antibiotics*

Antimicrobial resistance displays a global challenge for healthcare systems. Ever since their introduction to counteract clinical bacterial infections, bacteria of almost every phylogenetic family have responded to the increasing use of antimicrobials with adaption by mutational alteration or by transfer of resistance genes to other bacteria. The high consumption of antibiotics and inappropriate use are factors, which intensify the problem. There are many classes of antimicrobial agents available to treat clinical infections caused by *Escherichia coli* and they act in very different ways. To overcome the action of antibiotics bacteria have developed a broad spectrum of mechanisms of resistance which can be divided in three basic strategies: modification of the target (enzymatically or by mutation) , decreasing antibiotic concentration at the site of action either by reducing cell permeability (e.g. by downregulation of outer membrane porins) or by increasing the export of antibiotics (e.g. by over-expression of efflux pumps) as well as the production of modifying or degradative enzymes. Among the many classes of antibiotics, for the clinically important β-lactams and aminoglycosides the resistance mechanisms will be briefly explained, as these drugs are considered to be the most problematic in *E. coli* (Poirel et al., 2018). The third class of clinically relevant antibiotics, i.e. the fluoroquinolones (FQ) will be explained in more detail in this work.

### 3.2.1 ß-Lactams

The first β-lactam antibiotic to be discovered, that is also the first isolated "true", i.e., biosynthetic compound, was benzyl-penicillin, that was discovered in 1929 by Alexander

Fleming. It was introduced into clinical practice only about ten years later. β-Lactams act by preventing the biosynthesis of peptidoglycan. Beside penicillin, with cephalosporins, carbapenems and monobactams, three additional subclasses with altered or expanded spectrum of activity were detected and as the penicillins were used as scaffolds for the chemical modification to obtain more active derivatives. One major step in the development of β-lactam antibiotics is the introduction of aminopenicillins like ampicillin, which enabled the use of this antimicrobial compound to target different Gram-negative bacteria, methicillin to treat penicillin-resistant *Staphylococcus aureus* or oxyimino cephalosporins like cefotaxime and ceftazidime to overcome β-lactamase-mediated resistance in Gram-negative bacteria. ß-Lactamases include a group of enzymes that hydrolyze the amide bonding of the ß-lactam ring and are a highly effective mechanism of resistance against many β-lactams (Tooke et al., 2019).

### 3.2.2 Aminoglycosides

Aminoglycosides are produced by the genera *Streptomyces* and *Micromonospora* (Davies and Wright, 1997; Doi et al., 2016) present in the soil environment. Their antibiotic activity is enhanced in combination with a second antimicrobial agent, such as ß-lactams. This combination acts synergistically and thus is used to treat complicated infections like sepsis, pneumonia, meningitis and urinary tract infections. Members of the aminoglycoside class are e.g., gentamicin (from *Micromonospora*), kanamycin and streptomycin (from *Streptomyces*). Aminoglycosides interfere with ribosomal translation leading to bacterial cell death (bactericidal activity) (Poirel et al., 2018). Resistance to aminoglycosides can be due to mutational alteration of the target – the 16S rRNA and/or the S5 and S12 ribosomal proteins. The target of aminoglycosides, 16S rRNA, can also be enzymatically modified by 16S rRNA methylases to confer high-level resistance to some aminoglycosides, e.g., amikacin. (Fourmy et al., 1998; Griffey et al., 1999; Llano-Sotelo et al., 2009). The most widely distributed mechanism of resistance to aminoglycosides is the enzymatic modification of the aminoglycoside building blocks (aminohexoses or aminocyclitols) by three groups of aminoglycoside-modifying enzymes: acetyltransferases, nucleotidyltransferases and phosphotransferases (Poirel et al., 2018), resulting in the interference with binding to the target site (Poirel et al., 2018).

### 3.2.3 Quinolones and fluoroquinolones (FQ)

Quinolones represent a class of purely synthetic antibiotics that inhibit DNA replication by targeting bacterial type II topoisomerases, DNA gyrase and topoisomerase IV. The first representative of the quinolone class of drugs was nalidixic acid, a naphthyridone-based drug. It was first described by George Lesher in 1962 (Lesher et al., 1962). Later, in the 1970s, true 4-quinolones have been introduced to clinical usage, such as oxolinic acid. Later, in the 1980s, quinolones were chemically modified and resulted in the 1st generation 6-fluoro-4-quinolone-3carboxylic-acid derivatives, norfloxacin and ofloxacin (Andriole, 2005; Emmerson, 2003; Mitscher, 2005; Stein, 1988). Further modification of the N1-position substituents by, e.g., introduction of a cyclopropyl-moiety lead to the the 2nd generation fluoroquinolone ciprofloxacin. It has an increased activity against many Gram-negative bacteria by a significantly improved activity not only against the primary target DNA-gyrase, but also the secondary target, topoisomerase IV resulting in an extended spectrum including some Gram-positive pathogens, such as *Staphylococcus aureus*. Further chemical modifications resulted in levofloxacin representing the 3rd generation of fluoroquinolones with an improved activity against the primary target in Gram-positives, bacterial topoisomerase IV. Moreover, further developments by additional modifications affecting the C8-position of the fluoroquinolone core structure (e.g. in moxifloxacin, a 4th generation fluoroquinolone) were associated with enhanced pharmacokinetics and pharmacodynamics, especially including more Gram-positive and additionally some anaerobic pathogens. In summary, representatives of the four different classes of fluoroquinolones can be used to treat a broad variety of infections including urinary tract infections respiratory tract infections pyelonephritis, sexually transmittable diseases, skin and tissue infections, chronic bronchitis, nosocomial pneumonia and intra-abdominal and pelvic infections (Andriole, 2005; Emmerson, 2003; Mitscher, 2005; Stein, 1988)

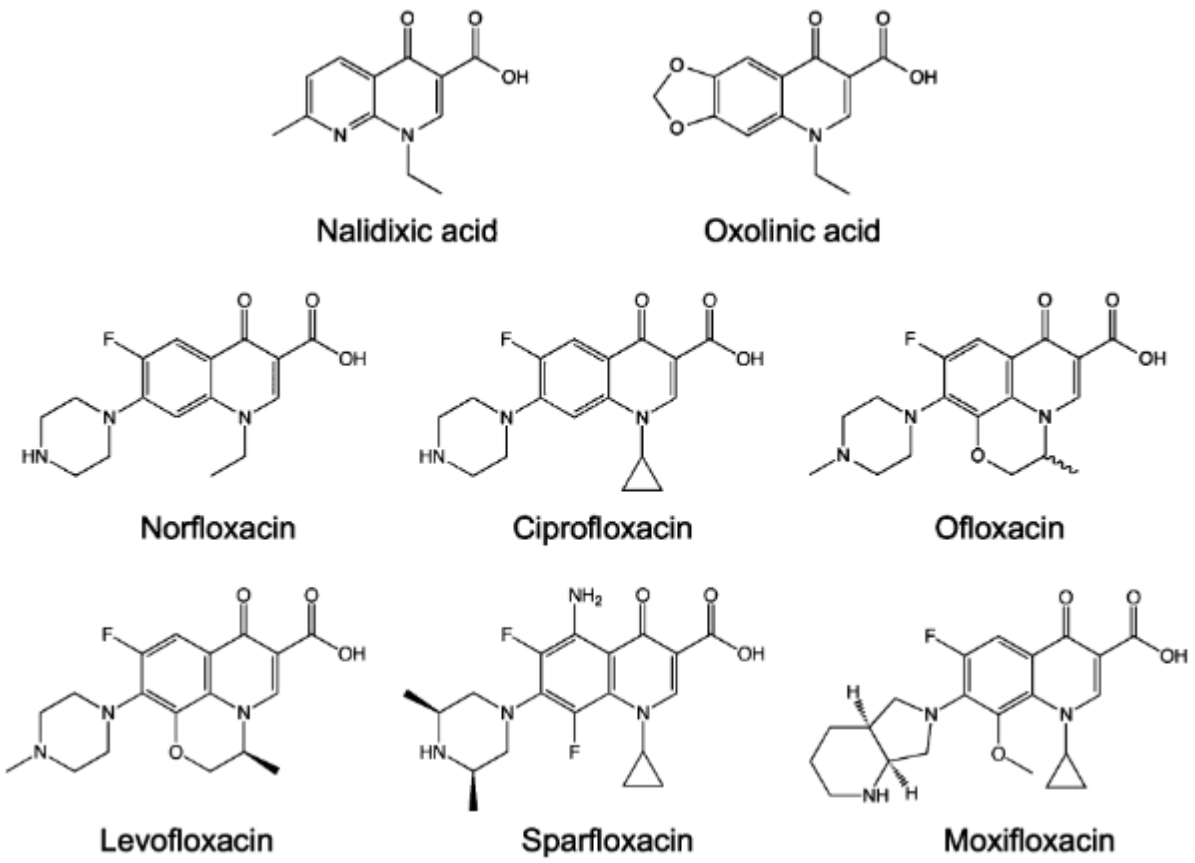


*Figure 1: Chemical structures of fluoroquinolones belonging to 1st generation (Norfloxacin), 2nd generation (Ciprofloxacin, Ofloxacin), 3rd generation (Levofloxacin, Sparfloxacin) and 4th generation (moxifloxacin) (Aldred et al., 2014).*

## *3.3 Bacterial type II topoisomerases*

Most bacterial species have two different type II topoisomerases, DNA gyrase (topoisomerase II) and topoisomerase IV. These enzymes in combination with type I topoisomerases (topoisomerase I and topoisomerase III) are involved in controlling the topological state of genomic bacterial DNA in the cell. In most bacteria covalently closed circular (ccc) chromosomal DNA is packed inside the cell in a so-called negatively supercoiled (i.e., underwind state) form, while in some others such as thermophilic archaea in an overwound state (i.e., positive supercoiling). The number of bp per 360° DNA turn of ccc ds DNA under physiological conditions is 10. Thus, the helix axis in this state of lowest energy, i.e., without any conformational constrains, is positioned in a plane and with each turn the two DNA strands are covalently intertwined once. Since this DNA molecule is about 500fold longer than a typical *E. coli* cell, the biological function of DNA topoisomerases is in collaboration with histone-like proteins to compact the ccc ds DNA molecule so that it fits into one cell. This is achieved by transiently introducing a dsDNA break, formation of a tyrosine-ester bond of either DNA gyrase subunit A to either 5'phosphat end of the cleaved ds DNA and, after

subsequent ATP binding, a directed passage of a remote DNA segment through the ds DNA break. This induces a conformational change in DNA gyrase followed by resealing of the DNA break and release of the DNA gyrase under ATP hydrolysis. As a result, the number of DNA-links is reduced by a factor of 2, while the number of DNA turns remains constant. As a result, the DNA molecule is underwound, i.e., negatively supercoiled which is detectable as a winding of the helix axis out of the plane. Repeated cycles of DNA gyrase action will lead to a more compact DNA molecule which finally is in a highly supercoiled state and a compact size to fit into the cell.

Although gyrase and topoisomerase IV share high structural similarities, their actual mechanisms of action differ. When gyrase promotes the formation of negative supercoils in DNA, topoisomerase IV works primarily by decatenating intertwined daughter chromosomes following replication and secondary by the removal of knots that have been accumulated in the DNA as a result of cellular processes. Both enzymes, gyrase and topoisomerase IV, consist of two distinct functional subunits and work as $A_2B_2$ heterotetramers. For gyrase, those subunits are called GyrA and GyrB, for topoisomerase IV in Gram-negative bacteria ParC and ParE, respectively. GyrA and ParC are the homologous A-subunits that contain the active-site tyrosine residue binding to the overlapping 5'-termini of the DNA. GyrB and ParE, respectively contain a single ATPase domain and a metal ion-binding domain essential for enzymatic activity. (Anderson and Osheroff, 2001; Champoux, 2001; Deibler et al., 2001; Deweese and Osheroff, 2010; Forterre et al., 2007; Forterre and Gadelle, 2009; Levine et al., 1998; Lindsey et al., 2014; Pitts et al., 2011; Pommier et al., 2010; Schmidt et al., 2010; Zechiedrich et al., 2000). As described by (Correia et al., 2017), the most frequent mutations within *Escherichia coli* are shown in Table 1.

*Table 1: Mutations detected in genes encoding subunits A and B of DNA gyrase and topoisomerase IV of clinically important pathogenic Escherichia coli strains described in the literature (Correia et al., 2017). In Enterobacteriaceae, the most common first-step mutation is a single mutation in the gyrA gene, which confers low-level resistance against quinolones. A second mutation often occurs within either Ser-80 or in the amino acid codon Glu-84 of the parC gene, that confers a moderate level of ciprofloxacin resistance. An additional mutation within gyrA is often associated with a high level of ciprofloxacin and a fourth mutation, the second in parC, is associated with the highest level of resistance (Fàbrega et al., 2009).*

| *gyrA* | *gyrB* | *parC* | *parE* |
|---|---|---|---|
| Tyr50Phe | Asp426Asn | Ala56Thr | Leu416Phe |
| Ala51Val | Lys447Glu | Ser57Thr | Ile444Phe |
| Ala67Ser | Ser492Asn | Asp69Glu | Leu445His/Ile |
| Gly78Cys | Glu466-Asp | Gly78Asp | Ser458Ala/Pro/Thr/Trp |
| Ser80Arg/Ile | Ser492Asn | Ser80Arg/Ile | Glu460Asp/Lys |
| Gly81Asp/Cys | | Ser83Leu | Ile464Phe |
| Asp82Gly | | Glu84Ala/Gly/Lys/Val | Ile529Leu |
| Ser83Ala/Ile/Leu/Trp/Tyr/Val | | Cys107Trp | |
| Ala84Pro/Val | | Ala108Thr/Val | |
| Asp87Asn/Glu/Gly/His/Tyr/Val | | | |
| Gln106Arg/His | | | |
| Ala119Glu | | | |
| Ala196Glu | | | |
| Arg237His | | | |

### 3.3.1 Inhibition of type-II topoisomerases by quinolones

The molecular target for the action of fluoroquinolones is the covalent DNA-enzyme complex. A noncatalytic $Mg^{2+}$ ion is chelated by the C3-carboxy/C4-keto groups of the quinolone and forms hydrogen bonds, e.g., in *Escherichia coli*, with the OH-residue of serine-83 and the β-carboxy group of aspartic acid-87 of gyrase subunit A (GyrA). In topoisomerase IV, that is the secondary target of quinolones in *Escherichia coli*, a serine at position 80 and a glutamic acid at position 84 are the respective ion chelators necessary for quinolone binding. Quinolones interfere with DNA supercoiling and relaxation by binding to and stabilizing the gyrase-DNA-cleaved complexes. This mechanism can also be adapted to topoisomerase IV. As mutations occur within serine 83, and aspartic acid 87, it was shown that the affinity for quinolones decreases, and as both residues mutate, quinolones can no longer stabilize cleavage complexes at clinically relevant concentrations (Aldred et al., 2013a, 2013b; Anderson and Osheroff, 2001; Drlica et al., 2009; Hooper, 2001, 1999; Wohlkonig et al., 2010).

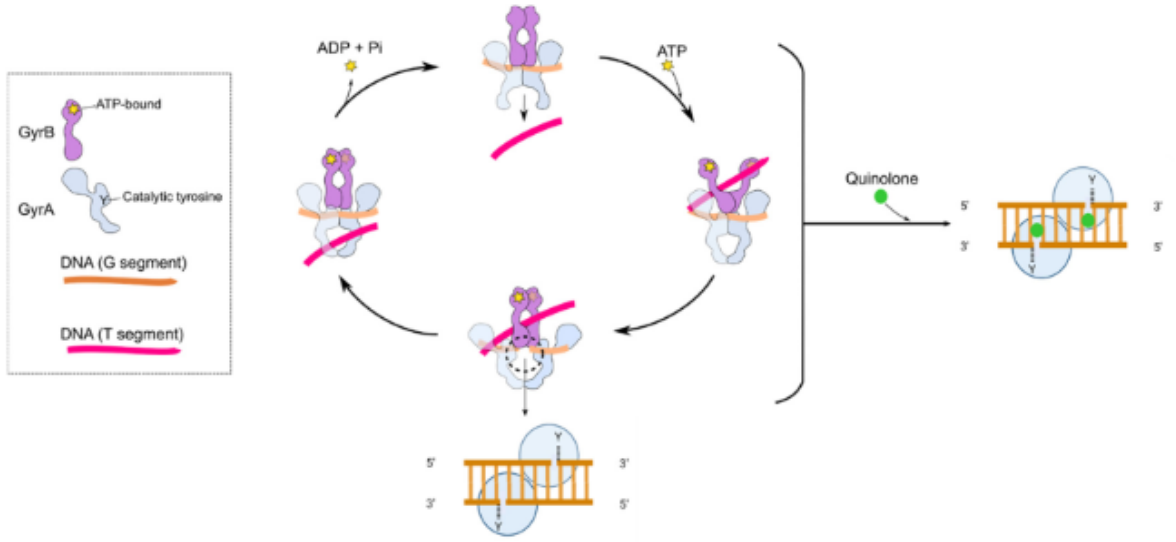


*Figure 2: Visualization of the proposed mechanism of DNA supercoiling by DNA gyrase and the stabilized cleavage complex by quinolones. The inset shows the GyrA (blue) and GyrB (purple) subunits. Y implies the the active site tyrosine, and the star implies the ATP-binding site. A G segment (orange) binds the GyrA dimer. ATP binds the N-terminal domain of GyrB, which closes the GyrB clamp (also known as the N-gate), targeting the T segment. The G segment becomes cleaved and the DNA gate widens, and the T segment is transported through the cleaved G segment. The G segment is re-ligated, and the T segment exits through the GyrA C-gate. The hydrolysis of ATP and the leaving of ADP + Pi resets the enzyme for another cycle. The lower inset shows the cleavage complex as indicated by a black-dashed circle. The right-hand panel shows the binding of quinolones (green spheres) in the cl (Bush et al., 2020).*

## *3.4 Bacterial resistance against quinolones*

As mentioned earlier, bacterial quinolone resistance is primarily associated with mutations affecting a serine and an additional acidic amino acid to prevent $Mg^{2+}$-associated formation of hydrogen bonds between the quinolone and the bacterial enzymes gyrase and topoisomerase IV. However, additional two mechanisms can cause quinolone resistance .

### 3.4.1 Plasmid-mediated quinolone resistance

When chromosomal mutations associated with quinolone resistance are being passed onto daughter cells of bacteria vertically, plasmid-mediated quinolone resistance can be transferred horizontally by conjugation. Three different types of plasmid-mediated quinolone resistance (PMQR) mechanisms are known: The first is represented by Qnr genes, that encode proteins (ca. 200 amino acids in size), that are forming a DNA-like structure. These structures compete with the natural substrate DNA for binding to gyrase and topoisomerase IV resulting in a decreased number of active targets. Besides these DNA-mimicking Qnr proteins, there is an additional plasmid-encoded mechanism, provided by AAC(6')-Ib-cr, an enzyme that is supposed to be derived from a close homologue, AAC(6')-Ib inactivating aminoglycoside

antibiotics. AAC(6')-Ib-cr acetylates the unsubstituted nitrogen of the C7-substituent, the piperazine ring in norfloxacin and ciprofloxacin resulting in a decreased antibiotic activity. The third mechanism of PMQR is presented by efflux pumps. Proteins like OqxAB, QepA1 and QepA2 have been identified to this date. (Cattoir et al., 2008; Guillard et al., 2013; Robicsek et al., 2006b; Rodríguez-Martínez et al., 2016; Strahilevitz et al., 2009; Sun et al., 2010; Tran et al., 2005a, 2005b; Tran and Jacoby, 2002; Xiong et al., 2011; Yamane et al., 2007). The mechanisms of efflux pumps and their role in fluoroquinolone resistance are described in the following chapter.

### 3.4.2 Chromosomally-encoded quinolone resistance

Small hydrophilic molecules such as nutrients or quinolones cannot pass the lipid bylayer of the outer membrane of Gram-negative bacteria. Instead, bacteria express proteins capable to form waterfilled transmembrane pores called porins. Uptake of fluoroquinolones through these porins is regulated by the type and the amount of porins. Thus, resistance to antibiotics can be increased by downregulating the expression of these porin proteins (Martinez-Martinez, 2003; Mitscher, 2005; Robicsek et al., 2006a; Strahilevitz et al., 2009; Tran and Jacoby, 2002). As already mentioned in 3.4.1, another way to reduce the intracellular fluoroquinolone concentration is the overexpression efflux systems. Chromosomally-encoded efflux systems can be regulated by chromosomal alterations inactivating genes that regulate these proteins, such as the local repressor AcrR silencing the AcrAB-TolC multiple drug resistance (MDR) efflux pump (Ma et al., 1996). Several chromosomally encoded efflux pumps show a broader substrate spectrum, while plasmid-mediated efflux-pump based resistance typically is drug-specific. Beside AcrAB-TolC belonging to the resistance-nodulation division (RND) family of efflux pumps four other classes are known: Major facilitator superfamily (MFS), ATP binding cassette (ABC) family, small multidrug resistance (SMR) family and multi-drug and toxic compound extrusion (MATE) family. Most commonly found in antibiotic-resistant *Escherichia coli* and other Gram-negative bacteria is the efflux system of the resistance-nodulation-division (RND) family type that affect multi-drug efflux (Poole, 2007). One of these RND family efflux pumps is the AcrAB-TolC efflux pump. Its efflux affects quinolones, macrolides, and others. Like other multidrug efflux pumps of RND-type, AcrAB-TolC consists of three functional subunits: the efflux pump (AcrB), the accessory protein AcrA in the periplasm and outer

membrane channel TolC as shown in Figure 3. Energy source for the efflux pump is the protone motif force across the cytoplasmic membrane.

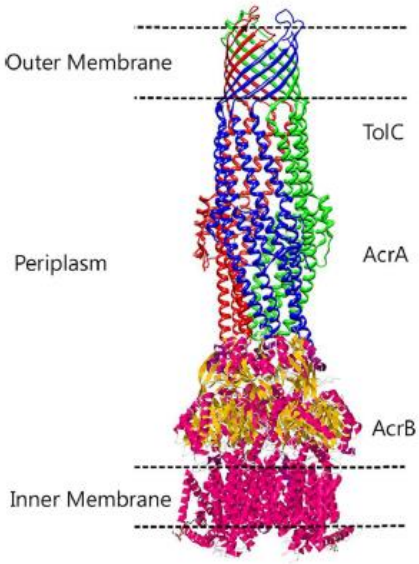


*Figure 3: Structure of AcrAB–TolC efflux pump of Escherichia coli (Puzari and Chetia, 2017).*

## *3.5 SOS response in bacteria*

Although the interaction of quinolones with gyrase and topoisomerase IV are well understood, the actual mechanism of how quinolone and gyrase/topoisomerase IV-interactions lead to bacterial cell death have been the focus of several molecular biological studies during the last years but are not yet completely understood. It has been common knowledge, that quinolones inhibit the supercoiling activity of DNA gyrase and the cleavage complex is a key structure for the induction of the SOS response triggering DNA repair mechanisms. This explains why quinolone-induced cell death is independent of supercoiling formation (Chow et al., 1988a).

Following DNA damage bacteria have evolved several DNA damage repair mechanisms. The SOS response is triggered by the accumulation of single-stranded DNA (ssDNA), e.g., by agents interfering with DNA-replication, ionizing radiation and UV light. Single-stranded DNA is generated when DNA polymerase III stalls e.g. at a gyrase-mediated ds DNA break while helicase continues unwinding and separating the DNA single strands (Higuchi et al., 2003; Pagès and Fuchs, 2003). Two proteins are essential in regulating the induction of the bacterial SOS response – LexA and RecA. In the absence of cellular stress, the LexA dimer functions as a transcriptional repressor, that prevents the expressions of a variety of genes, whose products are necessary for DNA repair after SOS induction (Luo et al., 2001; Walker,

1984; Zhang et al., 2010). LexA binds to promoter regions, called SOS boxes upstream of so-called SOS genes and blocks transcription. RecA acts as a regulator of LexA, due to its co-protease function, which is activated by binding to ssDNA resulting in the cleavage of LexA. RecA-induced cleavage of LexA occurs between Ala84-Gly85 (Little, 1991) resulting in a lower affinity of LexA to DNA and a subsequent exposure of residues that target LexA for ClpXP and Lon protease degradation (Neher et al., 2003). As soon as RecA has been activated, promoter-bound LexA proteins are degraded, resulting in transcriptional activation of SOS genes (Little and Mount, 1982), which include genes encoding enzymes for excision repair, homologous recombination, DNA replication and the arrest of cell division. For other genes regulated by LexA the function is still unknown. Although many genes are induced by RecA-mediated cleavage of LexA, they are differently expressed with respect to mRNA levels and are not expressed simultaneously (Courcelle et al., 2001; Fernández de Henestrosa et al., 2002; Quillardet et al., 2003).

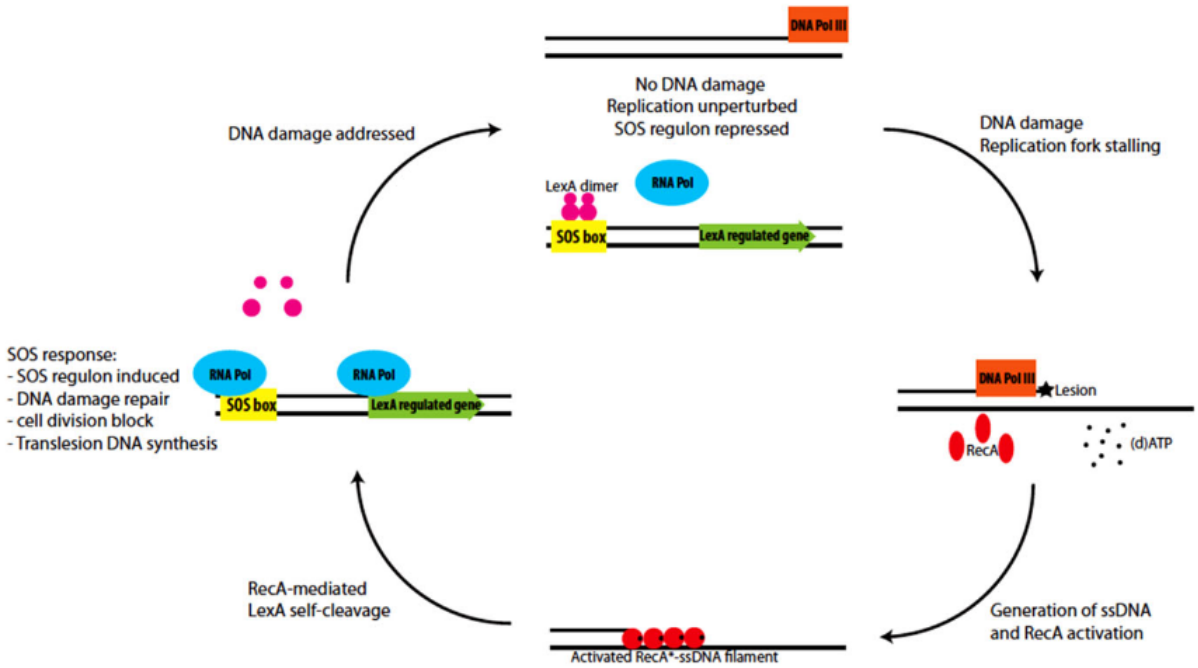


*Figure 4: Schematic representation of the SOS response in Escherichia coli. As soon as DNA damage leads to a stalled replication fork, ssDNA is being formed, which results in RecA activation by formation of RecA-activated ssDNA filaments, which lead to the cleavage of LexA. As soon as LexA is released from its binding to DNA and undergoes degradation, LexA regulated genes can then be expressed, which results the translation of SOS-related proteins (Maslowska et al., 2019).*

## *3.6 SOS response and reactive oxygen species (ROS)*

It has been shown that the fluoroquinolone ciprofloxacin triggers the formation of mutations by inducing transient differentiation of a mutant-generating subpopulation by reactive oxygen species. It was shown that mutagenesis induced by quinolones, occurs within a subpopulation

of the culture, where ubiquinone-electron transfer in combination with SOS signaling lead to accumulation of reactive oxygen species, which in turn activate the Sigma-S ($\sigma^S$) general stress response, that allows mutagenic DNA-break repair (Pribis et al., 2019).

### *3.7 Quinolone-mediated bacterial killing and reactive oxygen species*

As in previous paragraphs explained, quinolones block DNA replication and transcription by binding to and stabilizing a covalent complex of DNA and gyrase. While this event might explain a bacteriostatic effect of quinolones, it cannot provide a plausible explanation for the known bactericidal effects of quinolones (Chow et al., 1988b; Gellert et al., 1977; Snyder and Drlica, 1979; Sugino et al., 1977). From early experiments two types of bactericidal effects of quinolones have been postulated: (1) DNA lesions cause double strand breaks themselves which lead to cell death. (2) quinolone-topoisomerase-DNA ternary complexes stimulate the accumulation of toxic reactive oxygen species (ROS). Later work, however, has provided evidence for a third mechanism. It has been shown, for example, that nalidixic acid, a non-fluorinated naphthyridine-derivative, chemically closely related to quinolones, requires RNA and protein synthesis for bactericidal activity as well as when cells are suspended in nutrient free saline. In the absence of nutrients, energy metabolism and ROS accumulation is shut down when cells are treated with quinolones. Without nutrients, cells go into hibernation und downregulate energy-providing pathways, e.g., the respiratory chain. Without active respiration, the formation of water from ½ $O_2$, $2H^+$ and $2e^-$ decreases. This way, there is no electron transfer to oxygen, which is necessary for ROS. Therefore, saline suspension has the same effect on ROS as inhibition of protein synthesis, which is known to suppress ROS production. Fluoroquinolones, like ciprofloxacin and moxifloxacin, that were developed later, do have a bactericidal effect in the absence of energy metabolism, i.e., in saline and in the absence of protein synthesis. Norfloxacin, on the other side, kills cells in saline but not if protein synthesis is inhibited. These examples were proposed to represent killing of *Escherichia coli* by three distinct mechanisms A, B and C, respectively (Hong et al., 2020; Smith, 1986). All three mechanism have shown to accumulate ROS either during drug treatment or after the removal of the respective quinolone. The mechanisms of action of reactive oxygen species on bacterial cells as well as the cells' response to counter harmful ROS is explained in the following paragraph.

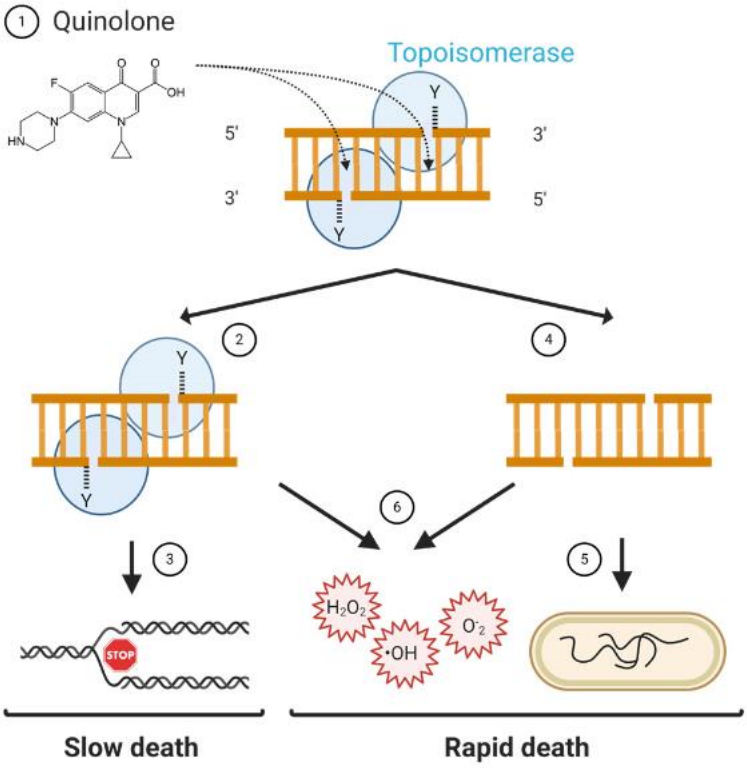


*Figure 5: Model of quinolone lethality. 1) As described in 3.3.1, quinolones stabilize the DNA cleavage complex with topoisomerases. 2) When the cleavage complex is not resolved, it leads to 3) inhibition of replication and transcription, which in turn, leads to slow death of the bacterial cell. However, if the cleavage complex is removed, it leads to 5) chromosomal fragmentation and rapid bacterial cell death. 6) Little is known, how reactive oxygen species are produced by either resolved or unresolved DNA cleavage complexes, but the formation of those, lead to rapid death of bacterial cells, like already discussed in 3.7. (Bush et al., 2020)*

## *3.8 Biological activities of reactive oxygen species*

Reactive oxygen species (ROS) can be generated endogenously in bacteria. When grown aerobically and molecular oxygen is available as an electron acceptor, reduced reactive oxygen species can be formed, such as superoxide anions ($O_2^{\bullet -}$), hydrogen peroxide ($H_2O_2$) and hydroxyl radicals (OH•) by reactions of molecular oxygen with univalent electron donors, like metal centers, such as $Cu^{1+/2+}Fe^{2+/3+}$ in cytochroms of the repsiratory chain, dihydroflavin cofactors ($FADH_2$ cofactors) as well as quinones (Imlay, 2013). Reactive oxygen species are highly reactive and lead to damage of essential cellular components, like DNA, lipids and proteins. To resist harmful oxidants, most organisms, such as *Escherichia coli*, have enzymes like superoxide dismutases, catalases and peroxiredoxins that convert harmful ROS to harmless oxygen. The exposure of proteins to reactive oxygen species leads to covalent modifications that destabilize and inactivate proteins. Having an electron rich sulfur atom in the side chain, the amino acids cysteine and methionine are sensitive to oxidation. However, bacteria like *Escherichia coli* also contain mechanisms to repair these oxidated residues in the

periplasm (Ezraty et al., 2017). For instance, the inner membrane-bound protein MsrQ uses electrons from the quinone pool and in combination with periplasmatic MsrP, a molybdopterin-containing oxidoreductase, reduce methionine residues of proteins that have been oxidized (Brokx et al., 2005; Gennaris et al., 2015). Additionally, proteins of the Dsb family can repair oxidized cysteine residues in periplasmatic proteins, also by use of electrons from the quinone pool (Bader et al., 1999; Bardwell et al., 1991; Depuydt et al., 2009; Dutton et al., 2008; Kadokura and Beckwith, 2009; Shevchik et al., 1994). However, there are also enzymes that require oxidation to be activated. For example, the protein OxyR, a transcriptional activator, becomes activated through Cys oxidation to respond to oxidative stress by activating genes to decrease the harmful effects of oxidative stress (Zheng et al., 1998). There are additional transcriptional factors, that can be regulated by – not just reactive oxygen species – but even the availability or unavailability of oxygen as described in the following chapter. In contrast to $O_2^{\bullet -}$ and $H_2O_2$, which do not directly damage DNA, $OH^{\bullet}$ reacts with almost all organic molecules, including the bases and ribose residues of DNA and RNA. This particularly affects guanine, which is more easily oxidized than the other bases due to its low reduction potential. One of the most common products of guanine oxidation is 8-oxo-guanine (7,8-dihydro-8-oxoguanine), which has a high mutagenic potential due to its capability to form a mismatch with adenine (Foti et al., 2012).

Though it was long thought that the membrane fatty acids of *Escherichia coli* are generally resistant to ROS-induced damage (Imlay, 2003), evidence for oxidative damage to these membrane components was provided: It was shown that *E. coli* lacking the oxidative stress defense regulator OxyR exhibits increased levels of a lipid peroxidation marker when exposed to tert-butyl-hydroperoxide, which induce lipid peroxidation in membranes (Yoon et al., 2002).

## 3.9 *Gene* regulation *by oxygen*

### 3.9.1 FNR

*Escherichia coli* is a facultative anaerobic microorganism, able to grow in aerobic as well as in anaerobic environments. Under anaerobic condition, aerobic respiratory pathways are replaced by anaerobic respiratory or fermentative pathways, depending on which electron acceptors are currently available (Clark, 1989; Spiro and Guest, 1990). During anaerobic

growth, terminal electron acceptors like fumarate, nitrate, nitrite, trimethylamine-N-oxide (TMAO), dimethyl sulfoxide (DMSO) as well as tetrahydrothiophene-1-oxide are used (Stewart, 1988). In the absence of oxygen, the anaerobic pathway needs to be induced, hence a transcriptional activator for the expression of genes encoding enzymes of anaerobic respiratory pathway needs to be activated. One such key transcriptional activator is the fumarate and nitrate reductase regulator (FNR). FNR contains an iron-sulfur-cluster ($[4Fe\text{-}4S]^{2+}$ cluster) and is activated when environmental oxygen is getting scarce. FNR controls the expression of more than 200 genes, upregulating those described above and repressing such genes that are involved in aerobic respiration. When FNR is exposed to oxygen, the iron-sulfur cluster converts from $[4Fe\text{-}4S]^{2+}$ to $[2Fe\text{-}2S]^{2+}$, inactivating the enzyme through monomerization (Mettert and Kiley, 2015).

Molybdoenzymes, proteins, that carry molybdenum cofactors, present a group of enzymes with functions especially involved in anaerobic respiratory pathways as described (3.8). Molybdoenzymes are to some extent regulated by FNR, such as the *fdnG*, *narG*, and *dmsA* gene products, which contain molybdenum-cofactors (Berg and Stewart, 1990; Lamberg and Kiley, 2000). Genes regulated by FNR in response to anerobic respiration or genes regulated by molybdate more specifically ModE, are of great interest for this study. As it will be described in 3.13, the highly quinolone resistant strain *Escherichia coli* MIVb, an in-vitro selected mutant, which resulted from a FQ-promoted selection process, has acquired, alongside with other target and off-target mutations, a mutation in gene *modB*.

## *3.10 Gene regulation by oxidative stress*

### 3.10.1 SoxR and SoxS

Another iron-sulfur cluster protein that controls the regulation of a vast group of genes is SoxR, which utilizes its [2Fe-2S] cluster to respond to and to initiate detoxifying mechanisms against oxidative stress and subsequently activates SoxS. As described earlier, oxidative stress is not induced by molecular oxygen but by reduced oxygen species, such as superoxide anions ($O_2^{\bullet -}$), hydrogen peroxide ($H_2O_2$) and hydroxyl radicals ($OH^{\bullet}$), which are generated by electron transfer to molecular oxygen. Oxidation of [2Fe-2S] of SoxR leads to its activation and redirects the promoter DNA elements to initiate RNAP promoted transcription (Chiang and Schellhorn, 2012; Kobayashi et al., 2014; Mettert and Kiley, 2015). When SoxR senses redox-cycling

compounds as described before in this chapter, SoxS is activated and initiates the transcriptional activation of more than 100 genes, including superoxide dismutases *sodA* (Lu et al., 2003), DNA repair enzymes and efflux pumps *acrAB* (Lu et al., 2003) or their regulators *marA* (Alekshun and Levy, 1999), to name a few (Mettert and Kiley, 2015). Moreover, transcription of other genes activated by SoxR/S include *acnA* and *fur* (Zheng et al., 1999), which encode proteins with FeS-clusters and *nfsA* a member of the *mar*-regulon (Paterson et al., 2002).

### 3.10.2 OxyR

As already described in 3.8, OxyR belongs to the transcriptional regulators that response to the presence of reactive oxygen species, by forming a disulfide bond that alters its capability of binding to DNA. In *Escherichia coli*, the oxidized form of OxyR promotes the transcription of a vast number of genes in response to oxidative stress to minimize damage of proteins, lipids and DNA. These genes include, e.g. *katG*, *fur* and *dsbG*, that hast already been described in 3.8 (Imlay, 2015; Zheng et al., 2001).

## *3.11 Molybdenum and molybdoenzymes*

Molybdoenzymes have bound molybdopterin-cofactors as a functional group (3.11.4) which promote redox reactions, e.g., in the nitrate respiratory pathway and other pathways where electron transport is essential. Molybdenum-cofactor (MoCo) is generated by coupling its biologically active form, molybdate, to either a pterin component of molybdopterin guanine dinucleotide (MGD) or to an iron-sulfur cluster, which is specific for nitrogenases (Iobbi-Nivol and Leimkühler, 2013).

### 3.11.1 Uptake of molybdenum

Molybdenum can be imported by *Escherichia coli* cells as biological active oxyanion molybdate ($MoO_4^{2-}$) by three different transport systems: (1) a low affinity CysPTWA sulfate-thiosulfate permease, (2) a non-specific transport mechanism that also transports sulfate, selenate and selenite and (3) the ModABC system, which has a high affinity to molybdenum (Aguilar-Barajas et al., 2011; Self et al., 2001).

The high affinity transport mechanism by molybdate transport proteins ModABC belongs to the ATP-binding cassette (ABC) superfamily of transporters which is widely distributed in

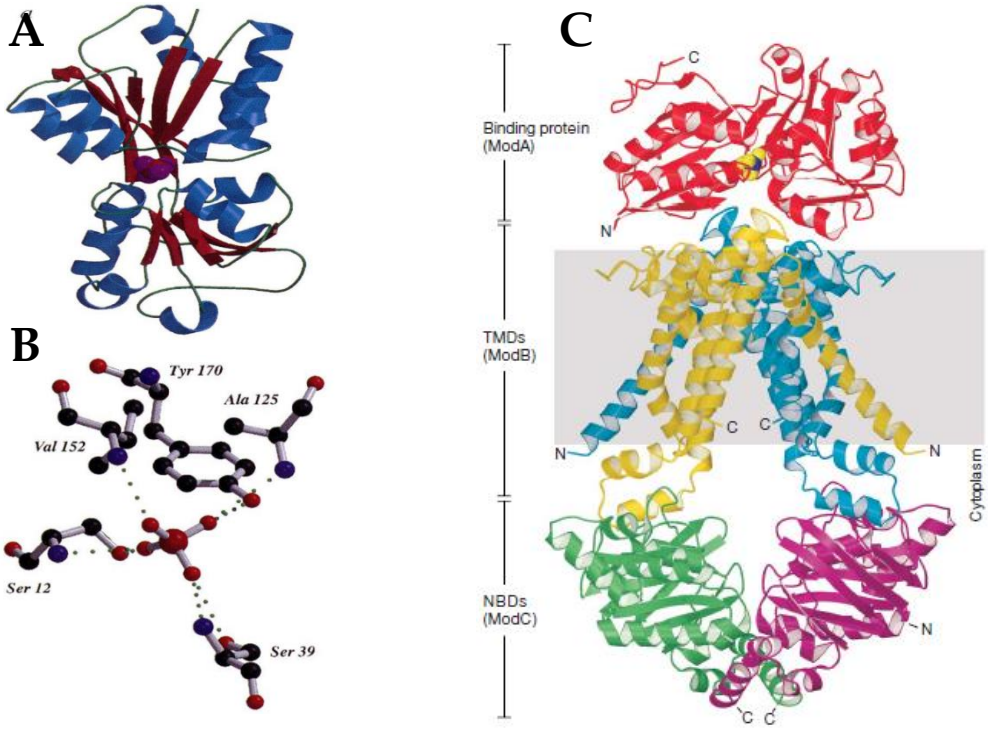


*Figure 6: Figure A shows the crystal structures of Escherichia coli ModA with α-helices shown inblue, β-strands in red and loop regions in green. B, Stereoview of the anion binding site of ModA. C, Crystal structure of ModB₂C₂ and ModA of Archaeglobus fulgidus (Hollenstein et al., 2007; Hu et al., 1997).*

prokaryotes as well as eukaryotes. In *Escherichia coli*, the transporter consists of a transmembrane protein ModB, a cytosolic ATP-binding protein ModC as well as an extracellular molybdate-binding protein, ModA, which bind molybdate and passes it to the integral membrane protein. Although the complete crystal structure of ModABC has been explored in *Archeoglobus fulgidus*, only the structure of ModA has been identified in *Escherichia coli*. Structural models of individual protein ModA or the ternary complex ModABC are shown in Figure 6.

### 3.11.2 Regulation of molybdate influx

In *Escherichia coli*, all three proteins of the ModABC transporter are encoded by the *modABC* operon, whose expression is regulated by ModE. The transcriptional regulator, ModE, , represses the expression of the *modABC* operon in availability of intracellular molybdate at micromolar concentrations (Grunden et al., 1996). ModE consists of an N-terminal helix-turn-helix motif and a C-terminal molybdate binding region. After binding of molybdate, ModE changes its conformational state, resulting in an increased binding affinity to the *modA*

promoter region and therefore represses the transcription of the operon (Zupok et al., 2019). Not only is *modABC* expression dependent on the regulation by ModE, but also a group of other genes being regulated by the ModE-molybdate complex (3.11.3). Upstream of these genes, DNA sequences called Mo-boxes, which consist of AT-rich sequences as part of the consensus sequence ATCGCTATATA-N6/7-TATATAACGAT bind the ModE-molybdate complex resulting in transcriptional activation (Anderson et al., 2000; McNicholas et al., 1997)

### 3.11.3 Genes regulated by molybdate

Many genes regulated by ModE-bound molybdate encode iron-sulfur-cluster proteins, like *hycABCDEFGHI*, constituents of the formate hydrogenlyase complexes and *narGHJI*, that encodes a respiratory nitrate reductase for anaerobic growth (Hasona et al., 1998). Other nitrate reductases are also regulated by ModE (McNicholas and Gunsalus, 2002). Nitrate reductases are enzymes that use nitrate as an electron acceptor during anaerobiosis, analogous to oxygen during aerobiosis (Bonnefoy and Demoss, 1994). Other proteins, that carry a molybdenum-cofactor for electron transfer, like the dimethyl sulfoxide (DMSO)/trimethylamine N-oxide (TMAO) reductase, encoded by the *dmsABC* operon, are also regulated by ModE-boundmolybdate (McNicholas et al., 1998).

Also many enzymes involved in electron transport carry a molybdenum-cofactor, as described in 3.11. The formation of this molybdenum-cofactor is a result of the modification of a guanine-triphosphate (GTP) in four steps with the incorporation of molybdenum as shown in Figure 7. The respective enzymes are regulated by the operons *moaABCDE*, *mobAB, moc, moeAB* and *mog* (Iobbi-Nivol and Leimkühler, 2013), whereas *moaABCDE itself*, like *modABCD*, is regulated by ModE (McNicholas et al., 1997).

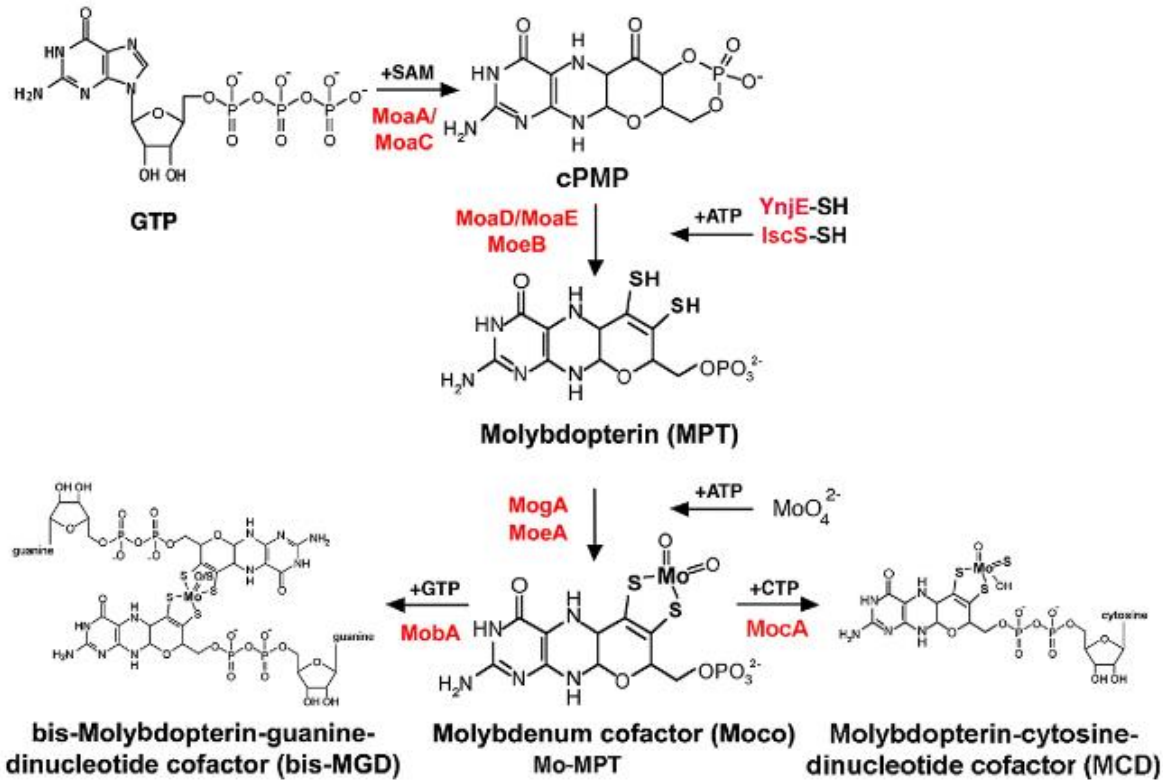


*Figure 7: The biosynthesis of Moco in E. coli and the proteins involved in the individual steps of the pathway. The basic form of the molybdenum cofactor is a 5,6,7,8-tetrahydropyranopterin (MPT) with a unique dithiolene group coordinating the molybdenum atom. (Iobbi-Nivol and Leimkühler, 2013)*

### 3.11.4 Molybdoenzymes in *Escherichia coli*

As described earlier, enzymes that contain molybdenum-cofactors in either one of three different configurations, are enzymes that catalyze reactions of electron transport processes. In general, molybdoenzymes are categorized into three different families in *Escherichia coli*. These are the xanthine oxidase family, sulfide oxidase family and DMSO reductase family.

The family of xanthine oxidases in *Escherichia coli* consist of three enzymes: the Aldehyde oxidoreductase PaoABC, the xanthine dehydrogenases XdhABC and the enzyme XdhD that has not been characterized yet. These enzymes are involved in reactions with water as a source of oxygen with a two-electron transfer hydroxylation and oxo-transfer and typically catalyze the hydroxylation of carbon centers (Hille, 1996; Iobbi-Nivol and Leimkühler, 2013).

Members of the family of sulfide oxidases catalyze the reduction of oxidized sulfur groups of proteins. Among the members of this family is MsrP of the MsrPQ complex, formerly known as YedYZ, that has already been described in 3.8. It reduces oxidized sulfur-containing methionine residues which are generated as a consequence of damage caused by reactive oxygen species to proteins (Ezraty et al., 2017; Iobbi-Nivol and Leimkühler, 2013). Enzymes of

the DMSO reductase family generally catalyze sulfur- or proton transfer reactions, hydroxylation and non-redox reactions. In *Escherichia coli*, this family includes the dissimilatory nitrate reductases, trimethylamine-N-oxide (TMAO) reductases, DMSO reductase and biotin sulfoxide reductases, that all catalyze reactions in the absence of oxygen (Iobbi-Nivol and Leimkühler, 2013; Magalon et al., 2011). Most of these enzymes are located in the periplasm and are membrane-bound. The transfer of these proteins to the periplasm is promoted by the twin-arginine-translocation (Tat) pathway, facilitated by an N-terminal signal peptide, harboring a consensus motif with arginine residues within the amino acid sequence motif (S/T)-R-R-x-F-L-K (Berks, 1996). In *Escherichia coli*, this sequence motif has been identified in the DMSO reductase DmsA, the formate dehydrogenases FdnG and FdoG, the periplasmatic nitrate reductase and its electron donor protein NapA and NapG as well as the TMAO reductase TorA (Berks et al., 2005).

As indicated in this chapter, molybdoenzymes catalyze reactions predominantly in the periplasm, catalyze redox reaction in response to harmful ROS reagents, that occur under aerobic conditions or enable dissimilatory pathways in the absence of oxygen by the DMSO reductase family during anaerobiosis.

### *3.12 RNA Polymerase*

By using ribonucleotides (rNTPs) as a substrate and DNA as a template, within *Escherichia coli*, the RNA polymerase (RNAP) enables the synthesis of ribonucleic acid (RNA). It consists of four subunits, $\alpha$, β, β′ and ω with different functions in the complex. The $\alpha$-subunit, encoded by the gene *rpoA*, is a 36.5 kilodalton (kDa) subunit, catalyzes the assembly of the RNAP holoenzyme and interacts with transcription factors. The β-subunit, encoded by *rpoB*, is 150.4 kDa in size and promotes the binding of DNA, RNA, nucleoside triphosphates (NTPs), the synthesis of the RNA, and is also the binding site for sigma-factors (σ factors), described in detail in the following paragraph. Subunit β′, encoded by the gene *rpoC*, is 155.0 kDa in size, and, thus, is the largest subunit of the RNAP. It shares some similarity with the β-subunit, binds DNA as well as σ factors, promotes RNA synthesis and contains the active site of the enzyme. This site is formed by two double-ψ-β-barrel (DPBB) domains, one provided by the β-subunit, the other by the β′-subunit, however, the DPBB of the β′-subunit contains an aspartic acid triade -DFDGD-, to coordinate catalytic $Mg^{2+}$- ions for the nucleotidyl transfer

reaction. The ω-subunit is encoded by *rpoZ*. Although its biological function has only minimally been studied, the ω-subunit was proposed to promote RNA folding, since an *Escherichia coli ΔrpoZ* strain was copurified with a protein chaperone (Basu et al., 2014; Mukherjee et al., 1999; Sutherland and Murakami, 2018).

It has been shown that the β-subunit of the RNAP plays a critical role as target for antibiotics. Rifampicin, an antibiotic used for the treatment of tuberculosis, binds in the center of the RNA extension pathway within the β-subunit and blocks the elongation of the nascent RNA transcript. Resistance against Rifampicin emerges by mutations within *rpoB*, especially those affecting amino acid residues 507 to 533 (Sutherland and Murakami, 2018).

For this work, however, the β'-subunit, encoded by *rpoC* is of higher interest: As described in 3.13, the highly fluoroquinolone-resistant mutant *Escherichia coli* MIVb, isolated in a FQ-promoted stepwise selection process, harbors, alongside with other target and off-target resistance mutations, two mutations in *rpoC*.

## *3.13 Escherichia coli MIVb*

To generate highly FQ-resistant mutants of *Escherichia coli*, a wild-type strain has been isolated from a patient with a history of no known antibiotic use and stepwise selected on increasing concentrations of nalidixic acid and ciprofloxacin (Heisig and Tschorny, 1994) resulting in the isolation of five consecutive mutants of *Escherichia coli* WT using increasing concentrations of quinolones: *Escherichia coli* MI, MII, MIII and MIVa and MIVb. During this process, the *Escherichia coli* parent strain WT, had acquired different target and off-target mutations known to be associated with fluoroquinolone resistance. As described in 3.4, target mutations affect genes that encode subunits of either bacterial gyrase, *gyrA* and *gyrB,* or topoisomerase IV, *parC* and *parE*, respectively. In addition, a non-target FQ-resistance mutation in gene *marR* encoding a repressor of the *mar* operon was identified. Together with the MarA transcriptional activator the AcrAB-TolC efflux system as well as many other genes of the mar regulon are overexpressed (Ruiz and Levy, 2010). In stage IV of this selection process, two different high-level FQ-resistant mutants have been isolated: MIVa and MIVb. Both contain as off-target mutation not known to be associated with FQ-resistance one *rpoC* mutation already detected in their common parent mutant MIII. In addition, *Escherichia coli* MIVa harbors a in *clpA* mutation and a *yccJ*, regulated by CsgD, which is a transcriptional regulator of biofilm

formation (Brombacher et al., 2003). *Escherichia coli* MIVb has a second *rpoC* mutation (3.12) and a mutation in *modB*, encoding the transmembrane unit of the ModABC transporter for molybdate (3.11.1).

In summary, compared to its genuine progenitor strain *Escherichia coli* WT, MIVb carries mutational alterations within the following enzymes:

*Table 2: Mutations in Escherichia coli MIVb*

| ***Enzyme*** | **GyrA** | **ParC** | **MarR** | **RpoC** | **YccJ** | **ModB** |
|---|---|---|---|---|---|---|
| *Position* | S83L, D87G | S80I | H120fs X178 | P246Q, ::A1227 | A6E | L106M |

However, only the mutation P246Q in RpoC and L106M in ModB are the mutations by which *Escherichia coli* MIVb differs from its direct progenitor, *Escherichia coli* MIII. Notably, *E. coli* MIVb posseses a CIP MIC of 256 μg/ml and *E. coli* MIII 64 μg/ml.

# 4. Aim of this work

As mentioned above, two mutations were detected in *Escherichia coli* mutant MIVb, that separates it from its direct progenitor, *E. coli* MIII – A C to A substitution within the gene *modB* at position 316 as well as a C to A substitution within *rpoC* at position 737. Both mutations occurred during selection at the highest possible minimum inhibitory concentrations (MIC) of FQ ciprofloxacin. These mutations lead to amino acids exchanges in the proteins ModB (leucin is replaced with a methionine at position 106) and RpoC (proline replaced with glutamine at position 246).

In a previous work, it was observed, that the combination of *rpoC* C737A together with a deletion at position 1227 in *rpoC*, leads to a significant higher MIC of fluoroquinolones as well as an altered temperature sensitivity (D. Rönfeldt, unpublished).

The mutation within *modB* has not yet been described in the literature. Since *modB* encodes the transmembrane unit of the ModABC transport system, which is associated with molybdate influx, we hypothesized that mutations within this gene might lead to altered influx of this trace ion. To investigate the impact of the ModB-L106M mutation on the molybdate influx in a genetic wildtype background, the *modB* C316A mutation was introduced into *E. coli* WT, lacking any other mutation that emerged during the FQ-selection process.

We have further hypothesized that the combination of mutations in *modB* and *rpoC* might result in a combined effect. Thus, to investigate a potential synergistic effect, *modB* C316A as well as *rpoC* C737A were both introduced into *E. coli* WT.

As a control it was investigated whether additional mutations in MIVb, i.e. *modB* C316A and *rpoC* C737A, which have already been identified in MIVb immediate progenitor mutant MIII, were separately introduced into *Escherichia coli* MIII.

When *modB* C316A was introduced into *E. coli* strains, a molybdate influx measurement system was subsequently introduced into the strains to determine ModB-L106M associated molybdate uptake.

After molybdate levels were assessed in the *E. coli* mutants, expression levels of molybdate-regulated genes were determined with quantitative realtime-PCR (qRT-PCR). As explained in 3.11.3, molybdate in combination with the transcriptional activator ModE, promotes the expression of many genes involved in respiratory pathways.

Simultaneous investigation of the transcriptome of *Escherichia coli* MIII and MIVb (A. Heisig, personal communication) addressed additional genes of interest, that have also been included in this work. These observations highlighted the role of *rpoC* on gene regulation for ROS detoxification, that was further assessed with qRT-PCR in this work.

In a final step, the roles of mutations in *Escherichia coli* MIVb in response to fitness restoration were determined. For this investigation, *Escherichia coli* MIVb was grown in antibiotic-free LB broth and was incubated for a maximum of 300 generations. Subsequent sequencing of the genome showed mutations that conferred to fitness restoration in this process.

# 5. Materials

## 5.1 Chemicals

| *Chemicals* | *Source* |
|---|---|
| *2 x RNA Loading dye* | Thermo Scientific |
| *6 x DNA Loading dye* | Thermo Scientific |
| *Agarose peqGold universal* | Peqlab |
| *Ammonium chloride ($NH_4Cl$)* | Merck |
| *Ampicillin-Na-salt* | Sigma |
| *Anhydrotetracycline* | Chemodex AG |
| *Calcium chloride-dihydrate* | Merck |
| *Casein hydrolysate (acid)* | Oxoid |
| *Chloramphenicol* | Acros Organics |
| *Ciprofloxacin-HCl* | Bayer |
| *D-Glucose-Monohydrate* | Roth |
| *Dimethyl sulfoxide (DMSO)* | Merck |
| *Disodium phosphate heptahydrate ($Na_2HPO_4 \cdot 7H_2O$)* | Roth |
| *Dodecylsulfate-Na-salt in pellets (SDS)* | Serva |
| *Ethanol abs.* | VWR |
| *Ethidium bromide (EtBr)* | Qiagen |
| *Ethylenediaminetetraacetate (EDTA)* | Roth |
| *Glacial acetic acid* | VWR |
| *Glycerol* | Fluka |
| *Hydrogen Chloride (37%)* | Grüssing |
| *L-Arabinose* | Fluka |
| *Magnesium sulfate Heptahydrate ($MgSO_4 \cdot 7H_2O$)* | Roth |
| *Methyl viologen dichloride hydrate* | Sigma |
| *Monopotassium phosphate ($KH_2PO_4$)* | Roth |
| *Na-molybdate-dihydrate* | Merck |
| *Nucleoside triphosphates (dNTPs)* | Roche |
| *Potassium actetate* | Merck |
| *Potassium chloride* | Merck |
| *PyroMark annealing buffer* | Qiagen |
| *PyroMark binding buffer* | Qiagen |

| | |
|---|---|
| *RNA Protect* | Qiagen |
| *Sodium chloride (NaCl)* | Roth |
| *Sodium hydroxide (NaOH)* | Roth |
| *Spectinomycin-sulfate* | Roth |
| *Straptavidin-sepharose* | Cytiva Sweden |
| *Thiamine-HCl* | Sigma |
| *TRIS, buffer grade* | Roth |
| *Tryptone/Peptone from casein* | Roth |
| *Yeast Extract* | Merck |

## 5.2 Buffers

| *Buffers* | *Components* |
|---|---|
| *GTE Buffer* | 50 µl 1 M D-glucose-monohydrate, 25 µl 1 M TRIS, 20 µl 0.5 M ethylenediaminetetraacetate , 20 µl RNAse A (10µg/µl), ad 1 ml $H_2O$ |
| *Lysis buffer for alkaline lysis* | 200 µl 1 M sodium hydroxide, 100 µl sodium dodecylsulfate (10% w/v), ad 1 ml H2O |
| *Neutralizing buffer* | 60 ml 5 M potassium acetate, 11.5 ml glacial acetic acid, ad 100 ml H2O |
| *PSQ washing buffer* | 10 mM TRIS, pH = 7.6, adjusted with glacial acetic acid |
| *TAE buffer (50 x)* | 2 M TRIS, 50 mM ethylenediaminetetraacetate, pH = 8, adjusted with glacial acetic acid |

## 5.3 Enzymes

| *Enzymes* | *Source* |
|---|---|
| *Dpn1 FastDigest* | Thermo Scientific |
| *EcoRI FastDigest* | Thermo Scientific |
| *Lysozyme* | Roth |
| *Q5 Polymerase* | New England Biolabs |
| *RNAse A* | AppliChem |
| *Taq-Polymerase* | Thermo Scientific |
| *T4 DNA Ligase* | Thermo Scientific |

## 5.4 Growth media

| *Medium* | *Composition* | *Source* |
|---|---|---|
| *LB Agar (Luria/Miller)* | 10 g/l tryptone, 5 g/l yeast extract, 10 g/l sodium chloride, 15 g/l agar-agar, pH = 7 | Roth |
| *LB Broth* | 10 g/l tryptone, 5 g/l yeast extract, 10 g/l sodium chloride, pH = 7 | Roth |
| *M9 caso amino acids broth* | 5 g casein hydrolysate (acid), 6 g disodium phosphate heptahydrate, 3 g monopotassium phosphate, 0.5 g sodium chloride, 1 g ammonium chloride, ad 1 L $H_2O$. Adjust pH to 7. Autoclave at 121 °C for 15 minutes, then add:<br>1 ml of 1 M magnesium sulfate heptahydrate, 10 ml D-glucose-monohydrate (20% w/v), 1 ml of 1 mg/ml thiamine-HCl, 1 ml of 0.1 M calcium chloride, all components sterilized | Own preparation |
| *Müller-Hinton Broth* | 2 g/l beef infusion, 17.5 g/l casein peptone (acidic hydrolysate), 1.5 g/l corn starch, pH = 7.4 | Roth |
| *SOB* | 20 g/l tryptone, 0.58g/l sodium chloride, 0.18 g/l potassium chloride, 0.95 g/l magnesium chloride, 2.47 g/l magnesium sulfate, 5 g/l yeast extract, ad 1 l H2O, autoclave for 15 minutes at 121 °C | Own preparation |
| *SOC* | 20 g/l tryptone, 0.58g/l sodium chloride, 0.18 g/l potassium chloride, 0.95 g/l magnesium chloride, 2.47 g/l magnesium sulfate, 5 g/l yeast extract, ad 1 L $H_2O$, autoclave for 15 minutes at 121 °C | Own preparation |
| *Standard Nutrient Broth I* | 15 g/l peptone, 3 g/l yeast extract, 6 g/l sodium chloride, 1 g/l glucose, pH = 7.5 | Roth |

## 5.5 Supplies

| *Supplies* | *Source* |
|---|---|
| *96 plate black Thermo Nunclon Delta Surface* | Thermo Scientific |
| Biometra® T Gradient | Analytik Jena |
| Biometra® T personal | Analytik Jena |
| Biometra® T3 | Analytik Jena |
| *Biosphere Filter Tips* | Sarstedt |
| *Butylrubber seals* | Glasgerätebau Ochs |
| *Cary ® 50 UV-Vis Spectrophotometer* | Varian |
| *Centrifuge 5804R* | Eppendorf |
| *CryoPure tubes* | Sarstedt |
| *Cuvettes, 1.5 ml semi-micro disposable* | Brand |
| *Electrophoresis chambers* | Peqlab |
| *Electroporation cuvettes, 1 mm gap* | Peqlab |
| *Electroporation unit Pulse Controller II and Gene Pulser II* | Bio-Rad |

| | |
|---|---|
| *Emission filter 485 nm* | Berthold Technologies |
| *Emission filter 535 nm* | Berthold Technologies |
| *Erlenmeyer flasks* | Schott |
| *Excitation filter 430 nm* | Berthold Technologies |
| *Geldoc UVP Solo* | Analytik Jena |
| *Heating Block MB-102* | Biozym |
| *Heating-Block* | Heidolph Instruments |
| *Herasafe Cleanbench* | Heraeus |
| *Hungate flasks 120 ml* | Glasgerätebau Ochs |
| *Hungate tubes 12 ml* | Glasgerätebau Ochs |
| *Incubators* | Heraeus |
| *Injekt-F needles for syringes* | B. Braun |
| *MikroWin 2000* | Berthold Technologies |
| *Minisart filter units* | Sartorius |
| *Mithas LB 960* | Berthold Technologies |
| *NanoDrop 2000* | Thermo Scientific |
| *NanoDrop 2000 Software* | Thermo Scientific |
| *OCelloScope* | BioSense Solutions |
| *PCR Cycler TAdvanced* | Analytik Jena |
| *Petri dishes* | Sarstedt |
| *Plate seals for 96-well plates* | Sarstedt |
| *PSQ 96 MA Pyrosequencing system* | Biotage |
| *PSQ 96 plate low* | Biotage |
| *QuantStudio Software* | Thermo Scientific |
| *RNA PCR Cycler Peqlab primus advanced* | VWR |
| *Rotary shaker I: Incubating Oribital Shaker* | VWR |
| *Rotary shaker II: Certomat R+H* | B. Braun Biotech |
| *Safe Seal Tubes (1.5 ml)* | Sarstedt |
| *Simple Reads software for Cary ® 50 UV-Vis Spectrophotometer* | Varian |
| *TC Plate 96* | Sarstedt |
| *Thermo Nunclon 96, Thermo Scientific for OCelloScope measurements* | Thermo Scientific |
| *Tubes, 15 ml and 50 ml* | Sarstedt |

| | |
|---|---|
| *UniExplorer software for OCelloScope measurements* | BioSense Solutions |
| *ViiA 7 Real-Time PCR System* | Thermo Scientific |
| *VisionWorks software for Geldoc UVP Solo* | Analytik Jena |
| *Vortex Genie 2* | Scientific Ind. |

## 5.6 Kits

| *Kit* | *Company* |
|---|---|
| *Luna Universal qPCR Mastermix* | New England Biolabs |
| *GeneJet* | Thermo Scientific |
| *Monarch Plasmid Mini Prep* | New England Biolabs |
| *InnuPrep Pure PCR Kit* | Analytik Jena |
| *Monarch Total RNA Miniprep Kit* | New England Biolabs |
| *Monarch RNA Cleanup Kit* | New England Biolabs |
| *LunaScript RT Supermix* | New England Biolabs |
| *Pyromark Gold 96 Q96 Reagents PSQ Enzymes* | Qiagen |

## 5.7 Bacterial strains

| *Bacterial strain* | *Genotype* | *Source* |
|---|---|---|
| *E. coli BW25113* | $F^-$ DE(araD-araB)567 lacZ4787(del)::rrnB-3 $LAM^-$ rph-1 DE(rhaD-rhaB)568 hsdR514 | (Baba et al., 2006) |
| *E. coli DH5a* | $F^-$ Φ80*lac*ZΔM15 Δ(*lac*ZYA-*arg*F) U169 *rec*A1 *end*A1 *hsd*R17($r_K^-$, $m_K^+$) *pho*A *sup*E44 *thi*-1 *gyr*A96 *rel*A1 $\lambda^-$ | Thermo Scientific |
| *E. coli JM09* | *endA1, recA1, gyrA96, thi, hsdR17 (rk -, mk+), relA1, supE44, Δ(lac-proAB), [F´ traD36, proAB, laqIqZΔM15]* | Promega |
| *E. coli JW0747-1* | F-, *Δ(araD-araB)567*, *ΔlacZ4787*(::rrnB-3), *ΔmodB736::kan*, $\lambda^-$, *rph-1*, *Δ(rhaD-rhaB)568*, *hsdR514* | (Baba et al., 2006) |
| *E. coli MIII* | *$gyrA^-$, $parC^-$, ΔmarR, rpoC(3682::ctg), $yccJ^-$* | (Heisig and Tschorny, 1994) |
| *E. coli MIII/ModB-L106M* | *$gyrA^-$, $parC^-$, ΔmarR, rpoC(3682::ctg), $yccJ^-$, $modB^-$ (316C>A)* | This work |
| *E. coli MIII/RpoC-P246Q* | *$gyrA^-$, $parC^-$, ΔmarR, $rpoC^-$ (737C>A), rpoC(3682::ctg), $yccJ^-$,* | D. Rönfeldt |
| *E. coli MIVb* | *$gyrA^-$, $parC^-$, ΔmarR, $rpoC^-$ (737C>A), rpoC(3682::ctg), $yccJ^-$, $modB^-$* | (Heisig and Tschorny, 1994) |
| *E. coli WT* | *$gyrA^+$, $parC^+$, $marR^+$, $rpoC^+$, $yccJ^+$, $modB^+$* | (Heisig and Tschorny, 1994) |
| *E. coli WT/ModB-L106M* | *$gyrA^+$, $parC^+$, $marR^+$, $rpoC^+$, $yccJ^+$, $modB^-$ (361C>A)* | This work |

| | | |
|---|---|---|
| *E. coli WT/ModB-L106M/RpoC-P246Q* | *gyrA*$^{+}$, *parC*$^{+}$, *marR*$^{+}$, *rpoC*$^{-}$ *(737C>A), yccJ*$^{+}$, *modB*$^{-}$ *(361C>A),* | This work |
| *E. coli WT/RpoC-P246Q* | *gyrA*$^{+}$, *parC*$^{+}$, *marR*$^{+}$, *rpoC*$^{-}$ *(737C>A), yccJ*$^{+}$, *modB*$^{+}$ | D. Rönfeldt |

## 5.8 Oligonucleotides

| *Oligonucleotide* | *Base pairs* | *Sequence (5'-3')* |
|---|---|---|
| *acnA_3_2399_EcoWT_RT* | 20 | CGTTCAAACGATTCGGCAAT |
| *acnA_5_2300_EcoWT_RT* | 20 | TTGCCGGGAAAGAGTATGGA |
| *acrA_3_954_EcoWT_RT* | 17 | ACGCGGCGTACGGGTTA |
| *acrA_5_855_EcoWT_RT* | 20 | CACTCTGCTGCCGGGTATGT |
| *arcA_3_599_EcoWT_RT* | 19 | GTACGGTCGTGCGGTTTCA |
| *arcA_5_500_EcoWT_RT* | 19 | GCGCCATGCTTCACTTCTG |
| *arcB_3_2151_EcoWT_RT* | 20 | ATGCCCTTCCTCAACAATGC |
| *arcB_5_2052_EcoWT_RT* | 20 | CGGGTTAGCGGTGTTTGAGA |
| *CRISPR_[modB_375rv_EscCol_noSCAR]* | 82 | ATCAACACCTTCCAGCGCCAGACG AATTGCCCGCACCATCATCGGAAA AGACATGACAGCGGCAGCGAGAA CCGCACCGCGC |
| *CRISPR_[rpoC_C737A_noSCAR]* | 80 | ACGACCACCATCCAGCGGAA CCAGCGGACGCAGATCTGGC TGCAGTACCGGCAGAACGGT CAGGATCATCCACTCTGGTT |
| *deoA_3_1238_EcoWT_RT* | 20 | GCTTCCTGCCAGCTGTTTTC |
| *deoA_5_1139_EcoWT_RT* | 21 | GCGTCGGCTTTACTGATATGG |
| *dmsA_3_444_EcoWT_RT* | 22 | CAGCGCCTGTGAATAGATCTCA |
| *dmsA_5_380_EcoWT_RT* | 20 | AAGATCCGCAGGCTAATCCA |
| *fdhF_3_240_EcoWT_RT* | 22 | CCAGGAAACAGGTTCGAGTTTG |
| *fdhF_5_141_EcoWT_RT* | 21 | TGGCTGGGACTTCATTAACGA |
| *fdnG_3_636_EcoWT_RT* | 20 | CGTTTGCGAGTTTGCATCAC |
| *fdnG_5_295_EcoWT_RT* | 18 | GGTGTCGCGCGTAAAGGT |
| *fur_3_194_EcoWT_RT* | 21 | GCGTCGTCAAACTGGTTCAGT |
| *fur_5_95_EcoWT_RT* | 21 | ATCACGTCAGTGCGGAAGATT |
| *hcr_3_877_EcoWT_RT* | 23 | TCACCGTATATTCACCGGAAATC |
| *hcr_5_778_EcoWT_RT* | 20 | GAGGCGCTGGAAAGCAATAA |
| *hycE_3_991_EcoWT_RT* | 21 | TACTGAAGTCGCGAGCGATTT |
| *hycE_5_892_EcoWT_RT* | 20 | GTGCAGGAGCTGGTGGATGT |
| *katG_3_2029_EcoWT_RT* | 24 | CTGTGTATTTCACTTCGCCAGTTT |

| | | |
|---|---|---|
| *katG_5_1930_EcoWT_RT* | 24 | GTGAACTTGCTGGATATGCGTTAC |
| *marA_3_216_EcoWT_RT* | 21 | CGATTCACCCTGCATATTGGT |
| *marA_5_117_EcoWT_RT* | 21 | ATATGGCTTCGAGTCCCAACA |
| *mlaE_3_468_EcoWT_RT* | 25 | GTAATGAAATAACTCCAGCCCAGAA |
| *mlaE_5_367_EcoWT_RT* | 20 | ATGCGCGCTACAGAGCAACT |
| *moaA_3_826_EcoWT_RT* | 21 | CACCAAACAGGCAGAGATGGA |
| *moaA_5_727_EcoWT_RT* | 20 | GCCGGAGAGATTGGCCTTAT |
| *modB_315rv_ARMS_MIVb_CAT* | 18 | AATTGCCCGCACCATCAT |
| *modB_315rv_ARMS_MIVb_CCT* | 18 | AATTGCCCGCACCATCCT |
| *modB_315rv_ARMS_MIVb_CTT* | 18 | AATTGCCCGCACCATCTT |
| *modB_467rv_EscCol* | 20 | CACCGAGCGAACGAGCGAAT |
| *modB_9fw_EscCol* | 20 | ACCGATCCAGAATGGCAGGC |
| *msrQ_3_300_EcoWT_RT* | 22 | CAACTCCAGCAATGCGTAACTG |
| *msrQ_5_229_EcoWT_RT* | 19 | CGCCGCCTGTTAGGCTTAT |
| *napA_3_622_EcoWT_RT* | 19 | CGTCAGCCTGCTCGATGTC |
| *napA_5_523_EcoWT_RT* | 19 | AACGCGCGTCACTGTATGG |
| *narL_3_297_EcoWT_RT* | 20 | CAGTGCGGTGACCACATCTT |
| *narL_5_198_EcoWT_RT* | 20 | CGGTCTGGAAACGCTGGATA |
| *narV_3_485_EcoWT_RT* | 21 | CCCACCAGCTTCATCATTTCA |
| *narV_5_420_EcoWT_RT* | 22 | TGGGTTAACCACCATTCCTTTT |
| *nfsA_3_425_EcoWT_RT* | 20 | AGTTCCGTCACCGCTTCAAT |
| *nfsA_5_326_EcoWT_RT* | 19 | CAATGATGGCGCAGAATGC |
| *norV_3_609_EcoWT_RT* | 20 | GCTGAACGGCGTCAGGATAT |
| *norV_5_510_EcoWT_RT* | 21 | GCACTACTGCGACGAGCATCT |
| *nrfA_3_785_EcoWT_RT* | 20 | GCTTTCAGCATTGGCGTTTT |
| *nrfA_5_686_EcoWT_RT* | 20 | GGGATGACGGCATGAAAGTC |
| *oppA_3_839_EcoWT_RT* | 21 | CCACTACGGTAGCGGTTGACA |
| *oppA_5_740_EcoWT_RT* | 19 | GCAGCCCGACCTACTGGAA |
| *oxyR_3_690_EcoWT_RT* | 20 | CATGTTGCGCAGAGTTTCCA |
| *oxyR_5_591_EcoWT_RT* | 19 | TCACTGTTTGCGCGATCAG |
| *pKDsgRNA_3_5546_Biotin_PsQ* | 20 | TTCGCTAAGGATGATTTCTGGA |
| *pKDsgRNA_5_5255* | 22 | TTCGCTAAGGATGATTTCTGGA |
| *pKDsgRNA_5_5316_PSQ_Seq* | 20 | GTGATAGAGATACTGAGCAC |
| *pKDsgRNA_modB_5_5336_no2* | 43 | TGTCATGTCTTTTCCGCTGAGT TTTAGAGCTAGAAATAGCAAG |
| *PtetR_pKDsgRNA_3_5335* | 43 | CGAATTGCCCGCACCATCAGG TTTTAGAGCTAGAAATAGCAAG |
| *rpoC_3_1138_Eco_WT* | 24 | GAACCAGCGGACGCAGATCTGGTT |

| | | |
|---|---|---|
| *rpoC_3_760M_ARMS_wMM_EcoMIVb* | 24 | GAACCAGCGGACGCAGATCTGGTT |
| *rpoC_5_-91_Eco* | 24 | GAACCAGCGGACGCAGATCTGGTT |
| *sdhA_3_1136_EcoWT_RT* | 21 | ACCACATCTTCGCCTTTCTCA |
| *sdhA_5_1037_EcoWT_RT* | 21 | CGATTCCGGTAATTCCAACCT |
| *sodA_3_596_EcoWT_RT* | 20 | GCTGCTTCGTCCCAGTTCAC |
| *sodA_5_497_EcoWT_RT* | 20 | GCCTGGATGTGTGGGAACAT |
| *soxS_3_240_EcoWT_RT* | 22 | CAGGTCCATTGCGATATCAAAA |
| *soxS_5_182_EcoWT_RT* | 16 | TGGCCGCCGTTGAGTT |
| *torA_3_303_EcoWT_RT* | 18 | TGCCCCTTCGTGAATTCG |
| *torA_5_224_EcoWT_RT* | 20 | ACGTTCGTGGTCAGGTGTTG |
| *ynfG_3_367_EcoWT_RT* | 20 | TGTGCCCTTTTTCAGCATTG |
| *ynfG_5_304_EcoWT_RT* | 18 | TGCCGCTACTGCCACATG |

## *5.9 Plasmids*

| *Plasmids* | *Source* |
|---|---|
| *pBlueScript II SK (+)* | (Nakanishi et al., 2013) |
| *pCas9cr4/pCas9-CR4* | Addgene |
| *pKDsgRNA-ack* | Addgene |
| *pKDsgRNA-modB* | This work |
| *pKDsgRNA-rpoC737* | D. Rönfeldt |
| *pYN627 MolyProbe* | (Nakanishi et al., 2013) |

# 6. Methods

## *6.1 Storage und cultivation of bacterial strains*

For the long-term storage of selected strains, inoculated bacteria were cryo-conserved at minus 80 °C. For this, 10-30 customary plastic pearls, standard-1-boullion with 87% glycerol in a 1:1 ratio in 1 ml were autoclaved at 121 °C and 2 bar for 20 minutes. 100 µl of a 3 ml LB-bouillon overnight culture, that was inoculated under sterile conditions (HERAsafe® cleanbench, Heraeus Instruments) with a single colony from a bacterial strain, were added to 1 ml of the cryo tube, incubated for 1 h at room temperature. Subsequently, the bacteria-bouillon mixture was discarded by pipetting and the leftover pearls were stored in the cryo tube at -80 °C.

When plating cryo conserved strains on agar plates, one pearl inside the tube was plated on the agar plate (usually LB agar plates), under sterile conditions, and an aseptic technique while

streaking for isolated colonies was performed by using a heat-sterilized loop. Usually, the strains were incubated at 37° C and overnight (about 16 hours). This, however, can differ among the strains, since some plasmids are heat-sensitive and/or have a drastically altered growth speed and need more time to show visible colonies on the agar plate. Incubated agar plates were stored at 4 – 7 °C to a maximum of 4 weeks.

Overnight cultures were prepared by taking one peal from a cryo tube with a heat-sterilized loop or by transferring a single colony from a previously incubated agar plate with a sterile glas rod and placing it into 3 ml of autoclaved LB-bouillon. The inoculated bouillon was usually incubated at 37 °C and 130 rpm in a rotary shaker. Also, this could differ among bacterial strains. Heat-sensitive plasmids inside the bacteria required incubation at 30° C. There are also strains that formed inhomogeneous cell suspensions, when shaking at 130 rpm, so the speed had to be reduced to 80 rpm.

## *6.2 Serial dilution of cell suspensions*

When it is not clear, how many cells are inside a cell suspension, a serial dilution of the cell suspension in either saline or physiological sodium chloride solution can be performed. Usually, this procedure is used, when cell count is performed afterwards. But serial dilution can also be performed when the bacterial suspension of an overnight culture harbors too many cells and this amount needs to be reduced. This procedure is required, e.g. for determining the growth rates via OCelloScope, as described in 6.13, where a starting culture is needed that does not exceed $1x10^6$ cells or in the measurement of the minimum inhibitory concentration (MIC), as described in 6.4, where the cells of the overnight culture should also must not exceed this value.

A serial dilution, regardless of if it is done in saline, sodium chloride solution or in a nutrition medium, is performed by taking a tenth of the output solution and transfer it to a new solution that has 90% of the volume, consequently adding a tenth of the output solution would result in having 100% volume of a new solution. This new solution, then, consists of 10% output material, resulting in a 1:10 dilution. This process can be extended deliberately, for the count of viable cells, as described in the next chapter, cells are usually diluted in autoclaved, physiological sodium suspensions, with total volumes of 4.5 ml in glass test tubes. In this case, 500 µl (a tenth of 5 ml) of a cell suspension are transferred in 4.5 ml of 0.9% NaCl, vortexed,

resulting in a $10^{-1}$ (or 1:10) dilution and subsequently, 500 µl of that solution is transferred into a new tube with 4.5 ml 0.9% NaCl solution, resulting in a $10^{-2}$ (or 1:100) dilution. As described above, this process can be extended deliberately and in the case of cell counting, usually is extended to a $10^{-7}$ dilution (or 1:10,000,000).

## *6.3 Colony forming units*

The colony forming units (CFU) determines, how many viable cells are inside a cell suspension and excludes the count of unviable or dead cells. This process is performed, when a cell suspension is diluted in 1:10 ratios over several steps (in this case 7 times from $10^{-1}$ to $10^{-7}$) in an autoclaved, physiological sodium chloride solution. Then, 50 µl of each dilution step from $10^{-4}$, $10^{-5}$, $10^{-6}$ and $10^{-7}$ is plated on a LB Agar plate, if necessary, supplemented with antibiotics. By using a sterile glass rod, the cell suspension is dispensed homogenously over the plate. The agar plate is then incubated at 37 °C and overnight (about 16 h), depending on the bacterial strain. As soon as colonies are visible, the number of cells in the output solution can be calculated by using the following formula:

$$CFU\ per\ milliliter = \frac{Amount\ of\ colonies}{Plated\ volume\ (50\ ml)\ x\ serial\ dilution}$$

## *6.4 Minimum inhibitory concentrations*

The minimum inhibitory concentration (MIC) defines to lowest concentration of an antimicrobial agent that hinders visible bacterial growth. The procedure in this work was the microdilution method, where a cell suspension was taken from an overnight culture, diluted 1:1000 in Müller-Hinton bouillon and 50 µl were transferred to the wells of a 96-well plate (TC Plate 96 Well, Suspension, R, SARSTEDT AG & Co. KG), that contained 50 µl of twice the respective MIC. In all cases MICs were tested with three biological samples with at least two determinations. For each plate, the used medium was tested to rule out contaminants by adding 50 µl of not inoculated medium in the wells. The plate was subsequently sealed and incubated at 37 °C and overnight (about 16 hours) in an incubator. After that, the lowest concentration of the tested agent was determined by the absence of visible cell sediments in the wells.

## 6.5 *Alkaline lysis*

The principle of alkaline lysis is based on the different capacity of renaturating chromosomal and plasmid DNA and is used to extract plasmid DNA from bacteria. The method was first described in 1979 by Birnboim and Doly (Birnboim and Doly, 1979). To isolate plasmid DNA, 3 ml of an overnight culture are centrifugated for 3 min at 5,000 rpm. The supernatant is then discarded and to the leftover cell pellet was added 100 µl ice-cooled GTE buffer and resuspended subsequently. The glucose and TRIS in the buffer lead to stabilized osmolarity and pH value, which prevents an early-stage cell death. The chelator EDTA and its binding to $Mg^{2+}$ and $Ca^{2+}$ ions destabilize the bacterial cell wall. GTE buffer contains RNAse A, so that in the case of nucleic acid release, RNA will be degraded. Then, the mixture is added 200 µl of lysis buffer and inverted immediately until the mixture is homogenous. Sodium dodecylsulfate (SDS) and sodium hydroxide (NaOH) in the lysis buffer, degrades the bacterial cell wall and nucleic acids will be denaturated by NaOH. After this step, 150 µl of neutralizing buffer are added to the mixture and chilled on ice for 3 minutes subsequently. The neutralizing buffer contains a lightly acidic milieu with potassium acetate, which leads to renaturation of nucleic acids. During this process, plasmid DNA can renaturate properly, according to its structure, chromosomal DNA, however, cannot renaturate and precipitates along with parts of the cell wall, proteins and potassium dodecyl sulfate. The precipitate is centrifuged for 5 min at 15,000 rpm and 400 µl of the supernatant are transferred to a new tube. Subsequently, 800 µl of ethanol (>96%) are added into the tube and the mixture is then centrifuged for 15 minutes and 15,000 rpm. The supernatant is then carefully discarded, and the precipitate is subsequently washed with 70% ethanol. The tube is then centrifuged under the same conditions and the washing step is repeated. The supernatant is discarded, and the pellet/precipitate is dried at 37 °C for about 20 minutes. The DNA can be incorporated in 30-50 µl of either $dH_2O$ or in elution buffer from Monarch Plasmid Mini Prep Kit (New England Biolabs).

## 6.6 *Agarose gel electrophoresis*

The method of agarose gel electrophoresis primarily enables the differentiation between DNA molecules by their respective size as well as the determination of its concentration. It is based on the differentiated distances that nucleic acids travel across a gel matrix within, due to

negatively charged phosphate groups within the nucleic acid. Here, the travel speed of linear dsDNA behaves reversely proportional to the logarithm of the molecular weight (Helling et al., 1974). The travel speed additionally depends on the voltage und structure of the nucleic acid. The matrix consists of agarose, which has previously been boiled in 0.5-fold TAE buffer and the boiled solution then forms a gel consistency once it cools down. To detect nucleic acids later, the agarose solution for as long as it remains liquid, has to be supplemented with ethidium bromide. Ethidium bromide intercalates within nucleic acids and enables the visual detection under UV light. The amount of ethidium bromide is generally 0.5-1 µl of a 1% solution, depending on the size of the gel. The amount of agarose determines the separation of nucleic acids in the gel. When low percentages (usually 0.8 – 1%) of agarose are useful to distinguish between nucleic acids of larger size (e.g., digested plasmid DNA), higher percentages (>1.5%) of agarose are useful to distinguish between nucleic acids of smaller size (e.g., 100 – 500 bp). This is because of the pores that agarose builds within the gel, higher concentrations lead so smaller pores, lower concentrations to large pores. When the still liquid agarose solution is poured into an electrophoresis system, a comb (10-20 well combs, Peqlab) is generally placed into the solution and once the gel is solidified, the comb is then pulled out subsequently and forms wells inside the gel, where samples can be put into later. After the solidification of the gel, the system is filled with 0.5-fold TAE buffer to ensure the electric diffusion of electrons within the system. To determine the size of the nucleic acid fragments, a DNA ladder that contains DNA fragments of known size, is generally injected to the first well of the gel. The samples, which are to be investigated, are then filled/injected (usually by using a pipette) to the remaining wells, however, they have usually been supplemented with a loading dye, that contains xylene cyanol and bromophenol blue. This enables to determine the travel speed of the fragments, since these reagents are visible with the human eye – xylene cyanole travels alongside 300 bp fragments and bromophenol blue travels alongside 3000 bp fragments within a 1% agarose gel. Once the experiment is set up, the electrophoresis chamber (Peqlab) is then attached to a power supply, the voltage and the current can be set and after turning on the system, the negatively charged nucleic acid fragments travel across the agarose gel in the direction of the anode.

To visualize the DNA fragments, the agarose gel is (after the power supply is shut down) placed into a gel documentation system (Analytik Jena), on top of a UV-table that is supplied

with a camera. Once the UV light is turned on, nucleic acid fragments become visible and can be documented with a shot of the camera inside the system.

## 6.7 *$CaCl_2$-based transformation of bacterial strains*

To introduce plasmid DNA or oligonucleotides into bacterial strains, calcium chloride is used to increase cell permeability, which enables the incorporation of foreign nucleic acids.

Overnight cultures were diluted in a 1:100 ratio in 50 ml SOB media within a 300 ml sterilized Erlenmeyer flask (Schott) and subsequently incubated in a rotary shaker at 130 rpm and 37 °C to an optical density of $OD_{600}$ = 0.4. Subsequently, cells were chilled on ice for 10 minutes and for cell harvest, transferred to a 50 ml Falcon Tube (Sarstedt) and centrifugated for 10 minutes at 5,500 rpm at 4 °C. The supernatant was discarded, and cell pellet was inoculated in autoclaved, 0.1 M ice-cold $CaCl_2$ solution and resuspended. After chilling the samples on ice for additional 10 minutes, an additional centrifugation step was done under the same conditions. After discarding the supernatant, cells were inoculated in 1 ml of autoclaved, 0.1 M ice-cold $CaCl_2$ solution and resuspended. After another 10 minutes of chilling on ice, cells were split to 200 µl aliquots in 1.5 ml SafeSeal reaction tubes (Sarstedt) for transformation. Concentrations of nucleic acids did not exceed 100 ng and after addition of DNA to the sample, tubes were incubated on ice for 45 minutes. To transfer nucleic acids into the cells, they were exposed to 42 °C for 2 minutes to induce a heat shock and subsequently chilled on ice for 2 minutes. At last, heat-shocked cells were supplemented with 1 ml of 37 °C warm SOC media, transferred to a sterile glass tube and incubated for 45 min, 37 °C and 130 rpm in a rotary shaker. For plating, cells were split to 50, 100, and 200 ml aliquots and plated on LB Agar plates, in most cases supplemented with one or more antibiotics.

## 6.8 *Electroporation*

Another method to transform bacterial strains with nucleic acid is the electroporation method. This method is preferred, when transformation efficiencies of the $CaCl_2$ method are not sufficient to transform cells that are not K-12 strains or seemed to be difficult to transform in general, e.g., *Escherichia coli* MIII. During electroporation, bacterial strains are exposed to an electric impulse, which increases cell permeability and increases the incorporation of foreign

nucleic acids. The success of this method lies on avoiding any kind of salts in the cell suspension, which might cause a short circuit within the electroporation cuvettes.

Overnight cultures were diluted in a 1:100 ratio in 50 ml SOB media within a 300 ml sterilized Erlenmeyer flask (Schott) and subsequently incubated in a rotary shaker at 130 rpm and 37 °C to an optical density of $OD_{600}$ = 0.4. Subsequently, cells were chilled on ice for 10 minutes and for cell harvest, transferred to a 50 ml Falcon Tube (Sarstedt) and centrifugated for 10 minutes at 5,500 rpm at 4 °C. The supernatant was discarded, and cell pellet was incorporated in 15 ml of autoclaved, ice-cold $dH_2O$ and resuspended. Cells were centrifugated and incorporation in water under the same conditions for additional two times. After that, cells were incorporated in 500 µl of autoclaved, ice-cold $dH_2O$ and resuspended within a 1.5 ml SafeSeal reaction tube (Sarstedt). The 500 µl of cell solution was split into 50 µl aliquots, that were subsequently supplemented with nucleic acids, which concentrations did not exceed 500 ng and chilled on ice for additional 10 minutes. Cells were then transferred to an electroporation cuvette with 1 mm gap (Peqlab), which was subsequently placed into the gene pulser II (Bio-Rad), attached to a pulse controller II (Peqlab) electroporation system. Electric impulse was induced with 1.8 kV, 25 µF and 200 Ω. After induction, cells were transferred to 1 ml SOC medium (pre-heated to 37 °C) in a sterilized glass tube and incubated in a rotary shaker for 1 h at 37 °C and 130 rpm. For plating, cells were split to 50, 100 and 200 ml aliquots and plated on LB Agar plates, in most cases supplemented with one or more antibiotics.

## *6.9 Pyrosequencing*

Pyrosequencing is a method of sequencing DNA, where DNA polymerization by DNA polymerase can be monitored by measuring phosphate production, that can be detected by light. Oligonucleotide primer annealing to the template strand of the DNA that is to be sequenced enables DNA synthesis by extending the 3'-end of the DNA. The system repeatedly injects dATP, dCTP, dGTP, dTTP, and as the correct complementary dNTP is injected, inorganic pyrophosphate is released. The enzyme ATP-sulfurylase then catalyzes with the use of pyrophosphate ($PP_i$) and adenosine 5'-phosphosulfate (APS) ATP and $SO_4^{2-}$. ATP then works as a cofactor for the enzyme luciferase, that oxidizes luciferin to oxyluciferin and light, which can then be detected.

However, before the sequencing starts, the DNA-sequence to be sequenced must be amplified via polymerase chain reaction (PCR). In this PCR, a biotinylated primer is used, that enables streptavidin-associated binding and subsequent removal of the untagged strand from the amplified DNA. As described above, the enzyme luciferase uses dATP as a substrate. Accordingly, the injection of dATP would lead to signals, regardless of DNA-synthesis. For this reason, a dATP analogue, deoxyadenosine $\alpha$-thio triphosphate (dATP-$\alpha$-S) is used for injection instead.

The PCR protocol for the pyrosequencing template is described in 6.10.3. The products of the PCR were used subsequently as follows:

Preparing the PCR plate - First, the strepdavidin-sepharose beads (Cytiva Sweden AB) were vortexed shortly, until a homogenous suspension was visible. Then, for each tested sample, 3 µl of strepdavidin-sepharose beads were mixed with 20 µl $dH_2O$ and 37 µl binding buffer (PyroMark® Binding Buffer, QIAGEN GmbH). The mixture was then added into the well of a 96-well plate (PSQ 96 Plate Low, Biotage AB), 20 µl of biotinylated PCR product was added subsequently, sealed and subsequently incubated on a plate shaker for 5 min (Vortex Genie 2, Scientific Ind.).

Preparing the primer plate - Then 40 µl annealing buffer (PyroMark® Annealing Buffer, QIAGEN GmbH) were mixed with 8 µl sequencing primer (pKDsgRNA_5_5316_PSQ_Seq, 5pmol/µl) and added into the well of another 96-well plate (PSQ 96 Plate Low, Biotage AB).

The workstation for the preparation of biotinylated PCR products bound to strapdavidin-sepharose beads in this experiment was the PSQ 96MA (Biotage, Sweden). Four reservoirs for liquids were filled: 1) $dH_2O$, 2) 70% ethanol, 3) 0.2M NaOH and 4) Washing buffer (10 mM Tris-HCl, pH 7.6 adjusted with glacial acetic acid). An additional reservoir (not included in the workstation) was filled with 5% bleach (5 %(v/v) DanKlorix (Colgate-Palmolive)). After activation of the pump of the work table, the aspirator tips (Vacuum Prep Tool) were dipped in 5% bleach for 5 seconds, subsequently washed in $dH_2O$ for 20 seconds. Then, the aspirators were placed above the PCR plate (removal of seal beforehand) and dipped in the wells to soak up the complete mixture in the well. Now biotinylated PCR products, attached to strepdavidin-sepharose beads are attached to the filter tip of the aspirators and are ready for further process, where untagged single DNA strands are filtered out.

Removal of untagged DNA strands – Aspirators were then placed in a reservoir, that was filled with 70% ethanol for 5 seconds, subsequently in 0.2 M NaOH for 5 seconds (denaturation of

double strand DNA) and finally in washing buffer for 5 seconds. The aspirators of the Vacuum Prep Tool were then turned upside down and dried for 10 seconds.

Incubation of DNA coupled beads with sequencing primer – The Vacuum Prep Tool was the carefully placed above the primer plate, but not dipping inside the wells. The vacuum was then turned off and the prep tool with its aspirators was placed in the sequence primer plate to incubate DNA coupled streptavidin-sepharose beads with the sequence primer. The PSQ plate (previous sequence primer plate) was then placed on a heating block (MR 3001, Heidolph Instruments GmbH & Co. KG) and incubated for 10 min at 65°C for sequence primer annealing.

The PSQ plate was then placed in the PSQ 96MA, following the instructions given by the PyroMark Q96 Software. Substrates, enzymes and dNTPs were delivered by PyroMark® Gold Q96 Reagents (QIAGEN GmbH).

## *6.10 CRISPR-Cas9-based editing of genes*

CRISPR-Cas9-mediated gene engineering is nowadays a commonly used tool in molecular biology and its use has been steadily increased since its release about ten years ago. The system uses a Cas9 endonuclease that targets a specific DNA strand with 20 bp of size, which can be introduced into the cell by plasmid transformation (Jinek et al., 2012). The PAM-site (Protospacer adjacent motif), where Cas9 endonuclease sets its cut, needs to be located adjacent to the triplet NGG, a base that is followed by 2 guanines. When Cas9 cuts genomic DNA, this will lead to cell death, because in *Escherichia coli*, there is no non-homologous end joining mechanism for DNA repair (Bowater and Doherty, 2006). It has been shown that a Cas9-expressing plasmid, combined with the λ-Red recombineering plasmid pKD46 have the ability to insert or delete genes at a single chromosomal locus (Pyne et al., 2015). In this work, CRISPR no-SCAR (Scarless Cas9 Assisted Recombineering) method (Reisch and Prather, 2015) is being used as a tool to create *Escherichia coli modB* and *rpoC* mutants.

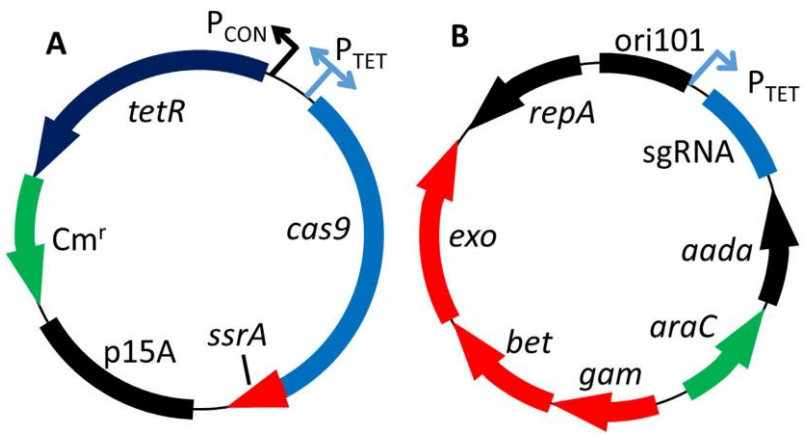


*Figure 8: Schematic map of the no-SCAR plasmids. (A) Schematic of the plasmid pCas9cr4 which has cas9 expressed under control of the $P_{TET}$ promoter and tetR constitutively expressed. (B) Schematic of the plasmid pKDsgRNA-ack which has the sgRNA expressed under control of the PTET promoter and the three genes that compose the λ-Red system under control of the arabinose inducible promoter $P_{araB}$ (Reisch and Prather, 2015).*

As shown in Figure 8, the system consists of 2 plasmids. On the first plasmid, pCas9cr4, shown in A, there is an inducible promoter ($P_{TET}$) for Cas9 endonuclease (cas9). As shown in B, the plasmid pKDsgRNA-ack is used for the expression of single guide RNA under control of the $P_{TET}$ promoter and three λ-Red genes under the control of the arabinose inducible promoter $P_{araB}$.

The First step in this process is to create a pKDsgRNA-*modB* plasmid, that contains the guiding sequence for the Cas9 endonuclease, next to the PAM-Site. For the construction of this plasmid, a pKDsgRNA-ack plasmid was taken as a template for a rolling circle PCR, where an individually constructed primer introduces the N20-sequence into the plasmid. The following primer was used to mediate Cas9 associated double-strand break in *modB*.

### 6.10.1 Rolling circle PCR

The principle of a rolling circle PCR is similar to the principle of a regular polymerase chain reaction, however, circular DNA, in form of a plasmid is being used as a template as opposed to linear DNA. To replicate the whole plasmid, one can set the primers to positions adjacent to each other so that during elongation, the complete sequence of the plasmid is reconstructed, since the primers direct elongation in opposing directions. The final construct, however, is not a circular PCR product but a linear double-strand DNA. This is because the adjacent primers are not connected with each other. However, after rolling circle PCR, there can be a subsequent ligation so that the beginning bases of the fragment are being connected and henceforth become circular DNA.

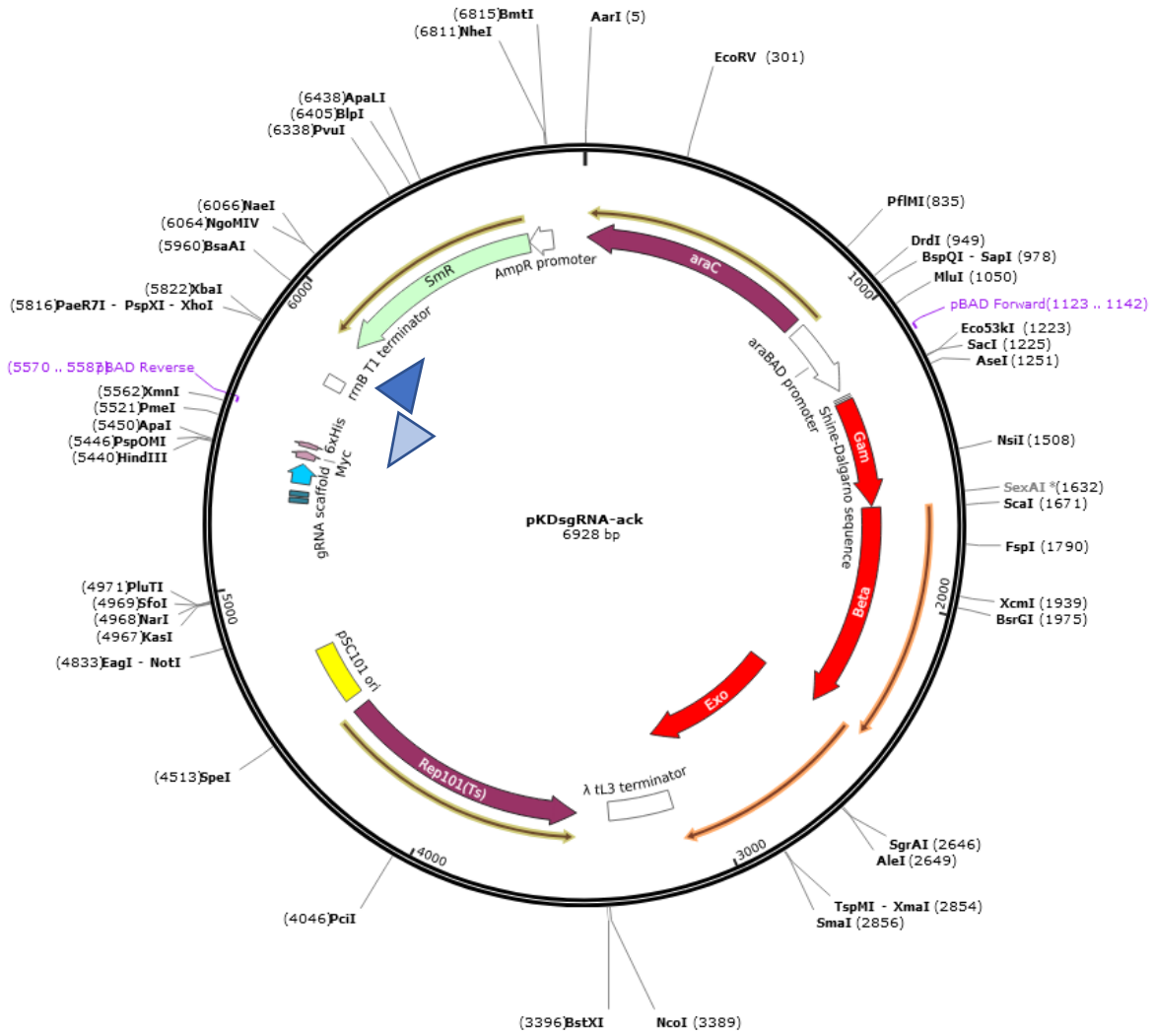


*Figure 9: Gene map of pKDsgRNA-ack. Primers used for rolling circle PCR are tagged with blue triangles. (Source: Addgene).*

During the process of rolling circle PCR, however, the amplicon can be modified by using primers that contain - apart of their complementary sequence – an additional sequence that will then be integrated into the plasmid by elongation. This method is being used to introduce an altered N20 sequence into pKDsgRNA-ack. During the rolling circle PCR, pKDsgRNA-ack is the original template for the reaction. Here, two adjacent primers are used, whereas the 5′ primer contains the N20 sequence, including the PAM-site.

This generates a plasmid, that is different to its progenitor. Here, rolling circle PCR is used as a method to create a pKDsgRNA plasmid with a *modB*-N20 sequence for directing Cas9 endonuclease to a cut within *modB* at position 316.

The Following PCR setup was used to create pKDsgRNA-*modB*:

*Table 3: Components and PCR setup for rolling circle PCR to generate a modified pKDsgRNA plasmid*

| Component | Volume [µl] |
|---|---|
| **$H_2O$ Invitrogen** | 54.5 |
| **Q5 Reaction Buffer** | 20 |
| **10 µM 3′-Primer (PtetR_pKDsgRNA_3_5335)** | 5 |
| **10 µM 5′-Primer (pKDsgRNA_*modB*_5_5336)** | 5 |
| **dNTPs** | 10 |
| **Q5 High Fidelity Polymerase (2U/µl)** | 1 |
| **pKDsgRNA-ack** | 4.5 |

| Step | Temperature | Duration |
|---|---|---|
| **Initial Denaturation** | 98 °C | 2 minutes |
| **30 Cycles** | 98 °C | 10 seconds |
| | 64 °C | 30 seconds |
| | 72 °C | 210 seconds / 0.5 m per kb (7 kb) |
| **Final Extension** | 72 °C | 5 minutes |
| **Hold** | 4 °C | ∞ |

Subsequently, the Fragment was analyzed on a 1% agarose gel electrophoresis. To digest remaining pKDsgRNA-ack plasmid in the sample, the whole PCR was enzymatically digested, using DpnI and the following components, as shown in Table 4. The complete digest was incubated at 37°C for 1 h.

*Table 4: Components for DpnI digest*

| Components | Volume [µl] |
|---|---|
| **$H_2O$ Invitrogen** | 42 |
| **Fast Digest Buffer 10X** | 12 |
| **PCR sample** | 60 |
| **FastDigest Dpn1** | 6 |

After digest, the whole sample was loaded into three wells of a 0.8% agarose gel and subsequently separated with electrophoresis at 100V for 30 min. The gel was stained in ethidium bromide and bands of 6948 bp size were extracted, using a Gel Extraction Kit (InnuPrep, Analytik Jena). For DNA quantification, the isolated, digested PCR products were pooled and analyzed on another 1% agarose gel after electrophoresis for estimating DNA concentration.

### 6.10.2 Ligation of pKDsgRNA-*modB*

After a rolling-circle PCR, there is no intact plasmid, instead there is a linear PCR product, that needs to be ligated to subsequently form a plasmid. For T4-Ligase mediated ligation, following protocol was used, as shown in Table 5 and incubated for 16 hours at 16°C and subsequently inactivated at 65°C for 10 minutes.

*Table 5: Components of the T4 Ligase protocol*

| Component | Volume [µl] |
|---|---|
| **DNA from gel extraction (~100 ng)** | 16.5 |
| **T4 Ligase Buffer** | 2 |
| **T4 Ligase** | 1.5 |

After ligation, $CaCl_2$-transformation was used to transform *Escherichia coli* DH5α as described in 6.7. For cell count of competent cells, a serial dilution was performed as described in 6.2. After transformation, cells containing pKDsgRNA-*modB* plasmid underwent alkaline lysis to isolate the plasmid as decribed in 6.5. Then the isolate was used for an enzymatic digest of EcoRV with following procedure as shown in Table 6:

*Table 6: Components of the EcoRV digest of pKDsgRNA-modB*

| Component | Volume [µl] |
|---|---|
| **$H_2O$ Invitrogen** | 7 |
| **Fast Digest Buffer** | 2 |
| **FastDigest EcoRI** | 1 |
| **pKDsgRNA-*modB* from alkaline lysis** | 10 |

The enzymatic digest was incubated for 30 minutes at 37°C. The whole digest was then added 2 µl of bromophenol-containing 6X loading dye and analyzed in a 1% agarose gel after electrophoresis at 100V for 1 hour. The results are shown in Figure 12.

### 6.10.3 Pyrosequencing

To determine the N20 sequence of the pKDsgRNA-*modB* plasmid, pyrosequencing was used as described in 6.9. For the creation of a biotinylated PCR product, following PCR setup was used as described in Table 7.

*Table 7: PCR components and protocol for pyrosequencing*

| Component | Volume [µl] |
|---|---|
| **$H_2O$ Invitrogen** | 31.4 |
| **Taq-Puffer (10X)** | 4 |
| **10 µM 3'-Primer (pKDsgRNA_3_5546_Biotin_PsQ)** | 0.8 |
| **10 µM 5'-Primer (pKDsgRNA_5_5255)** | 0.8 |
| **dNTPs** | 1.2 |
| **Taq-Polymerase (5U/µl)** | 1 |
| **pKDsgRNA-*modB* From alkaline lysis** | 0.8 |

| Cycle | Temperature | Duration |
|---|---|---|
| **Denaturate** | 94°C | 3 min |
| **45 Cycles** | 94°C | 30 sec |
| | 60°C | 40 sec |
| | 72°C | 30 sec |
| **Extension** | 72°C | 5 min |
| **Hold** | 4°C | ∞ |

The PCR products were then added 6 µl of bromophenol-containing 6X loading dye and analyzed on a 1% agarose gel. The results are shown in 7.1.1. After that, the PCR products were used for pyrosequencing as described in 6.9.

### 6.10.4 Transformation of *Escherichia coli* WT and derivates

The next step for CRISPR-Cas9 mediated gene editing was to introduce both plasmids, pCas9cr4 and pKDsgRNA-*modB* into *Escherichia coli* WT and MIII strains. However, for successful transformation assays, both plasmids needed to be isolated from WT background. To do so, $CaCl_2$-transformation protocol was used, as described in 6.7, to introduce pCas9cr4 and pKDsgRNA-*modB* into *Eschericia coli* WT. After transformation, cells were plated on LB Agar plates, supplemented with I) 100 µg/ml Chloramphenicol (pCas9cr4 transformants) or II) 100 µg/ml spectinomycin (pKDsgRNA-*modB* transformants). For isolation of WT-background plasmids, a plasmid mini prep (New England Biolabs) was used, according to the manufacturers protocol. Furthermore, both plasmids were introduced into *Escherichia coli* WT and *Escherichia coli* MIII, in consecutive Electroporation transformation protocols as described in 6.8. Transformed cells were then plated on LB Agar plates, supplemented with I) 100 µg/ml

Chloramphenicol (pCas9cr4 transformants) or II) 100 µg/ml spectinomycin (pKDsgRNA-*modB* transformants) or II) 100 µg/ml Chloramphenicol **and** 100 µg/ml spectinomycin. By doing so, double-transformants were established and designated *Escherichia coli* WT + pCas9cr4 + pKDsgRNA-*modB* as well as *Escherichia coli* MIII + pCas9cr4 + pKDsgRNA-*modB*.

### 6.10.5 Transformation with oligonucleotides

For oligonucleotide transformation, *Escherichia coli* WT + pCas9cr4 + pKDsgRNA-*modB* as well as *Escherichia coli* MIII + pCas9cr4 + pKDsgRNA-*modB* were used for electroporation protocol as described in 6.8, however, for induction of λ-Red genes, cells were grown to an $OD_{600}$ of 0.3 and subsequently induced with 500 µl of 20%(w/v) of L-Arabinose (Sigma) in a total volume of 50 ml. Electroporation was performed with 2 µl of 10 µM Oligonucleotide CRISPR_[*modB*_375rv_EscCol_noSCAR]. Competent cells and were plated on LB Agar, supplemented with either spectinomycin and chloramphenicol (growth control) and spectinomycin (Spec), chloramphenicol (Clm) and anhydrotetracycline (aTet) (activity control). Transformants were plated on LB Agar plates with spectinomycin, chloramphenicol and anhydrotetracycline. Concentrations of Spec = 100 µg/ml, Clm = 100 µg/ml, aTet = 0.1 µg/ml with serial dilutions as described in 6.2. Plating results are shown in Table 21.

### 6.10.6 Test of ARMS-PCR primer

To identify mutational integration in the genome of *Escherichia coli*, amplification-refractory mutation system (ARMS) was used. The principle of this method is to perform a polymerase chain reaction, with the usage of sequence-specific primer that allows the amplification of the gene of interest only when the exact sequence is given. There is a variety of protocols on how to design sequence-specific primers. Here, we apply the protocol of Little et al. (Little, 1995) to find the best combination of primers to detect the single nucleotide polymorphism in the gene *modB*, that lead to C→A at position 316 within CRISPR-Cas9 mediated strains of *Escherichia coli* WT and *Escherichia coli* MIII.

For this a consistent forward primer and 3 variants of the reserve primer, with different bases at the second last position to the 3'-end were used.

The primers that were used are shown in the following Table 8. The varying bases are tagged in bold.

*Table 8: Primers used to establish a detection of modB SNP*

| Name of the primer | Sequence |
|---|---|
| ***modB*_315rv_ARMS_MIVb_CCT** | AATTGCCCGCACCATC**C**T |
| ***modB*_315rv_ARMS_MIVb_CTT** | AATTGCCCGCACCATC**T**T |
| ***modB*_315rv_ARMS_MIVb_CAT** | AATTGCCCGCACCATC**A**T |

To figure out, which set of primers are suitable for the detection of C→A in *modB*, single colonies of *Escherichia coli* MIVb were taken as a template for the ARMS-PCR, *Escherichia coli* WT colonies were taken as a negative control, respectively.

Furthermore, it was tested, if dimethyl sulfoxide (DMSO) enhances sequence-specific binding of primers. DMSO is a chemical, sometimes used in polymerase chain-reactions to inhibit the formation of secondary structures, which can be interfering during PCR. For PCR setup, 50% of the reverse primer was used, compared to the forward primer. A shortage of sequence-specific primers that only bind to mutational sequences was also found to decrease non-specific primer binding. For these reasons, the following PCR setup came up, as shown in Table 9.

*Table 9: Components and setup for ARMS-PCR*

| Component | Volume [µl] | Cycle | Temperature | Duration |
|---|---|---|---|---|
| **$H_2O$ Invitrogen** | 18.925 | **Denaturate** | 98°C | 2 min |
| **Dreamtaq-Buffer (10X)** | 3 | **30 Cycles** | 98°C | 10 sec |
| **10 µM 3'-Primer *modB*_-170fw** | 0.75 | | 58°C | 30 sec |
| **10 µM 5'-Primer *modB*_315rv_ARMS_MIVb_CCT, or *modB*_315rv_ARMS_MIVb_CTT, or *modB*_315rv_ARMS_MIVb_CAT** | 0.375 | | 72°C | 30 sec |
| **dNTPs** | 3 | **Extension** | 72°C | 5 min |
| **Taq-Polymerase (5U/µl)** | 0.2 | **Hold** | 4°C | ∞ |
| **DMSO or $H_2O$** | 0.75 | | | |
| **Boiling DNA template (*Escherichia coli* MIVb or WT colony, Boiled in 100 µl $H_2O$)** | 3 | | | |

### 6.10.7 ARMS-PCR

As shown and described in in the previous chapter, the combination of primers with 3'-Primer *modB*_-170fw and 5'-Primer *modB*_315rv_ARMS_MIVb_CTT were further used for the detection of *modB* C→A single nucleotide polymorphism. The protocol for the PCR reaction is shown in Table 9 (with -CTT primer and DMSO) and adjusted to the number of colonies that were tested.

### 6.10.8 DNA sequencing analysis of genomic DNA

To determine, if CRISP-Cas9 mediated gene editing of *modB* was successfully proceeded in *Escherichia coli* WT and *Escherichia coli* MIII, potentially positive clones were picked for Sanger sequencing. For that, boiled DNA from ARMS-positive clones was used as a template for a PCR, purified PCR products were analyzed the on a 1% agarose gel and sent it to one of our partner laboratories for Sanger sequencing.

The first step was the PCR of *modB*, which setup is shown in the following Table 10.

*Table 10: Components and setup of PCR for Sanger Sequencing*

| Component | Volume [µl] |
|---|---|
| **10X DreamTaq Buffer** | 12.5 |
| **10 mM dNTPs** | 12,5 |
| **10 µM Forward Primer (*modB*_9fw_EscCol)** | 1,5 |
| **10 µM Reverse Primer *modB*_467rv_EscCol** | 1,5 |
| **Boiling DNA** | 0 |
| **DMSO** | 0 |
| **DreamTaq DNA Polymerase** | 1 |
| **Ad $H_2O$ 100 µl** | 71 |

| Cycle | Temp. | Duration |
|---|---|---|
| **Initial Denaturation** | 98°C | 3 minutes |
| **30 Cycles** | 98°C | 30 seconds |
| | 62,5°C | 30 seconds |
| | 72°C | 20 seconds / 0,5 m per kb (476 bp) |
| **Final Extension** | 72°C | 5 minutes |
| **Hold** | 4°C | ∞ |

The master mix was split into 20 µl aliquots, 5 µl of boiling DNA of positive clones were then added, making a total volume of 25 µl of each PCR reaction. 5 µl of $H_2O$ was added as a negative control in one of the samples. As shown in Table 10, a PCR product of 476 base pairs in size was expected in the forthcoming agarose gel electrophoresis.

### 6.10.9 DNA purification of PCR products and Sanger sequencing

To purify the amplicon of *modB* after polymerase chain reaction, InnuPREP PurePCR Kit (Analytik Jena) was used. To do so, the total volume of 25 µl of PCR products were used for the purification. For each sample, a spin filter was set into a receiver tube. Then, 500 µl of binding buffer were added onto the spin filter. Subsequently, 25 µl of PCR product were added and mixed by pipetting up and down 2-5 times. The tubes were then placed in a microcentrifuge and spun for 1 minute at 11,000 x g. The flow-though was discarded and the samples were spun an additional time for 2 minutes at 11,000 x g. The spin filter was then placed into an elution tube and 10 µl of elution buffer were added to the center of the spin filter. The samples were then incubated for 1 minute prior to a final centrifugation step to elute the DNA at 11,000 x g for 1 minute.

The purified amplicon was then analyzed, by pipetting 1 µl of the sample on a 1% agarose gel, supplemented with ethidium bromide (0.5 µl on 50 ml agarose gel) after electrophoresis for 1 hour at 100V, to estimate DNA concentration and check for a clean band after PCR. A DNA concentrations of 30-35 ng per microliter was estimated, the requirement for Sanger sequencing was 60 ng/µl, or 2 µl of each sample was used for sequencing. A sequencing primer (*modB*_9fw_EscCol) was added according to the instructions (5 pmol/µl) of the partner laboratory (Eurofins GATC). The total volume of the sequencing samples was 10 µl. The results of the sanger sequencing are shown in Figure 16.

### 6.10.10 Plasmid curing

After detection of positive clones with Sanger sequencing, successfully gene edited strains still contained both plasmids, which are necessary for CRISPR-Cas9 mediated gene editing. These plasmids, pKDsgRNA-*modB* and pCas9cr4, needed to be excluded from the cells. For this, plasmid curing is an given option, as described in (Reisch and Prather, 2015). Since pKDsgRNA-*modB* is a derivate of pKDsgRNA-ack plasmid, which contains Rep101(Ts), which is a temperature-sensitive version of the RepA protein, needed for replication with the pSC101 origin, pKDsgRNA-*modB* can be degraded by incubation at temperatures at 37°C as opposed to 30°C, which was the essential incubation temperature for this plasmid. To exclude pCas9cr4 from cells, pKDsg-p15A plasmid can be transferred into pCas9cr4-containing cells. The pKDsg-p15A plasmid targets the p15A origin of replication of pCas9cr4, so that an induction

of the Cas9 endonuclease would lead to DSB of its own originated plasmid. Empirical laboratory experiments, however, have shown that pCas9cr4 plasmids can be excluded from *Escherichia coli* strains by incubating the cells without the involvement of selection markers for pCas9cr4, such as chloramphenicol for about 2 days at 37°C.

For plasmid curing, successfully CRISPR-Cas9 mediated *modB* mutant strains of *Escherichia coli* WT and *Escherichia coli* MIII, as determined by Sanger sequencing, were inoculated in 3 ml LB medium and incubated at 37°C for 16 hours. Cells were then transferred in a 1:100 manner to 50 ml of fresh LB medium and incubated for 8 hours. 50 µl of cell material was then plated on LB Agar plates and LB Agar plates, supplemented with 100 µg/ml chloramphenicol as well as LB Agar plates, supplemented with 100 µg/ml spectinomycin. This process was repeated after 16 hours, as the 50 ml cell suspension was diluted in a 1:1000 ratio in 50 ml of fresh LB medium that was incubated over night for 16 hours at 37°C and plated an additional time.

### 6.10.11 Creating an *Escherichia coli* WT/ModB-L106M/RpoC-P246Q double mutant by CRISPR-mediated gene editing

Since both mutations, *modB* C316A and *rpoC* 737 occur concomitantly in *Escherichia coli* MIVb, one of the last successors of FQ-based selection process, one aim of this work was to create a double mutant strain, carrying *modB* C316A and *rpoC* 737. For this purpose, *rpoC* C737A was introduced into *Escherichia coli* WT/ModB-L106M, the bacterial strain that was generated during the process in 6.10.1 - 6.10.10. The principle of this process was similar to 6.10.1 - 6.10.10, in this case, however, a different pKDsgRNA plasmid had to be used, as well as a different oligonucleotide and primers for ARMS-PCR. The introduction of *rpoC* C737A into *Escherichia coli* WT/ModB-L106M is being described in the following chapter.

The construction of a *rpoC*-737-carrying pKDsgRNA plasmid was assessed by rolling circle PCR, similar to 6.10.1 - 6.10.3. In this case, a N20 sequence was selected to initiate DSB at *rpoC* at position 737. The work for this was performed within a different study (D. Rönfeldt, unpublished) and the plasmid was designated pKDsgRNA-*rpoC*737. *Escherichia coli* WT/ModB-L106M was transformed with both plasmids, pKDsgRNA-*rpoC*737 and pCas9cr4 in an electroporation protocol as described in 6.8. Concentrations of chloramphenicol and spectinomycin were used in the same fashion as in *Escherichia coli* WT. Transformation of oligonucleotide was performed, using electroporation protocol as described in 6.8, however,

CRISPR_[*rpoC*_C737A_noSCAR] and not CRISPR_[*modB*_375rv_EscCol_noSCAR] was used here. Plating was performed as described in 6.10.5 and levels of chloramphenicol, spectinomycin and anhydro tetracycline matched to *Escherichia coli* WT. The results are shown in Table 22. For ARMS screening, the following PCR setup was used, as shown in Table 11.

*Table 11: ARMS-PCR screening components and PCR setup for rpoC C737A mutations*

| Component | Volume [µl] |
|---|---|
| **$H_2O$ Invitrogen** | 18.925 |
| **Dreamtaq-Buffer (10X)** | 3 |
| **10 µM 3'-Primer *rpoC*_3_760M_ ARMS_wMM_EcoMIVb** | 0.75 |
| **10 µM 5'-Primer *rpoC*_5_-91_Eco** | 0.375 |
| **dNTPs** | 3 |
| **Taq-Polymerase (5U/µl)** | 0.2 |
| **DMSO or $H_2O$** | 0.75 |
| **Boiling DNA template** | 3 |

| Cycle | Temperature | Duration |
|---|---|---|
| **Denaturate** | 98°C | 2 min |
| **30 Cycles** | 98°C | 10 sec |
| | 58°C | 30 sec |
| | 72°C | 30 sec |
| **Extension** | 72°C | 5 min |
| **Hold** | 4°C | ∞ |

As shown in Table 11, a PCR reaction for three samples of ARMS PCR screening. The amount of the component was adjusted to the number of colonies that were to be tested. To 9 µl of master mix was added 1 µl of boiling DNA of transformed clones, *Escherichia coli* MIVb boiling DNA (positive control) or *Escherichia coli* WT boiling DNA (negative control) or a no template control ($H_2O$). The PCR reactions were added 2 µl of bromophenol blue or a 6 X Loading Dye and were analyzed on a 1% agarose gel after electrophoresis at 100V for 1 hour. The results are shown in Figure 17. After detection of positive clones on agarose gel, a PCR was performed to amplify *rpoC* for Sanger sequencing. The PCR setup is shown in Table 12.

*Table 12: Components and setup of PCR for Sanger Sequencing of rpoC C737A mutation*

| Component | Volume [µl] |
|---|---|
| **$H_2O$ Invitrogen** | 18.925 |
| **Dreamtaq-Buffer (10X)** | 3 |
| **10 µM 3'-Primer *rpoC*_3_1138_Eco_WT** | 0.75 |
| **10 µM 5'-Primer *rpoC*_5_-91_Eco** | 0.375 |
| **dNTPs** | 3 |
| **Taq-Polymerase (5U/µl)** | 0.2 |
| **DMSO or $H_2O$** | 0.75 |
| **Boiling DNA template** | 3 |

| Cycle | Temparature | Duration |
|---|---|---|
| **Denaturate** | 98°C | 2 min |
| **30 Cycles** | 98°C | 10 sec |
| | 58°C | 30 sec |
| | 72°C | 30 sec |
| **Extension** | 72°C | 5 min |
| **Hold** | 4°C | ∞ |

The PCR products were then purified, using InnuPREP PurePCR Kit (Analytik Jena), according to the manufacturer's instructions. The purified PCR products were then supplemented with a sequencing primer *rpoC*_3_1138_Eco_WT according to our partner laboratories instructions (Eurofins GATC) and adjusted to a total volume of 10 µl. The results of Sanger sequencing are shown in Figure 18.

For plasmid curing, successfully CRISPR-Cas9 mediated *rpoC* mutant strains of *Escherichia coli* WT/ModB-L106M as determined by Sanger sequencing, were inoculated in 3 ml LB medium and incubated at 37°C for 16 hours. Cells were then transferred in a 1:100 manner to 50 ml of fresh LB medium and incubated for 8 hours. 50 µl of cell material was then plated on LB Agar plates and LB Agar plates, supplemented with 100 µg/ml chloramphenicol as well as LB Agar plates, supplemented with 100 µg/ml spectinomycin. This process was repeated after 16 hours, as the 50 ml cell suspension was diluted in a 1:1000 ratio in 50 ml of fresh LB medium that was incubated over night for 16 hours at 37°C and plated an additional time.

## *6.11 Determination of molybdate influx using FRET-technology*

To determine to incorporation of molybdate that is passing ATP-driven transporters through the cell membrane and to investigate the effects on that event caused by mutations in *modB*, a method that measures molybdate-influx in *E. coli* strains was established here.

In 2013, Nakanishi et. al published a work that included a plasmid-based Förster-Resonance Energy Transfer (FRET) system, that determines the incorporation of molybdate in living cells (Nakanishi et al., 2013). This system, called MolyProbe, is a constitutional expressed plasmid for the usage in *Escherichia coli* that expresses a Yellow Fluorescence Protein (YFP) that is coupled to a Cerulean Fluorescence Protein (CFP) over two molybdate-binding domains (MoBD) and are connected by optimized peptide linkers. MoBDs are from *Escherichia coli* ModE factor, a transcriptional factor, with high affinity to molybdate. In the presence of molybdate, MoBD confers an energy transfer among the fluorophores by a conformational change of the MolyProbe by annealing YFP to CFP. In this case, an excitation of YFP results in an energy transfer to CFP. This way, emission of CFP is possible, even though excitation wavelengths of YFP are used. With this, it is possible to assess molybdate binding to MolyProbe and thus, a decreased or increased amount of molybdenum inside the cell.

The genuine idea of the MolyProbe in Nakanishi's experiments was to assess levels of molybdenum in eukaryotes. For this purpose, the recombinant protein MolyProbe was expressed in an *Escherichia coli* DH5$\alpha$ strain, however, it was then purified, using a set of chromatography experiments for the usage in HEK cells – an investigation of molybdate levels in *Escherichia coli* itself had not been proceeded in their study.

The main goal of this project was to assess hypothetical effects on molybdate influx caused by a single nucleotide polymorphism in *modB*. However, it was first necessary to determine other data prior to an actual use of the system on *Escherichia coli* strains, that possessed *modB* mutations. This included the validation, if molybdate levels can assessed in *Escherichia coli* in general, the assessment of cell material, necessary to detect proper fluorescence signals and the selection of an appropriate growth medium.

### 6.11.1 Determination of molybdate levels in *Escherichia coli* JW0747-1 and BW25113

Here, for this investigation, an assessment of molybdate levels of *Escherichia coli* was validated by comparing a *modB* knockout-mutant, *E. coli* JW0747-1, with its progenitor strain, *E. coli*

BW25113. For this purpose, pYN627 was isolated from *E. coli* DH5α using a plasmid mini prep kit (Monarch Plasmid Miniprep Kit, New England Biolabs®). The same method was used to isolate pBlueScript II SK (+), a mock control plasmid, from *E. coli* DH5α. Then, *Escherichia coli* JW0747-1 and *Escherichia coli* BW25113 were transformed with pYN627 or pBlueScript II SK (+), using the $CaCl_2$ method as described in 6.7 and plated on LB Agar with 50 µg/ml ampicillin. Colonies of each transformed strain were picked, and a stock culture was prepared as described in 6.1. For molybdate level measurements, three colonies of BW35113 + pYN627 and JW0747-1 + pYN627 as well as one colony of BW25113 + pYN627 and JW0747-1 + pYN627 were cultured overnight in 3 mL of LB broth medium, supplemented with 50 µg/ml ampicillin at 30°C and 130 rpm in a rotary shaker. After 16 hours, cell suspensions were diluted 1:100 in 25 mL M9 caso amino acids broth, supplemented with 50 nM molybdate as well as 50 µg/ml ampicillin. Cells were incubated at 30°C and 130 rpm in a rotary shaker to an $OD_{600}$ = 0.7. Cells were transferred to 50 mL Falcon tubes, filling ½% of its volume and centrifugated at 5,000 x g and 4°C for 10 minutes. The supernatant was discarded, and pellets were washed, using 15 mL of 0.9% NaCl solution (autoclaved) to resuspend cells prior to an additional centrifugation step (5,000 x g, 4°C, 10 min). The supernatant was discarded, and cells were washed in a second step, using 15 mL of 0.9% NaCl solution (autoclaved) to resuspend cells prior to an additional centrifugation step (5,000 x g, 4°C, 10 min). Supernatant was discarded and cell pellets were diluted in 1 mL of 0.9% NaCl solution (autoclaved).

For molybdate quantification, 5 x 200 µl of each cell suspension was transferred in a black 96-well plate and analyzed in a multimode microplate reader (Mithras LB 940, Berthold Technologies), using the following program.

*Table 13: Properties of FRET measurement*

| Measurement options | |
|---|---|
| **Counting time** | 0.10 |
| **Lamp energy** | 60000 |
| **Excitation filter** | 430 |
| **Excitation aperture** | Normal |
| **Emission filter** | F535 |
| **Counter position** | Top |
| **Measurement operation** | By Plate |
| **2nd measurement** | Yes |
| **Excitation filter 2** | 430 |
| **Emission filter 2** | 495 |

As shown in Table 13, a protocol was used that first assessed a FRET signal with an excitation filter of 430 nm (excitation maxima of CFP) and an emission filter of 525 nm (emission maxima of YFP). In a second measurement, CFP values were analyzed, using 430 nm as an excitation wavelength and 480 nm for emission.

To determine background-corrected emission, FRET and CFP-values of pBlueScript II SK (+)-carrying strains were assessed and subtracted from MolyProbe-containing strains. After calculation of background-corrected emission, FRET values were set in correlation to CFP values. For this, a FRET/CFP ratio was calculated. The results are shown in 7.2.

### 6.11.2 Determination of molybdate levels in *E. coli* WT and CRISPR-Cas9 strains

After measuring the molybdate levels in *Escherichia coli modB*-knockout strain and its progenitor strain, molybdate levels of *E. coli* ModB-L106M were verified to determine gain or loss of function of the molybdate ABC transporter.

As mentioned in the previous chapter, MolyProbe plasmid pYN627 as well as the mock control vector pBlueScript II SK (+) were isolated from *Escherichia coli* DH5α strains. For the transformation of *Escherichia coli* wild-type and CRISPR-Cas9 strains (*E. coli* WT, *E. coli* WT/ModB-L106M and *E. coli* WT/ModB-L106M/RpoC-P246Q), electroporation protocol was used for a transformation assay as described in 6.8 and plated on LB Agar plates, supplemented with 50 µg/ml ampicillin. Colonies of each transformed strain were picked, and a stock culture was prepared as described in 6.1. For MolyProbe measurement, 6 colonies of each MolyProbe-carrying strain, i.e., *Escherichia coli* WT + pYN627 and *Escherichia coli* WT/ModB-L106M + pYN627 as well as 2 colonies of each pBlueScript II SK (+)-carrying strain, i.e., *Escherichia coli* WT + pBlueScript II SK (+), *Escherichia coli* WT/ModB-L106M + pBlueScript II SK (+) and *Escherichia coli* WT/ModB-L106M/RpoC-P246Q + pBlueScript II SK (+) were inoculated in 3 mL LB growth medium and incubated at 30°C at 130 rpm in a rotary shaker overnight. After 16 hours, cell suspensions were diluted 1:100 in 50 ml M9 caso amino acids broth medium, supplemented 50 nM molybdate as well as 50 µg/ml ampicillin. Cells were incubated at 30°C and 130 rpm in a rotary shaker to an $OD_{600}$ = 1.5. Cells were transferred to 50 mL Falcon tubes, filling ½% of its volume and centrifugated at 5,000 x g and 4°C for 10 minutes. The supernatant was discarded, and pellets were washed, using 15 ml of 0.9% NaCl solution (autoclaved) to resuspend cells prior to an additional centrifugation step (5,000 x g,

4°C, 10 min). The supernatant was discarded, and cells were washed in a second step, using 15 ml of 0.9% NaCl solution (autoclaved) to resuspend cells prior to an additional centrifugation step (5,000 x g, 4°C, 10 min). Supernatant was discarded and cell pellets were diluted in 1 mL of 0.9% NaCl solution (autoclaved).

For molybdate quantification, 5 x 200 µl of each cell suspension was transferred in a black 96-well plate and analyzed in a multimode microplate reader (Mithras LB 940, Berthold Technologies), using the program as shown in Table 13.

To determine background-corrected emission, FRET and CFP-values of pBlueScript II SK (+)-carrying strains were assessed and subtracted from MolyProbe-containing strains. After calculation of background-corrected emission, FRET values were set in correlation to CFP values. To do so, a FRET/CFP ratio was calculated, and the results are shown in Figure 20.

### 6.11.3 Statistics

FRET/CFP-Ratios of three biological samples were measured in each BW35113 and JW0747-1, respectively. The fluorescent background signals of one biological sample without MolyProbe (mock vector control) was assessed and subtracted from MolyProbe fluorescent signals. Background-corrected FRET/CFP-Ratios were determined with a 2-sided student's t-test to determine biological significances with a respectively indicated p-value of 0.018.

When molybdate levels of *Escherichia coli* wild-type strains (*E. coli* WT, *E. coli* WT/ModB-L106M and E. coli WT/ModB-L106M/RpoC-P246Q) were assessed, FRET/CFP-Ratios of six biological samples were measured for each strain. The average fluorescent background signals of two biological sample without MolyProbe (mock vector control) was assessed and subtracted from MolyProbe fluorescent signals. Background-corrected FRET/CFP-Ratios were assessed with a 2-sided student's t-test to determine biological significances with a respectively indicated p-value of 0.038.

## *6.12 qRT-PCR*

With quantitative real-time PCR (qRT-PCR), the detection of ongoing amplification processes can be observed by using fluorescent dyes. The system relies on measuring increasing amounts of fluorescent signals, which display the amount of DNA produced during every cycle. A single PCR reaction is determined by the PCR cycle, where the fluorescence signal rises above a threshold background levels (threshold cycle, Ct). Therefore, higher messenger RNA (mRNA) concentrations are indicated by a low Ct-value. The process of qRT-PCR consists of three steps: reverse transcriptase-based conversion of RNA to cDNA, the amplification of cDNA by PCR, and the detection and quantification of amplified products-referred as amplicons (Jozefczuk and Adjaye, 2011). For this purpose, total RNA is being extracted of cell material, that is subsequently synthesized to complementary DNA (cDNA) using a reverse transcriptase as an operating enzyme. This way, mRNA is transcribed to a DNA template for a polymerase chain reaction. The higher the number of starting templates, the higher the number of amplified products. A DNA-interlinked, fluorescent dye - in this work - SYBR Green, is used to visually detect amplified DNA that is illustrated as an increasing curve within an amplification plot. During experimental design, a $C_T$-threshold is set and defines when ΔRn reaches a certain value. ΔRn is the fluorescence signal of a reporter dye (in this work SYBR GREEN) divided by the fluorescence signal of a reference dye (in this work ROX). By doing so, a high expression level of an investigated gene leads to high amounts of cDNA and thus, more SYBR Green is being interlinked with DNA. With this, ΔRn of this gene will hit the threshold earlier and henceforth, will lead to a smaller $C_T$ value. In every experiment, a reference gene – in this work *dnaQ* – is being used to adjust the individual gene expression of a gene of interest to a housekeeping gene.

### 6.12.1 Growth and harvest of bacterial cells

#### *6.12.1.1 Aerobic growth*

For qRT-PCR under aerobic conditions, colonies of bacterial strains were taken from LB Agar plate with a glass rod, sterilely transferred to a 10 ml test tube with 3 ml LB broth medium and incubated at 37° C at 130 rpm in a rotary shaker for 16 hours. *Escherichia coli* MIII/RpoC-P246Q as well as *Escherichia coli* MIVb were incubated at 80 rpm to prevent strains from creating inhomogeneous, filamenting cell suspension. After 16 hours, cultures were diluted 1:100,

transferring 250 µl of bacterial suspension into a 250 ml Erlenmeyer flask, filled with 25 ml sterile LB broth medium. Cells were incubated at 37°C at 130 rpm or 80 rpm, respectively, to an $OD_{600}$ of 0.4. Optical densities were analyzed, using 1 ml cuvettes in a Photometer.

For *soxS* induction, respective amounts of paraquat were added to the cultures at $OD_{600}$ = 0.4 to achieve the MIC of respective strains in the medium. For each strain with wild-type background, paraquat was added to the media to attain a concentration of 750 µM. For each strain with MIII background, paraquat was added to attain a concentration of 550 µM in the medium. For paraquat-driven *soxS* induction, a 100 mM stock solution was prepared that was sterilized using a 0.2 µm non-pyrogenic Minisart® filter unit (Sartorius™) and a sterile 50 ml tube with 115x28 mm size (Sarstedt AG).

#### *6.12.1.2 Anaerobic growth*

For anaerobic growth, colonies of bacterial strains were taken from LB Agar plate with a sterile needle that was attached to a syringe, containing 0.5 ml of sterile LB broth medium. The colonies were then injected into butylrubber-sealed 12 mL hungate-tubes (Glasgerätebau Ochs), filled with 5 ml LB broth medium under anaerobic conditions and incubated for 24 h at 37°C without rotary shaking in an incubator (Heraeus Holding GmbH). After 24 hours, 0.5 ml of the bacterial suspensions were transferred into a new hungate-tube, filled with 5 mL LB broth medium under anaerobic conditions, using a sterile needle and a syringe. The new inoculated medium was then incubated for additional 24 hours at 37°C in an incubator without rotary shaking. After 24 hours, 0.5 mL of the bacterial cell suspensions were transferred into a butylrubber-sealed 120 mL serum flask (Glasgerätebau Ochs), containing 50 ml of LB broth medium under anaerobic conditions. Anaerobic medium was generated by filling the tubes and flasks with nitrogen gas for 10 min to evacuate oxygen in the vessels before autoclaving. The bacterial strains in the freshly inoculated, anaerobic medium were then grown to an $OD_{600}$ of 3.5. To measure the optical density of anaerobically grown strains, sterile needles attached to syringes were used to transfer inoculated medium to a cuvette.

For any bacterial harvest, 500 µL of cell suspensions were transferred to a 1.5 mL tube, filled with 1 mL of RNA Protect (Qiagen), incubated for 5 minutes at room temperature and centrifuged for 10 min. at 5.000 g in a centrifuge. The supernatant was discarded, and the cell pellet was stored at -80°C in a freezer.

### 6.12.2 Isolation of total RNA

RNA isolation was performed using Monarch® Total RNA Miniprep Kit (New England Biolabs®). As mentioned above, cell pellets of bacterial strains were stored in 1.5 mL tubes at -80°C. First, tubes were chilled on ice to thaw cell material. 105 µl of TE buffer were added and subsequently vortexed on a vortex machine. Then, tubes were incubated at 25°C in a rotary shaking incubator for 5 min at full speed. After that, 220 µl of RNA lysis buffer were added to the sample and tubes were vortexed an additional time for 10 seconds before a centrifugation step took place at 16,000 x g for 2 min. For gDNA removal, the gDNA removal column was placed in 2 mL collection tubes and 330 µL of the lysate was added to the column. Samples were centrifugated at 16,000 x g for 30 s. 165 µl ethanol (≥95%) was added to each sample and gently resuspended. Then, a RNA purification column was added to a 2 mL collection tube and the ethanol-mixture was added to the column. Each sample was centrifugated at 16,000 x g for 30 s, the flow-through was discarded and to the columns were then added 500 µl RNA priming buffer. An additional centrifugation step was added (16,000 x g for 30 s) and columns were then washed, using 500 µl wash buffer. After an additional washing step with 500 µl wash buffer and subsequent centrifugation (16,000 x g for 30 s), RNA elution was performed by adding 50 µl of nuclease-free water to the column, waiting for 1 min and centrifugation at 16,000 x g for 30 s.

### 6.12.3 RNA digest with DNAseI

Measurements of RNA quality and quantity were assessed using NanoDrop spectrophotometer. Purified RNA was used for a DNAseI digest, for the removal of residual DNA. Each sample of RNA was digested with DNAseI as shown in Table 14. The samples were then incubated at 37°C for 30 minutes, using an incubator.

*Table 14: Components for DNAseI digest*

| Component | Volume [µL] |
|---|---|
| **Millipore $H_2O$** | 6 |
| **RNA (ca. 2 µg)** | 10 |
| **DNase I Reaction Buffer with $MgCl_2$ (10x)** | 2 |
| **DNase I (RNase frei)** | 2 (2 Units) |
| **Σ** | 20 |

### 6.12.4 RNA purification

For RNA purification of DNAseI-digested nucleic acids, samples were taken from 6.12.3 and 30 µl of RNAse-free $H_2O$ was added to each sample to have a total volume of 50 µl. Subsequently, 100 µl of RNA cleanup buffer and 150 µl ethanol absolute were added to each sample. Cleanup columns were placed inside 2 mL collection tubes and sample/ethanol mixtures of 300 µl volume were added onto the columns and tubes were centrifugated at 16,000 x g for 1 min. After centrifugation, flow-through was discarded and 500 µl RNA cleanup wash buffer was added onto the column. Samples were centrifugated (16,000 x g, 1 min), flow-through discarded and an additional washing step was performed, using 500 µl RNA cleanup wash buffer, centrifugation (16,000 x g, 1 min), and discard of flow-through. For RNA elution, 20 µl of RNAse-free $H_2O$ was added onto the column, incubated at room temperature for 1 min and centrifugated at 16,000 x g for 1 min. Measurements of RNA quality and quantity were assessed using NanoDrop spectrophotometer.

### 6.12.5 Quality control of RNA on agarose gel electrophoresis

To assess RNA quality of purified RNA, samples were undergoing gel electrophoresis on an agarose gel. For that, 200 ng purified RNA of each sample was given 1:1 volume of 2 x RNA loading buffer in 0.2 mL non-pyrogenic PCR tubes, placed in a thermal cycler (Peqlab primus 25 advanced®, VWR) and incubated for 10 min at 70°C to diminish secondary RNA structures before running whole samples in a 1% agarose gel at 100 V for 1 h.

### 6.12.6 cDNA transcripts

After RNA quality check on agarose gel electrophoresis, purified RNA samples from 6.12.5 were used for cDNA synthesis. For cDNA synthesis, LunaScript™ RT SuperMix (New England Biolabs®) was used like described in Table 15. For each strain, a no-RT control mix was prepared to rule out genomic DNA contaminations in the samples (NAC = no amplification control). cDNA synthesis and no-RT controls were prepared in 0.2 mL non-pyrogenic PCR tubes.

*Table 15: Components of LunaScript RT Supermix*

| Component | Volume cDNA [µL] | Volume no-RT control [µL] |
|---|---|---|
| **Template RNA (150 ng)** | x | x |
| **LunaScript™ RT SuperMix (5x)** | 4 | - |
| **No-RT Control Mix** | - | 4 |
| **Nuclease-free H2O** | Ad 20 µL | Ad 20 µL |
| **Σ** | 20 | 20 |

Samples were placed in a thermal cycler (Peqlab primus 25 advanced®, VWR) and were undergoing following heating steps as shown in Table 16.

*Table 16: Protocol of cDNA synthsis*

| Step | Temperature [C°] | Time [min] |
|---|---|---|
| **Primer annealing** | 25 | 2 |
| **cDNA synthesis** | 55 | 10 |
| **Heat-inactivation** | 95 | 1 |
| **Idle** | 4 | ∞ |

### 6.12.7 Sample preparation and qPCR

For each investigated strain in qRT-PCR, a serial dilution of its cDNA was assessed, using *dnaQ* as the investigated gene. For this purpose, a threefold dilution was assessed, using cDNA and nuclease-free $H_2O$ in a 1:3 proportion for 5 times, resulting in a final 1:243 dilution as shown in Table 17. cDNA and NACs for qRT-PCR analysis were diluted in 1:10 proportion.

*Table 17: Dilution steps and preparation of cDNA*

| Dilution | cDNA [µL] | H2O (RNAse free) [µL] |
|---|---|---|
| 1:3 | 3 of cDNA | 6 |
| 1:9 | 3 of 1:3 | 6 |
| 1:27 | 3 of 1:9 | 6 |
| 1:81 | 3 of 1:27 | 6 |
| 1:243 | 3 of 1:81 | 6 |

NACs were diluted 1:10 in RNAse-free $H_2O$. QRT-PCRs were performed using Luna® Universal qPCR Master Mix (New Englang Biolabs®). For each set of primers, master mixes were prepared, containing 0,25 µM of reverse and forward primers each, RNAse-free $H_2O$ and Luna® Universal qPCR Master Mix as shown in Table 18, cDNA is not present in the master mixes.

*Table 18: Components and their volumes of a qRT-PCR of one sample*

| Component | Volume cDNA [µL] | Final concentration |
|---|---|---|
| **cDNA product <100 ng** | 2 | <50 ng/µL |
| **Forward primer (10 pmol/µL)** | 0.5 | 0.25 |
| **Reverse primer (10 pmol/µL)** | 0.5 | 0.25 |
| **Luna® Universal qPCR Master Mix** | 10 | 1 x |
| **Nuclease-free $H_2O$** | Ad 18 µL | |
| **Σ (with cDNA)** | 20 | 20 |

For each master mix, 18 µl were added to a well of the 96-well-plate, supplemented with 2 µl diluted cDNA or RNAse-free $H_2O$ for a no template control. For each strain, 18 µl of *dnaQ* master mix were added into a well, supplemented with 2 µL diluted NAC. The whole plate was analyzed, using ViiA7 Real Time PCR System (Thermo Scientific) and QuantStudio™ Software, undergoing PCR program as shown in Table 19 and using settings as shown in Table 20.

*Table 19: Protocol of qRT-PCRs in ViiA7 Real Time PCR System*

| Step | Temperature [°C] | Time [s] | Cycles |
|---|---|---|---|
| **Initial denaturation** | 95 | 60 | 1 |
| **Denaturation** | 95 | 15 | 40 |
| **Annealing/elongation** | 60 | 30 | |
| **Final denaturation** | 95 | 15 | 1 |
| **Melting point analysis** | 60 → 95 (0.5/s) | 60 | 1 |
| **Melting point analysis II.** | 95 | 15 | 1 |

*Table 20: Experimental properties and Setup Standards of qRT-PCR reaction of the ViiA7 System*

| **Experiment Properties** | |
|---|---|
| Block | Fast 96-Well Block |
| Experiment | Relative Standard Curve |
| Reagents | SYBR Green Reagent |
| Instrument Run | Fast |
| Include Melt Curve | Yes |
| Passive Reference | ROX |
| **Setup Standards** | |
| Target | dnaQ |
| # of Point | 5 |
| # of replicates | 1 |
| Starting Quantity | 243 |
| Serial Factor | 1:3 |
| Analysis Settings | |
| Threshold | 0.2 |

### 6.12.8 Data analysis and statistics

For analysis of $C_T$-values, $\Delta C_T$ was calculated with $C_{T\,target} - C_{t\,dnaQ}$. For expression values $2^{-(\Delta CT)}$ was calculated. For overall expression, expression mean values of 3 biological samples were calculated. For biological significance analysis, a 2-sided student's t-test was performed, using matrices with 3 single expression values, each.

## *6.13 Generating mutant MIVb-300*

To determine the roles of mutations in *Escherichia coli* MIVb in (I) quinolone susceptibility and II) bacterial fitness, *E. coli* MIVb was cultivated for over 300 generations in the absence of antibiotics. Thus, it could be demonstrated I) when and II) which genomic mutations during this process occur to confer the restoration of bacterial fitness with a concomitant increase of quinolone susceptibility.

Mutant MIVb was cultivated in 100 mL LB growth medium and incubated at 37°C and 80 rpm on a rotary shaker. With almost 2 hours of doubling time, the cell culture was diluted 1:1000 every 24 hours. That makes 12 generations each day. After 25, 100, 200 and 300 generations, 100 µl cell material was taken for cryo cultures. In addition, 500 µl cell material was taken for a serial dilution to $10^{-7}$ as described in 6.2. 50 µl of the last four dilutions ($10^{-4}$ to $10^{-7}$) were plated on LB Agar and LB Agar, containing 128 µg/ml ciprofloxacin (1/2 of *Escherichia coli* MIVb's genuine MIC to CIP).

To determine fitness restoration of *Escherichia coli* MIVb from generation 25 to 300, overnight cultures of each strain were cultivated for a OCelloScope measurement. The OCelloScope (BioSense Solutions) is a live-cell imaging system, which provides monitoring of developing cells and growing cultures within 6 to 96-well plates. The system is supplied with a camera that focuses on the wells, combining optical techniques such as phase contrast, brightfield and confocal-like microscopy. The system acquires images along the horizontal plane to form a Z-stack, generated by build in algorithms. The software enables live monitoring and graphical illustrations of the developing cells, that can be analyzed by growth kinetic algorithms. Here, the background corrected absorption (BCA) was determined, which is similar to optical density measurements.

For this, overnight cultures of selected strains were diluted 1:1000 in LB broth to a final cell population of ~$10^6$ CFU/ml. 100 µl of this cell suspension was transferred to the wells of a 96-well plate (Thermo Nunclon, Thermo Scientific), that was subsequently placed in the OCelloScope. For each strain, at least 3 biological samples were investigated, and each biological sample was at least measured 3 times.

To investigate genomic alterations within the strains, genomic DNA was extracted from each strain, using the Monarch Genomic DNA Purification Kit from New England Biolabs and sent to GeneWIZ, according to the company's instructions for next generation sequencing.

# 7. Results

## *7.1 CRISPR-Cas-9 mediated genome editing*

### 7.1.1 CRISPR-Cas-9 mediated genome editing of *modB*

To investigate the role of either mutation, in *modB* and *rpoC* individually, strains carrying either mutation alone or in combination had to be established. Thus, *Escherichia coli* WT, the quinolone-susceptible progenitor strain of MIVb, was subjected to CRISPR-Cas9-mediated gene editing for investigating the impact of a single or a double mutation in a wild-type background, lacking any other mutation that has emerged in MIVb during the selection with high doses of quinolones. Thus, first, *modB* C316A (resulting in amino acid exchange ModB-L106M) was introduced into *Escherichia coli* WT, using the CRISPR-no-SCAR system as described by (Reisch and Prather, 2015).

Further, to investigate the function of either one mutation that emerged in MIVb during the selection process, combined with additional mutations in the direct progenitor of the selection process, *Escherichia coli* MIII, CRISPR-Cas9-mediated gene editing was used to introduce these mutations individually into mutant MIII. Following the same protocol as mentioned above, *Escherichia coli* MIII/ModB-L106M was generated. Accordingly, *Escherichia coli* MIII/RpoC-P246Q, which has been generated in another project using the same procedure was used here as well (D. Rönfeldt, unpublished). All bacterial strains in this work are shown in 5.7.

To initiate CRISPR-no-SCAR editing, single guide RNA has to be prepared, using the

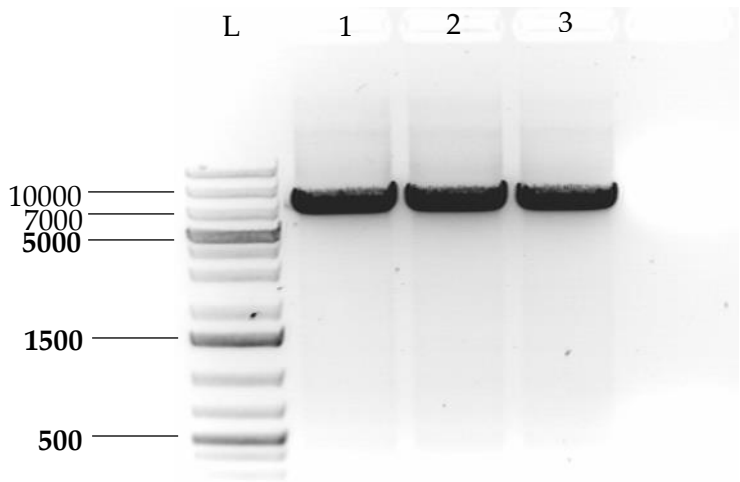


*Figure 10: DpnI digest of rolling circle PCR amplified products on a 1%(w/v) agarose gel after electrophoresis for 1h at 100V. (L) 1 kb plus GeneRuler DNA Ladder (Thermo Scientific). (1-3) Products of rolling circle PCR from 6.10.1] after DpnI digest. Numbers indicate respective size of fragments in base pairs.*

pKDsgRNA-ack plasmid as the origin of the sequence to be cut. For the preparation of the plasmid that contains the *modB* sequence, designated as pKDsgRNA-*modB*, rolling circle PCR was used to insert the *modB*-N20-sequence in pKDsgRNA-ack. The amount of DNA as well as its purity was subsequently measured with NanoDrop. Then, after a DpnI-digest, the PCR product was analyzed on an electrophoresis with agarose. As shown in Figure 10, PCR products of 6948 bp are indicated next to a DNA ladder (GeneRuler 1kb plus, Thermo Scientific™). Then the product was extracted, using the GeneJET Gel Extraction Kit (Thermo Scientific™) and the concentration of the extracted PCR product was determined as 20 ng/µl. Extracted PCR product was used for a ligation, using T4 DNA Ligase (see Table 5). Ligation Electrocompetent JM109 cells were transformed with the ligation and after 45 min incubation subsequently plated on LB Agar plates with 50 µg/ml ampicillin. Ampicillin-resistant colonies were replated on selective agar. Subsequently, plasmids were isolated by alkaline lysis (6.5) and digested with EcoRI. In accordance with the known sequence map (Figure 11), this yielded three fragments of pKDsgRNA-*modB* plasmid of 2,868 bp, 2,551 bp and 1,509 bp, as shown in Figure 12

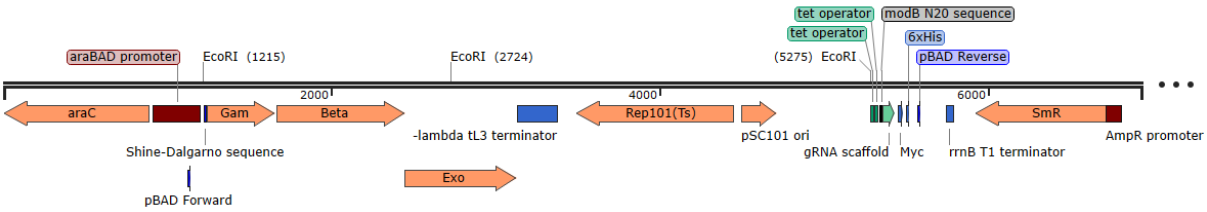


*Figure 11: Schematic illustration of pKDsgRNA-modB plasmid for CRISPR-Cas9 mediated gene editing. Restriction sites of EcoRI are indicated at position 1215, 2724 and 5275. The total size of the plasmid is 6928 base pairs.*

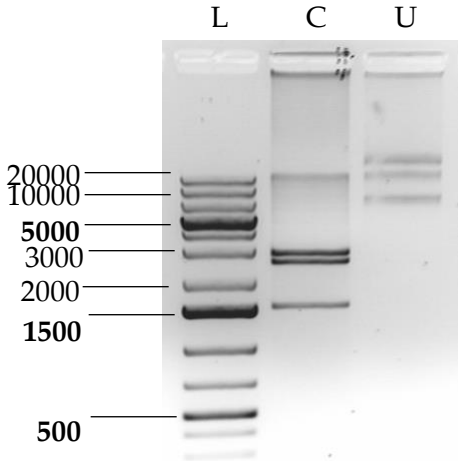


*Figure 12: EcoRI digest of pKDsgRNA-mod plasmid on a 1%(w/v) agarose gel after electrophoresis for 1h at 100V. (L) 1 kb plus GeneRuler DNA Ladder (Thermo Scientific). (C) EcoRI digest of pKDsgRNA-modB. (U) uncut vector pKDsgRNA-modB. Numbers indicate respective size of fragments in base pairs*

In the second lane, pKDsgRNA-*modB* sample from alkaline lysis was added to the agarose gel as a control reference.

#### *7.1.1.1 Pyrosequencing of pKDsgRNA-modB*

The N20 sequence of pKDsgRNA-*modB* was further verified by pyrosequencing, using pKDsgRNA-*modB*, obtained by alkaline lysis as a template. As shown in Figure 13, bands of about 300 bp in size in lanes 1 to 3 are indicative of the presence of a PCR product of 291 bp

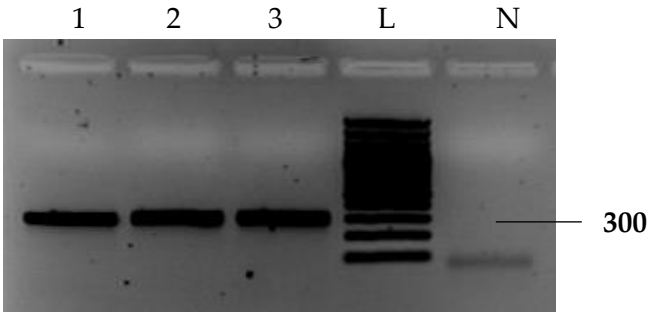


*Figure 13: Pyrosequencing PCR products on a 1%(w/v) agarose gel after electrophoresis for 1h at 100V. (1-3) PCR products of pyrosequencing PCR (L) 100bp plus GeneRuler DNA Ladder (Thermo Scientific). (N) No template control. Numbers indicate respective size of fragments in base pairs.*

size. Lane 4 shows a no template control. The given sequence 5'-CGAATTGCCCGCACCATCAGGTTTT-3' was confirmed by the result of the pyrosequencing (Figure 14).

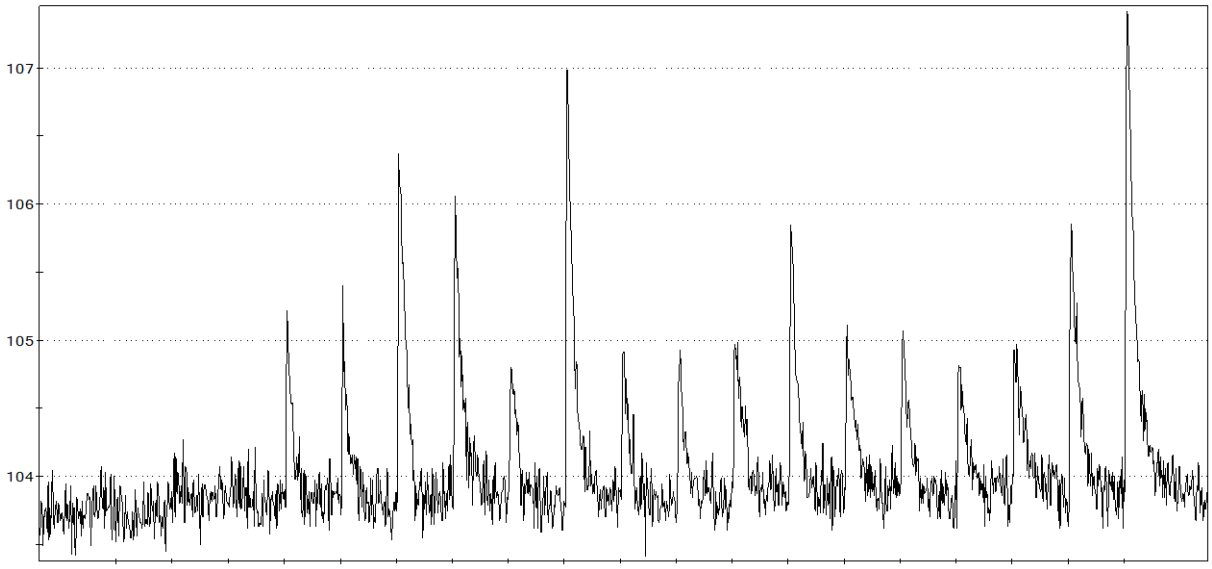


*Figure 14: Pyrogram of pKDsgRNA-modB plasmid. (E) Enzyme. (S) Substrate. (A) Adenine. (C) Cytosine. (G) Guanine. (T) Thymine. Resulting DNA sequence: 5'-CGAATTGCCCGCACCATCAGGTTTT-3'.*

#### 7.1.1.2 *Transformation with oligonucleotide CRISPR_[modB_375rv_EscCol_noSCAR]*

For the subsequent CRISPR-Cas9 no-SCAR procedure, the selected parental strains of *E. coli* WT and MIII to be edited, were first transformed with plasmid pCas9-CR4 isolated from *E. coli* JM109. Transformants were selected with 100 µg/ml chloramphenicol, before transforming them with plasmid pKDsgRNA-modB by electroporation. Double transformants grown in SOB medium to an optical density at 600 nm of 0.3, followed by arabinose induction. Competent cells were transformed with the respective oligonucleotide, using electroporation protocol. Following transfer into SOC medium for regeneration, transformants were diluted in 0.9% NaCl and plated on LB Agar plates, containing spectinomycin, anhydrotetracycline and a strain specific concentration of chloramphenicol.

*Table 21: Colony forming units of either electrocompetent cells of Escherichia coli WT + pCas9cr4 + pKDsgRNA-modB (WT) and Escherichia coli MIII + pCas9cr4 + pKDsgRNA-modB (MIII) after plating aliquots of serial dilutions from $10^{-1}$ to $10^{-7}$ on growth control plates (Spec, Clm), activity control plastes (Spec, Clm, aTet) or cells after oligonucleotide transformation. Percentages indicate gain or loss of CFUs between the columns.*

| **WT** | **Growth control** | | **Activity control** | | **Oligo transformation** |
|---|---|---|---|---|---|
| | $10^{-7}$ = 7 | **-99,95 %** | $10^{-7}$ = 0 | **+35%** | $10^{-7}$ = 0 |
| | | → | $10^{-6}$ = 0 | → | $10^{-6}$ = 0 |
| | | | $10^{-5}$ = 0 | | $10^{-5}$ = 0 |
| | | | $10^{-4}$ = 3 | | $10^{-4}$ = 4 ↓ |
| | | | | | $10^{-3}$ = 42 |
| **MIII** | **Growth control** | | **Activity control** | | **Oligo transformation** |
| | $10^{-7}$ = 18 | **-99,6 %** | $10^{-7}$ = 0 | **-78%** | $10^{-7}$ = 0 |
| | | → | $10^{-6}$ = 0 | → | $10^{-6}$ = 0 |
| | | | $10^{-5}$ = 4 | | $10^{-5}$ = 0 |
| | | | $10^{-4}$ = 44 | | $10^{-4}$ = 60 ↓ |
| | | | | | $10^{-3}$ = 627 |

Table 21 shows CFUs of both transformed strains, *Escherichia coli* WT and *Escherichia coli* MIII, after oligonucleotide transformation (Here designated WT and MIII) at respective dilution stages. In both strains, there is a decreasing number of CFU, when electrocompetent cells were plated on LB Agar with anhydrotetracycline (decrease from growth control to activity control). When compared to actual transformed strains (oligo transformation), CFUs increase to 35% in WT strain and decrease 78% in MIII, indicating a success of the oligo transformation process in WT. However, both transformed strains were further tested via ARMS-PCR for validating positive oligonucleotide transformation.

*7.1.1.3 ARMS-PCR screening of positive clones of modB C316A*

To verify that oligonucleotide transformation was successful, an ARMS PCR targeting the desired *modB*(C316A) mutation was performed. Template DNA was isolated from selected transformants grown on LB Agar plates containing respective concentrations of spectinomycin, chloramphenicol and anhydrotetracycline (see 7.1.1.2). For mutation detection, a 18 nt oligonucleotide was used, containing a two nucleotide mismatch affecting the respective *mod*B sequence in *Escherichia coli* MIVb (Table 8). As positive and negative controls,

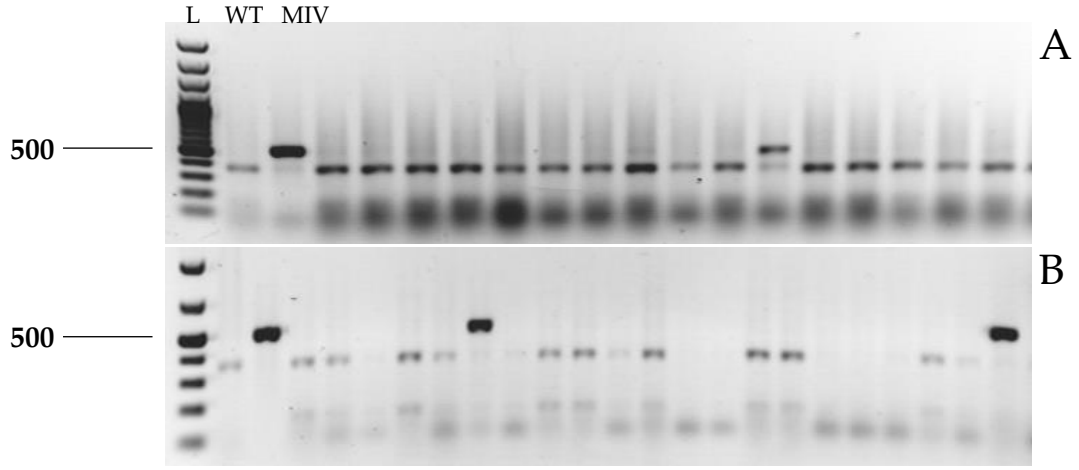


*Figure 15: ARMS-PCR screening of Escherichia coli WT (A) and Escherichia coli MIII (B) for modB C316A mutation. (L) 100 bp plus GeneRuler (Thermo Scientific). (WT) ARMS with boiling DNA of Escherichia coli WT as template (negative control). (MIV) ARMS with boiling DNA of Escherichia coli MIVb as template (positive control). Untagged lanes show the respective bands of the tested colonies. Numbers to the left indicate respective size of fragments in base pairs.*

PCR fragments of *modB* from MIVb (contains mutation in *modB* at pos. 316 C→A), WT (contains no mutation), respectively, were added to each sample. As shown in Figure 15A, results of ARMS-PCR screening for positive colonies shows, that most of the colonies were not transformed with the oligonucleotide. As shown in the first lane, ARMS-PCR of *Escherichia coli* WT shows a band that is repeatedly seen in most of all lanes. As indicated in lane 2, ARMS-PCR of *Escherichia coli* MIVb (contains the *modB* mutation C316A), the band is located at a higher position indicating successful mutagenesis. This specific band can also be observed in lane 13. Similar effects were detectable in results obtained for MIII positive controls. As shown in Figure 15B, lane 1 and 2, exactly matching those in Figure 15A, indicate a negative and a positive control, using as a template DNA from WT and MIVb, respectively. As shown here, two positive results are detectable in lanes 8 and 23. These two agarose gels are representative of the remaining agarose gels, used for ARMS-PCR screening. *modB* gene fragments from at least 3 positive amplicons of either WT or MIII, were amplified and used for sanger sequencing

(Eurofins Genomics GmbH). Among the samples investigated the following CRISPR-cas9-clones were identified as carriers of *modB* C316A): #WT13, #MIII8.

#### 7.1.1.4 *Sanger sequencing of modB.*

The mutation C316A leads to an ATG, instead of an CTG in the open reading frame, resulting in a methionine, replacing a leucin in the amino acid sequence. As shown in Figure 16, the DNA sequence shows ATGs instead of CTGs at the specific position.

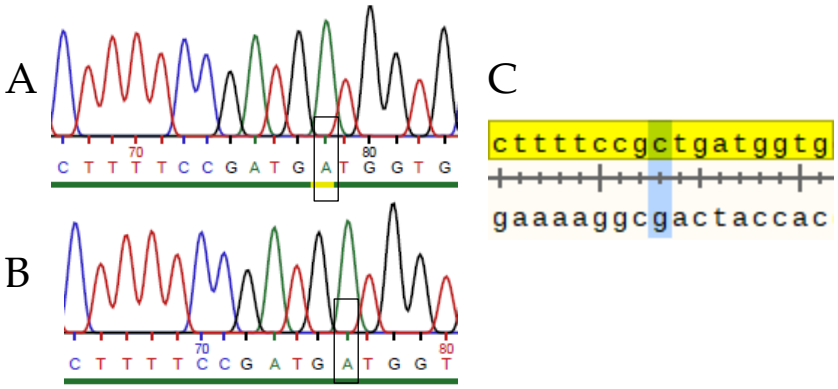


*Figure 16: Sequences of modB from Escherichia coli WT/ModB-L106M (A) and Escherichia coli MIII/ModB-L106M (B) attained with Sanger sequencing. At pos. 78 (A) and pos. 76 is an adenine, instead of a cytosine. (C) Sequence Escherichia coli WT. Shown are the positions 305 to 321 of modB. At position 316, CRISPR-Cas9-mediated strains show an A instead of C in the upper lane.*

Here, CRISPR-Cas mediated gene editing was used to generate *Escherichia coli* WT/ModB-L106M and *Escherichia coli* MIII/ModB-L106M. With his, the effects of the *modB* mutation in wild type and MIII background can be verified. *Escherichia coli* MIII/ModB-L106M/RpoC-P246Q, which also contains a *rpoC* mutation was established as well (next chapter).

### 7.1.2 Establishment of CRISPR-Cas9 mediated *Escherichia coli* variant *E. coli* WT/ModB-L106M/RpoC-P246Q

Since quinolone selection introduced two mutations, ModB-L106M and RpoC-P246Q into *Escherichia coli* MIVb, a double mutant, carrying both mutations in a wild-type background was generated subsequently. The purpose was to analyze, if these mutations in combination might have a synergistic effect on the bacterial strains. A CRISPR-Cas9 edited *rpoC* C737A mutation strain on wild-type background was already established in the lab, however, further gene editing seemed to be troublesome, since the activity control always showed a minor loss when compared to growth control as opposed to other strains (data not shown). The reason

for this is not well understood, however it was speculated that RNA-Polymerase activity played an essential role in this process, since *rpoC* encodes the β'-subunit of RNA-Polymerase, and it was hypothesized that this might lead to alterations within the transcriptome of the cell. To create an *Escherichia coli modB/rpoC* double mutant on a wild-type background, *Escherichia coli* WT/ModB-L106M was used as the output strain and CRISPR-Cas9 mediated gene editing was performed, using pKDsgRNA-*rpoC*737 plasmid and a *rpoC*737-oligonucleotide in ~80 nucleotides in size that was aimed to substitute *rpoC* during endonuclease activity of Cas9. The following paragraphs describe the CRISPR-Cas9 mediated gene editing of *Escherichia coli* WT/ModB-L106M to establish the *Escherichia coli* WT/ModB-L106M/RpoC-P246Q double mutant.

#### *7.1.2.1 Transformation of Escherichia coli WT/ModB-L106M with CRISPR plasmids*

As described in 6.10.4, the first step of this process is to transform the selected strains with both plasmids for CRISPR-Cas9-mediated gene editing, pKDsgRNA-*rpoC*737 to guide Cas9 endonuclease to its destination and pCas9cr4 to introduce the Cas9 enzyme into the cell. As opposed to the creation of *modB*-C316A-carrying strains, pKDsgRNA-*rpoC*737 plasmid was already established in the lab. Thus, *Escherichia coli* WT/ModB-L106M was transformed with a) pCas9cr4, that was already isolated from a wild-type background and subsequently b) pKDsgRNA-*rpoC*737. Transformants of pCas9cr4 (*Escherichia coli* WT/ModB-L106M + pCas9cr4) were plated on LB Agar plates, supplemented with 100 µg/ml chloramphenicol and transformants of pKDsgRNA-*rpoC*737 (*Escherichia coli* WT/ModB-L106M + pCas9cr4 + pKDsgRNA-*rpoC*737) were plated on LB Agar plates, supplemented with 100 µg/ml Chloramphenicol and 100 µg/ml Spectinomycin.

#### *7.1.2.2 Transformation of cells with rpoC oligonucleotide*

Transformed strains of 7.1.2.1 were then inoculated, grown to an $OD_{600}$ of 0.3 and subsequently induced with L-Arabinose as described in 6.10.5. Transformation of oligonucleotide was performed as described in 6.10.5. The results of the oligonucleotide transformation are shown in Table 22.

*Table 22: Colony forming units of either electrocompetent cells of Escherichia coli WT/ModB-L106M + pCas9cr4 + pKDsgRNA-rpoC737 after plating aliquots of serial dilutions from 10-1 to 10-7 on growth control plates (Spec, Clm), activity control plastes (Spec, Clm, aTet) or cells after oligonucleotide transformation. Percentages indicate gain or loss of CFUs between the columns.*

| RpoC | Growth control | | Activity control | | Transformation |
|---|---|---|---|---|---|
| | $10^{-7}$ = 1 | **-91,84%** | $10^{-7}$ = 0 | **+6.5%** | $10^{-7}$ = 0 |
| | $10^{-6}$ = 4 | → | $10^{-6}$ = 1 | → | $10^{-6}$ = 1 |
| | $10^{-5}$ = 42 | | $10^{-5}$ = 2 | | $10^{-5}$ = 2 |
| | $10^{-4}$ = 321 | | $10^{-4}$ = 30 | | $10^{-4}$ = X |
| | | | $10^{-3}$ = 262 | | $10^{-3}$ = 280 |

### *7.1.2.3 ARMS-Screening*

Transformed strains from 7.1.2.2 were subsequently used for ARMS-Screening to detect positive clones, that were the carrying *rpoC* C737A substitution mutation. For specific procedures, see 6.10.11. For positive controls for ARMS-PCR screening, boiling DNA of *Escherichia coli* MIVb was used. For negative controls, boiling DNA of *Escherichia coli* WT was used. The screening of positive clones is shown in the following Figure 17.

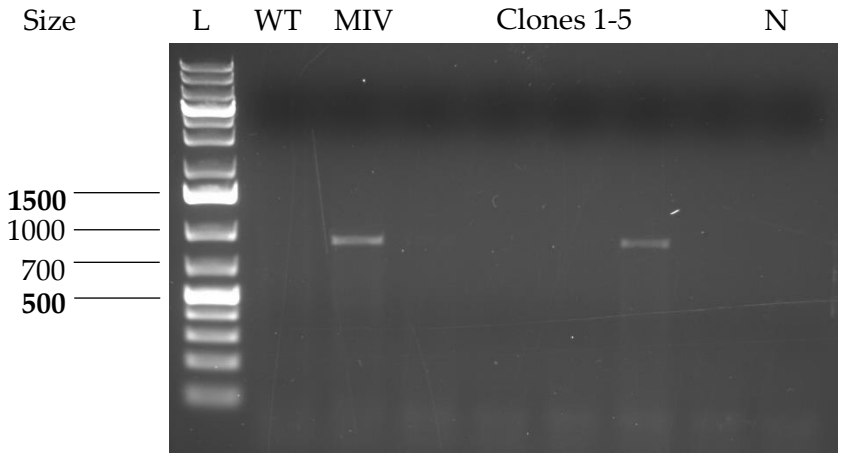


*Figure 17: Detection of rpoC C737A-variants in Escherichia coli transformants from 7.1.2.2 by ARMS-PCR on a 1%(w/v) agarose gel after electrophoresis for 1h at 100V. (L) 1 kb plus GeneRuler (Thermo Scientific). (WT) ARMS-PCR of Escherichia coli WT (negative control). (MIV) ARMS-PCR of Escherichia coli MIVb (positive control). (Clones 1-5) ARMS-PCR of transformants from 7.1.2.2, showing a positive match in lane 4. Each well represents a different clone. (N) No template control.*

As shown in Figure 17, a band is clearly visible at a position between 100 bp and 700 bp, as indicated by the DNA Ladder in well L. Within the ARMS-PCR of different clones, as indicated at the same size, a visible band at this specific position occurs in the second last of the tested clones. Figure 17 is a positive representation of at least 50 tested colonies from the transformation assay. Positive clones were picked and used for Sanger sequencing to confirm the C737A mutation within *rpoC*.

#### 7.1.2.4 *Sanger sequencing of positive clones*

Genomic DNA of the positive clones was extracted, using the Monarch genomic DNA extraction Kit (New England Biolabs), according to the manufacturer's instructions for a PCR reaction to amplify *rpoC* as described in 6.10.11. Subsequently, the amplicon was then synthesized and purified for Sanger sequencing. As shown in Figure 18, a mutation within the gene can be detected at nucleotide 737 of gene *rpoC* at position.

```
CTGCCGGTACTGCCGCCAGATCTGC
||||||||||||| ||||||||||||
CTGCCGGTACTGCAGCCAGATCTGC
```

*Figure 18: A nucleotide blast shows an alignment of the rpoC sequence from 724 to 748, where rpoC from WT (upper sequence) is aligned against the rpoC sequence from E. coli WT/ModB-L106M/RpoC-P246Q (lower sequence), that was determined by Sanger Sequencing.*

## 7.2 *FRET-based quantification*

We hypothesized that the mutation in *modB* might affect the molybdate uptake. To analyze this, a measurement system for molybdate levels *in vivo* was introduced here. The MolyProbe, a plasmid-based Förster-Resonance Energy Transfer (FRET) system, is directly affected by increased or decreased levels of the molybdenum trace ion. The recombinant protein consists of two metal binding site regions, coupled to a yellow fluorescence protein (YFP) and a cerulean fluorescence (CFP) protein. In case of molybdate binding, a subsequent conformational change occurs within the MolyProbe, leading to a spatial convergence between the two fluorescent domains. Subsequently, in case of excitation, energy transfer takes place between the domains. In this case, excitation of one domain does not only lead to an emission of itself but also of the approximated domain. With this, alterations in molybdate incorporation are detectable. Before analyzing a mutation in CRISPR generated mutants of *modB*, it was first investigated if a *modB*-knockout strain, JW0747-1 has decreased molybdenum levels when comparing it to its parental strain, BW25113.

### 7.2.1 FRET signaling in BW25113 and JW0747-1

As shown in Figure 19, FRET/CFP-Ratios drop 17.28%, when *modB*-knockout is present in *E. coli*, indicated by a decreasing FRET/CFP ratio in the *modB*-knockout strain *E. coli* JW0747-1. Since a permanent knockout of *modB* leads to a non-functioning molybdate ABC transporter membrane subunit, it was highly presumable that FRET/CFP-Rations would decrease, but unclear to what extent.

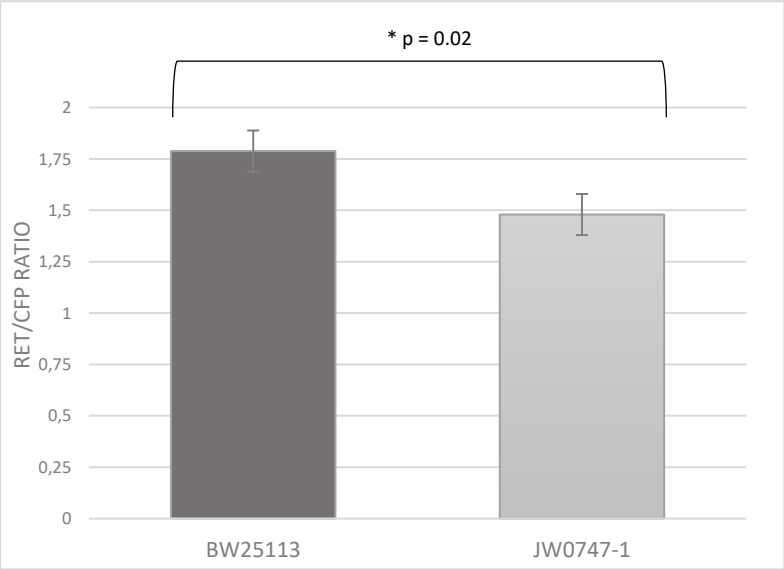


*Figure 19: FRET/CFP ratios of E. coli BW25113 and E. coli JW0747-1 strains in molybdate-supplemented growth medium. FRET/CFP ratios in modB-knockout JW0747-1 are at 1.48, whereas BW25113 shows 1.79. Statistical significance was assessed with a p-value of 0.02 with a 2-sided student's t-test.*

### 7.2.2 FRET signaling in *E. coli* CRISPR strains

After assessing the determination of molybdate uptake in *Escherichia coli* K-12 strains BW25113 and JW0747-1, those of *E. coli* WT/ModB-L106M and *E. coli* WT/ModB-L106M/RpoC-P246Q was determined. However, minor adjustments in the conditions of the cultivation process were made. When *E. coli* K-12 strains showed strong signals at $OD_{600}$ = 0.7, wild-type strains showed rather weak signals at this concentration of cell material. In this case, the cultivation process was extended to an $OD_{600}$ = 1.5.

Previously, *Escherichia coli* WT, *Escherichia coli* WT/ModB-L106M and *Escherichia coli* WT/ModB-L106M/RpoC-P246Q were transformed with either pYN627 or a mock control vector, pBlueScript II SK (+) for background signaling. Transformation of wild-type strains was performed using the electroporation protocol. As shown in Figure 20, FRET/CFP-Ratio drops from 0.77 to 0.72 when ModB-L106M was introduced into wild-type strains. When

RpoC-P246Q mutation is also introduced into the strain, ratios drop to 0.74. As mentioned before, cultivation processes had to be adjusted when measuring in wild-type *Escherichia coli*, in which the number of harvested cells were drastically increased to detect appropriate FRET and CFP signals *in vivo*. Yet, FRET/CFP-Ratios are only about 40% intensity, compared to *E. coli* K-12 strains.

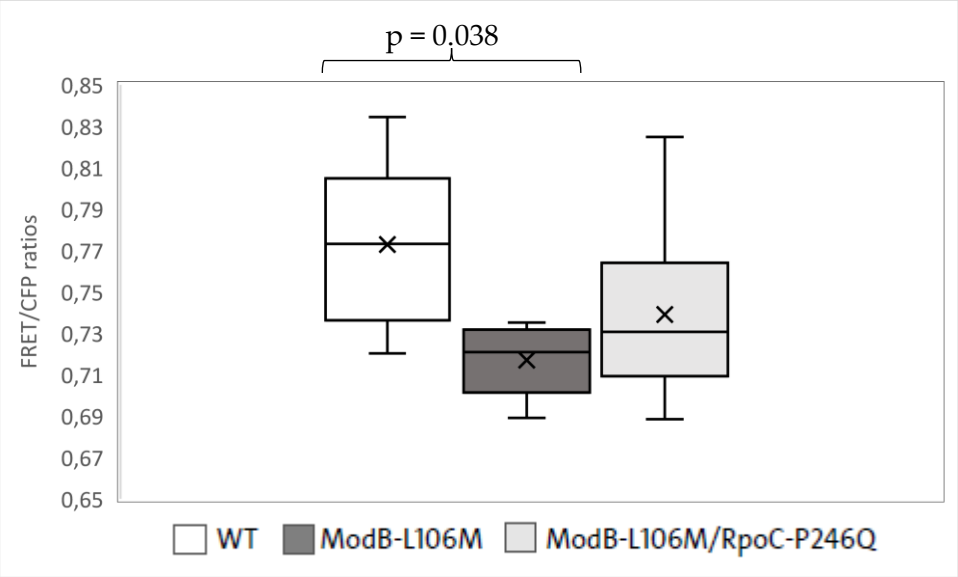


*Figure 20. FRET/CFP ratios of E. coli WT, E. coli WT/ModB-L106M and E. coli WT/ModB-L106M-RpoC-P246Q strains in molybdate-supplemented growth medium. FRET/CFP ratios of WT = 0.77, ModB-L106M = 0.72 and ModB-L106M/RpoC-P246Q 0.74. Statistical significance was assessed with a p-value of 0.038 for ModB-L106M, compared to wild type with a 2-sided student's t-test.*

*E. coli* K-12 strains have a very different phenotype than wild-type isolates. A difference in morphology results in different light scattering, when passing cell membranes. A general loss of fluorescence signals can be explained that way.

In both measurements, with a) *Escherichia coli* K-12 strains from keio collection and b) *Escherichia coli* wild-type isolates, six biological samples were investigated, respectively. Both experiments, the *modB* knockout in *E. coli* JW0747-1 as well as the loss of function mutation in *Escherichia coli* wild-type isolate, *E. coli* WT/ModB-L106M showed a significant reduction of molybdate uptake with a statistical significance of a) p = 0.02 and b) p = 0.038 when using a 2-sided student's t-test. Differences between *E. coli* WT and *E. coli* WT/ModB-L106M/RpoC-P246Q showed no statistical significance.

## *7.3 Gene expression analysis with qRT-PCR*

Quantitative real-time PCR is a commonly used technique for analyzing gene expression in cells. In this experiment, genes involved in the formation of reactive oxygen species, anaerobic growth as well as genes that are regulated by SoxS and ModE were analyzed. The aim was to determine, whether a mutation in *modB* or *rpoC* leads to differentiated gene expression.

A whole genome transcriptomics analysis prior to qRT-PCR (data not included in this work) revealed differences in genes between the strains MIII and MIVb. Since the difference between these strains are represented by two mutations, within *modB* and *rpoC*, it was unclear, if those differences could be referred to either one of them, or both. For this purpose, qRT-PCR was performed in CRISPR-Cas9-mediated mutants, *E. coli* MIII/ModB-L106M and *E. coli* MIII/RpoC-P246Q, lacking either one of those mutations. Transcriptomics data prior to this experiment revealed differentiated expression patterns in *msrQ*, *fdnG*, *soxS*, *ynfG*, *torA* and *narV*.

### 7.3.1 Genes regulated under anaerobiosis

Many of those genes are regulated by FNR, a key regulator to anaerobic growth. To underline differences in gene expression, cells were grown under aerobic and anaerobic conditions. To have a positive and a negative control, MIII and MIVb strains were taken into consideration as well. To determine the induction of anaerobic growth, *dmsA*, that is highly expressed under anaerobic conditions, was taken into the experiment as well. We can see that, under anaerobic growth conditions, *dmsA* levels increase up to a 130-fold times higher expression compared to expression of cells that grew under aerobic growth conditions, as seen in Figure 21.

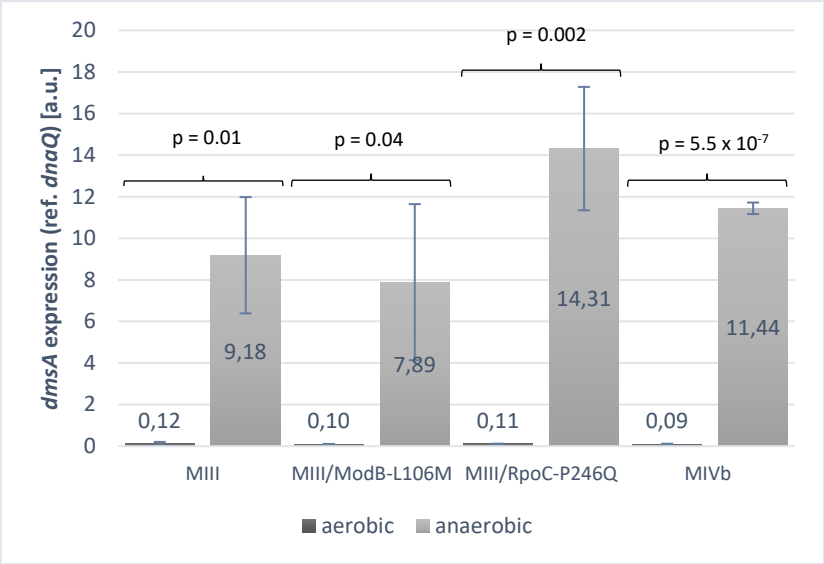


*Figure 21: Gene expression levels of dmsA from aerobic growth compared to anaerobic growth. When grown anaerobically, each strain showed increased expression of dmsA, compared to aerobically grown.*

Data analysis of *msrQ, fdnG, soxS, ynfG, torA and narV* gene expression during anaerobic growth revealed that the presence of RpoC-P246Q mutation within a strain leads to *fdnG* amounts similar to aerobic conditions, suggesting RpoC-P246Q to inhibit expression of *fdnG* during anaerobic growth as seen in Figure 22. When performing a 2-sided student's t-test, the comparison between a RpoC-P246Q carrying MIII and its progenitor strain showed a biol. significance of p = 0.01, with 25-fold lower levels of *fdnG* expression, when grown under anaerobic conditions. The other genes showed no differentiated expression, when grown anaerobically.

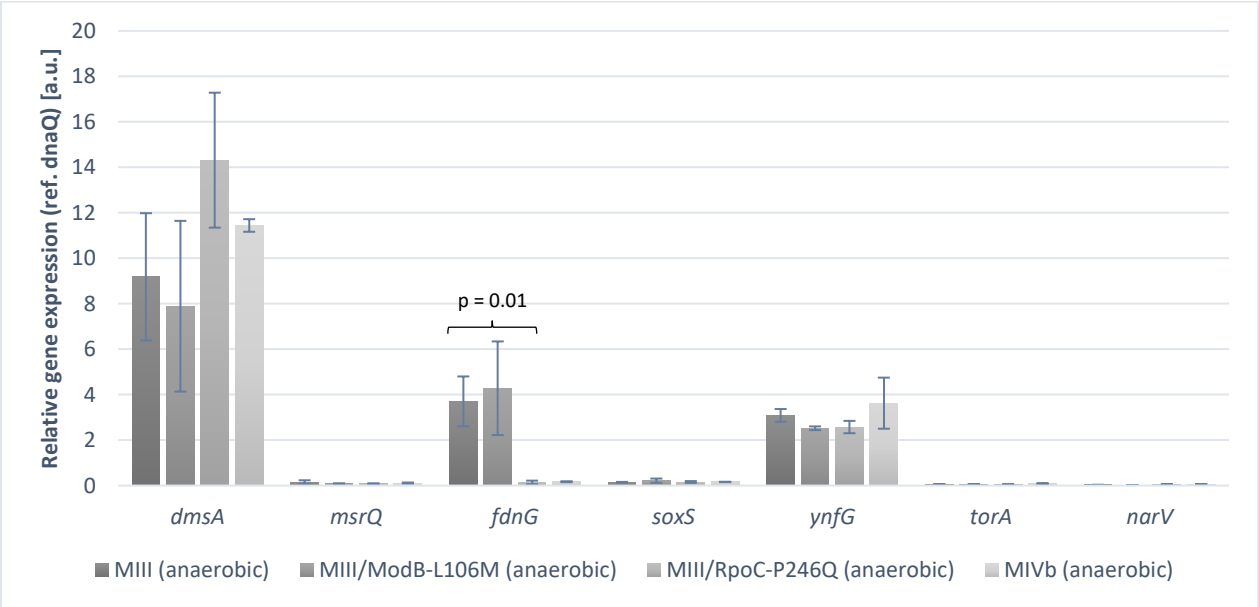


*Figure 22: Gene expression levels of dmsA, msrQ, fdnG, soxS, ynfG, torA and narV under anaerobic growth conditions. fdnG levels in strains with RpoC-P246Q are not induced by anaerobiosis.*

However, when the strains were grown under aerobic conditions, three strains, *E. coli* MIII/ModB-L106M, *E. coli* MIII/RpoC-P246Q as well as *E. coli* MIVb, showed decreased expression of *soxS*, a key regulator of a vast number of genes in response to oxidative stress. As seen in Figure 23, *soxS*-levels drop 3-fold, when ModB-L106M is present and drop about 6-fold when RpoC-P246Q is present (evaluation of a 2-sided student's t-test was performed with 3 biol. samples of MIII, which were either compared to MIII/ModB-L106M or MIII/RpoC-P246Q with n = 3, respectively).

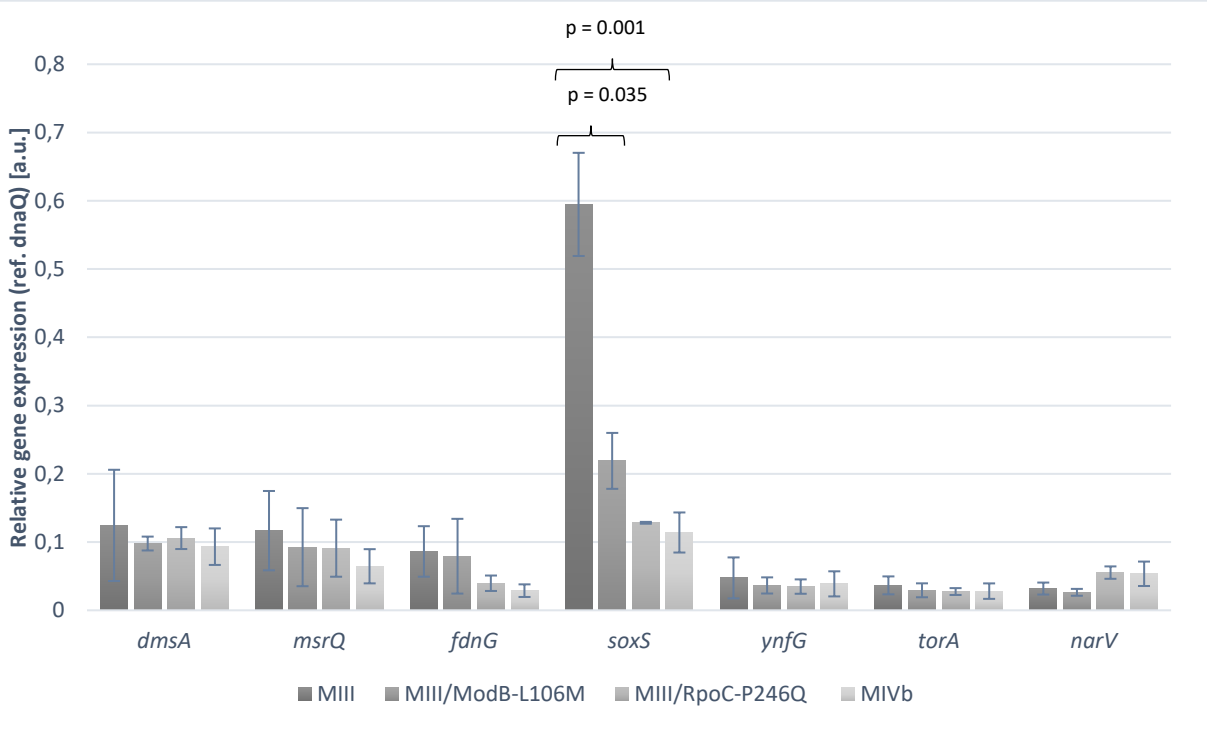


*Figure 23: Gene expression levels of dmsA, msrQ, fdnG, soxS, ynfG, torA and narV under aerobic growth conditions. In MIII/ModB-L106M, MIII/RpoC-P246Q as well as MIVb only little soxS expression can bee seen, compared to MIII.*

### 7.3.2 Gene regulation by *soxS*

Since *soxS*-levels decrease, when carrying ModB-L106 or RpoC-P246Q either alone or in combination (*E. coli* MIVb), it was further investigated, if an induction of *soxS* would lead to differentiated expression pattern in genes that are regulated by SoxS. For this approach, each strain was treated with the ROS-triggering agent paraquat with 1-fold of its MIC (MICs were taken from MIII or MIVb and adopted to MIII/ModB-L106M or MIII/RpoC-P246Q, respectively, paraquat MICs were provided from unpublished lab data) for 1 hour after attainment of an $OD_{600}$ = 0.4 and prior to harvest. Treatment of paraquat leads to formation of reactive oxygen species, thus an enhanced activation of *soxS*, as described by Zheng et al. (Zheng et al., 1999). To investigate *soxS*-regulated genes in response to oxidative stress, the

expression levels ROS-related genes were quantified with qRT-PCR. For that purpose, *soxS*-regulated genes like *acrA* (TolC efflux pump), *sodA* (Superoxid dismutase) or *oxyR* (Oxidative stress regulator), to name a few, were taken into analysis, most of them have been taken from an *E. coli* database (Keseler et al., 2021)

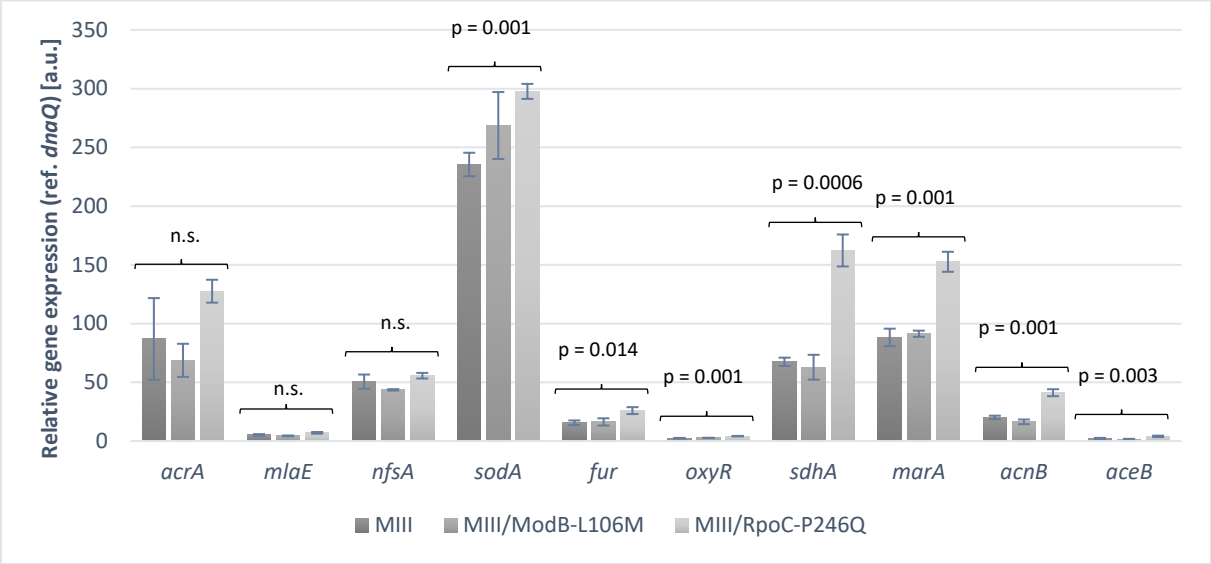


*Figure 24: Gene expression levels of soxS-regulated genes after soxS-induction with the ROS-triggering agent paraquat in E. coli mutants with MIII background. No significant alterations in acrA, mlaE and nfsA. MIII/RpoC-P246Q shows significantly higher expressions of sodA, fur, oxyR, sdhA, marA, acnB and aceB as compared to other strains.*

As shown in Figure 24, all investigated genes, except *acrA*, *mlaE* and *nfsA* showed significant higher expression levels, than in MIII, when the RpoC-P246Q mutation was present. A differentiated expression pattern of these genes was not detected in MIII/ModB-L106M. Statistical significances were determined using a 2-sided student's t-test with 3 biological samples of each strain. P-values are indicated over the bars. With this experiment it was able to determine the impact of RpoC-P246Q on gene regulation in response to oxidative stress. However, the observed differences in the expression of *soxS*-regulated genes cannot ascribed to RpoC-P246Q exclusively, since the progenitor strain MIII, that it was compared to, implicates six other mutations. Thus, it is possible that RpoC-P246Q plays a role in transcriptomics in response to oxidative stress, but possibly in combination with progenitor strain mutations that were introduced into the strain during quinolone selection.

### 7.3.3 Characterization of the SoxS regulon in wild-type background

To examine the possibility, if RpoC-P246Q promotes gene regulation upon oxidative stress in the absence of other mutations, the expression profiles of *soxS*-regulated genes in CRISPR-

Cas9-modified wild-type strains carrying RpoC-P246Q, were determined and compared to those of its progenitor strain, *Escherichia coli* wild-type under the same conditions as in 7.3.2. As shown in Figure 25, the observed upregulation of the *soxS*-regulon by RpoC-P246Q, as seen in MIII background (Figure 24) is diminished in the absence of MIII-mutations, as has been demonstrated in *E. coli* wild-type background. Neither one of the genes tested showed any significantly altered expression, neither driven by RpoC-P246Q or ModB-L106M in a wild-type background.

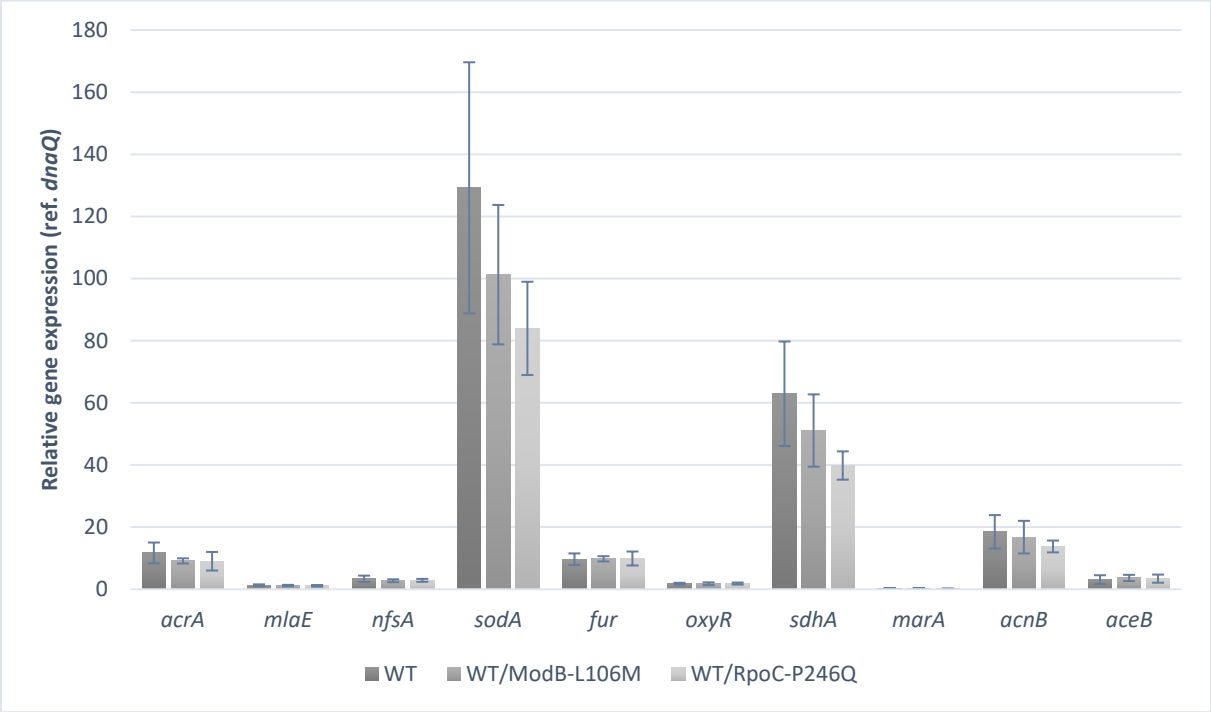


*Figure 25: Gene expression levels of soxS-regulated genes after paraquat treatment in E. coli mutants with wild-type background. No significant alterations are detectable within the stains.*

### 7.3.4 Molybdate regulated genes in *E. coli* WT/ModB-L106M

As indicated in Figure 20, ModB-L106M mutation results in a loss of function in the ModABC molybdate-transport protein. Since molybdate in association with *modE* controls a set of genes in *E. coli*, molybdate-regulated genes were analyzed by qRT-PCR: *modB*, *moaA*, *narL*, *oppA*, *napA*, *hycE* and *deoA*. To determine the impact on anaerobiosis on *modE*-regulon within MIII/ModB-L106M compared to MIII, cells were grown anaerobically to an $OD_{600}$ = 0.35 prior to cell harvest. RNA isolation, cDNA synthesis and qRT-PCR were performed subsequently as described in 6.12.2 - 6.12.8. As indicated in Figure 26, no significant differences in can be observed in *modE*-regulated genes within the MIII *modB*-mutant strain, when compared to its MIII progenitor during anaerobiosis.

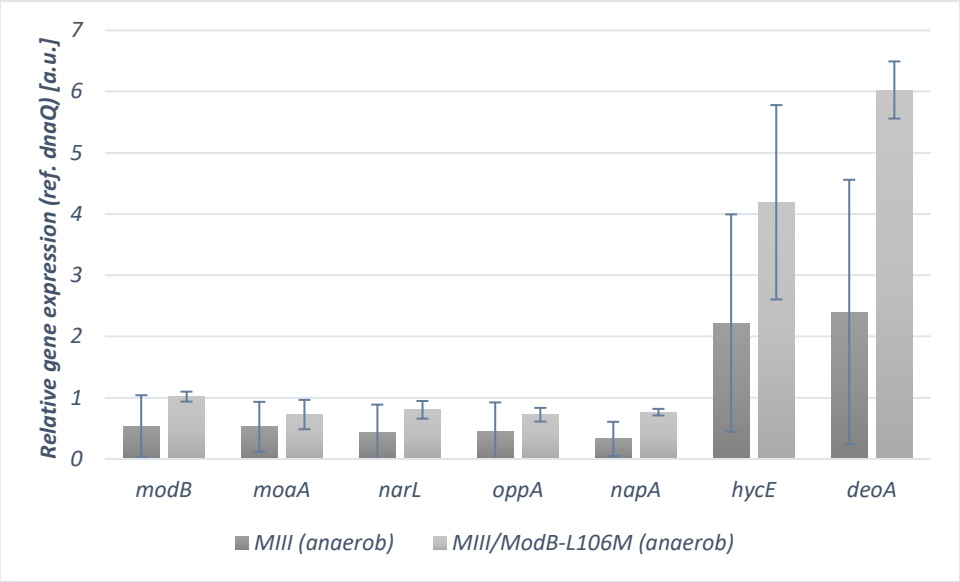


*Figure 26: Gene expression levels of molybdate/ModE regulated genes. Only little, but not statistically significant increasing expressions within molydate/ModE regulated genes can be observed within MIII/ModB-L106M, when compared to MIII.*

### 7.3.5 Summary qRT-PCR data

The first step in this process was to reproduce the data that was gathered during whole genome transcriptomics. For this purpose, expression profiles of *dmsA*, *msrQ*, *fdnG*, *soxS*, *ynfG*, *torA* and *narV* were analyzed since those genes showed minor differences during transcriptomic analysis. Since some of these genes play a role an anaerobiosis, thus cell harvest prior to qRT-PCR was performed under I) aerobic and II) anaerobic conditions to underline the effects that were observed during whole genome transcriptomics that exclusively took place in aerobic environment.

During aerobic growth, *soxS* expression levels dropped ~7-fold from MIII to MIVb during transcriptomics (data not shown). In quantitative real-time PCR, soxS-levels drop ~4.5-fold from MIII to MII/RpoC-P246Q (0.59 a.u. to 0.13 a.u.), ~2.7-fold from MIII to MIII/ModB-L106M (0.59 a.u. to 0.22 a.u.) and ~5.4-fold from MIII to MIVb (0.59 a.u. to 0.11 a.u.). With these observations, data achieved in whole genome transcriptomic analysis regarding the expression of *soxS* can be validated. Furthermore, they show not only the effect of one mutation that is present in MIVb, but rather both individually. However, it can be shown that the effect of RpoC-P246Q on *soxS* expression is significantly higher than the impact of ModB-L106M and highly resembles to expression level observed in *Escherichia coli* MIVb.

During aerobic growth, it was not able to reproduce the effects investigated during whole genome transcriptomics considering *dmsA*, *msrQ*, *fdnG*, *ynfG*, *torA* and *narV* with quantitative real-time PCR.

When *Escherichia coli* is grown anaerobically, the absence of oxygen promotes the expression of a set of genes, necessary for the usage of nitrogen as an electron acceptor. Three of these genes, *dmsA*, *fdnG* and *ynfG* are expressed severalfold-times during anaerobic growth as shown in Figure 22, compared to Figure 23 (*dmsA* = 92-fold, *fdnG* = 41-fold and *ynfG* = 77-fold expression in MIII, when grown anaerobically, compared to aerobic growth), indicating that cells entered anaerobic growth state prior to cell harvest. While *Escherichia coli* MIII and MIII/ModB-L106M showed an increased *fdnG* expression during anaerobiosis, RpoC-P246Q carrying strains are rather unaffected by this condition. As shown in Figure 22, *fdnG* expression levels drop 26-fold in MIII, when RpoC-P246Q mutation was introduced. The anaerobic state induces a 3.5-fold times higher expression of *fdnG* in MIII/RpoC-P246Q, compared to aerobic conditions, whereas MIII undergoes a 46-fold higher expression during anaerobic growth. With these data, the role of *rpoC* in *fdnG* expression can be underlined, whereas *modB* does not seem to have any impact. The genes *dmsA* and *ynfG* are unaffected by RpoC-P246Q.

When the genes *dmsA*, *msrQ*, *fdnG*, *ynfG*, *torA*, *narV* and *soxS* were analyzed during aerobic growth, significant differences within *soxS* were shown in Figure 23, when either ModB-L106M, RpoC-P246Q or both were introduced into MIII strains. Since SoxS is a key regulator to oxidative stress and affects a vast number of genes that play a role in the detoxification of reactive oxygen species, it was investigated, whether these genes might be affected by ModB-L106M or RpoC-P246Q. To distinguish the differences within these genes affected by MIVb-mutations and to induce the expression of genes regulated by SoxS, cells were treated with the ROS-inducing agent paraquat prior to cell harvest. For that purpose, *acrA*, *mlaE*, *nfsA*, *sodA*, *fur*, *oxyR*, *sdhA*, *marA*, *acnB* and *aceB* were taken into consideration for this investigation. As shown in Figure 24, RpoC-P246Q promotes a significant increase in most of them, whereas ModB-L106M has no relevance in this case. The only gene that is clearly unaffected by RpoC-P246Q is *nfsA*, a gene that is activated by MarA, Rob, and SoxS and is deactivated by OxyR (Paterson et al., 2002). As shown in Figure 24, *acrA* fails to show biological significance in its expression levels between MIII and MIII/RpoC-P246Q ($p = 0.065$), however, this due to an outlier in one of the examined MIII strains. Once the MIII *rpoC*-mutant is compared with the MIII *modB*-mutant, it can be observed that *acrA* levels rise to a 1.8-fold expression, when RpoC-P246Q is present. *mlaE* levels in MIII/RpoC-P246Q appear to be increased, yet closely fail to be statistically relevant.

Furthermore, the role of ModB-L106M and RpoC-P246Q in absence of other mutations in MIII was determined. For that purpose, paraquat-induced *soxS*-upregulation with subsequent qRT-PCR was performed in CRISPR-Cas9-mediated *E. coli* wild-type trains, WT/ModB-L106M and WT/RpoC-P246Q and compared to their parental strain, *Escherichia coli* WT. As shown in Figure 25, there are no major differences that are statistically relevant, showing that the effects of RpoC-P246Q shown in Figure 24 can only be achieved, when progenitor MIII mutations were introduced into the strain as well.

## *7.4 MIVb-300*

The Gram-negative strain *Escherichia coli* MIVb was established by R. Tschorny in 1993. It was the successor of a quinolone selection experiment to create highly quinolone-resistant *E. coli* strains. For that purpose, a clinical isolate of *Escherichia coli* wild type was extracted from stool sample of a patient, that was never exposed to antibiotics. Subsequently, the strain was cultivated in growth media with continual rising concentrations of nalidixic acid or ciprofloxacin. When MICs increased, the strain was passaged three times with constant concentrations of the respective antibiotic and subsequently incubated at higher concentrations of quinolones. After four selection cycles, the strains showed a ciprofloxacin MIC of 256 µg/ml, plated on agar and designated MIVb.

Although this mutant showed decreased susceptibility to fluoroquinolones, it also showed a concomitant loss of fitness, as indicated by a generation time of 120 minutes, compared to its progenitor, *Escherichia coli* wild type of about 25 minutes when grown in LB and 37°C in a rotary shaker at 130 rpm.

To compensate the bacterial fitness in this strain, and to investigate introducing mutations that would decrease the duplication time, *E. coli* MIVb was inoculated in LB, without selection by antibiotics. The cells were grown to stationary phase and subsequently diluted 1:1000 in fresh LB broth. This process was repeated until 25, 100, 200 and 300 generations passed. After 25, 100, 200 or 300 generations, an aliquot was plated on LB-agar and a stock culture was prepared. For each generation, cells were plated on LB-Agar and LB-Agar with 128 µg/ml CIP, to

determine increasing susceptibility against CIP. The strains were designated MIVb-25 (and MIVb-25-CIP), MIVb-50, MIVb-100, MIVb-200 and MIVb-300. Growth rates of each individual strain were assessed using the OCelloScope as described in 6.13. Three biological samples of

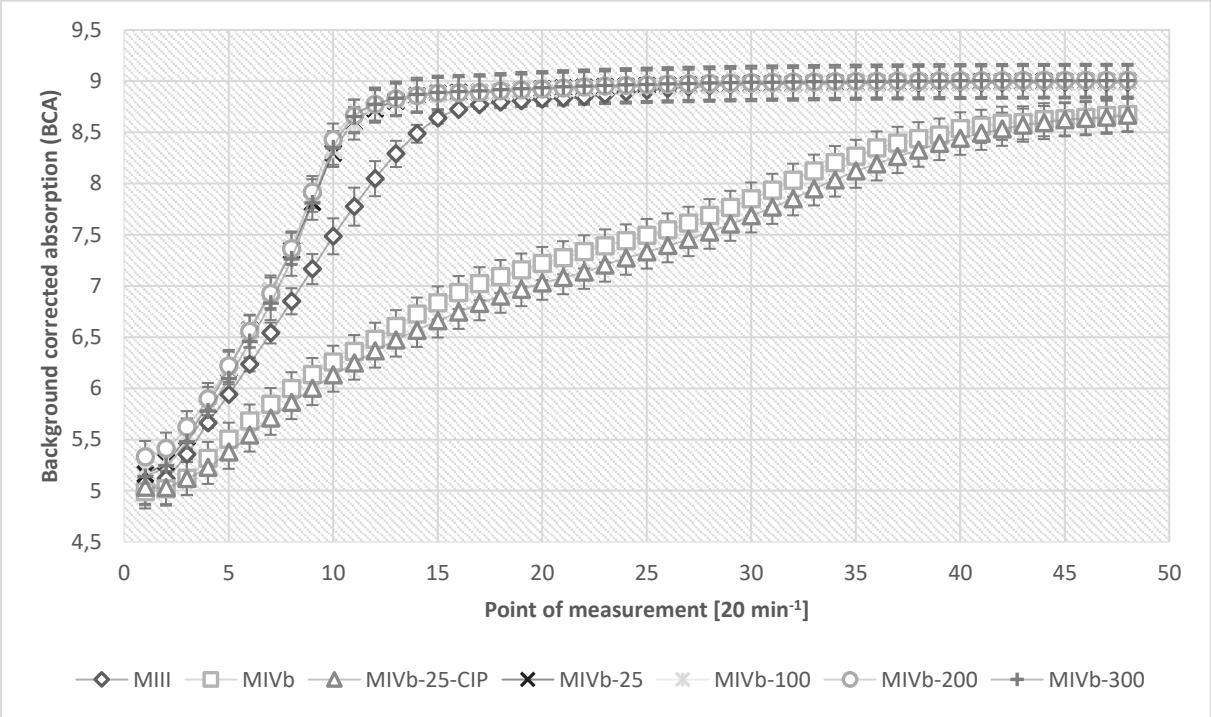


*Figure 27: OCelloScope measurement to assess the growth speed of the MIVb strain after generations have passed. As shown on the y-axis, background corrected absorption indicates the density of cell population. On the x-axis every number indicates the measurement after 20 minutes. Geometric figures represent figures as indicated in the legend. Strains after 25 generations exceed the growth speed of the progenitor strain, E. coli MIII.*

each strain were cultivated for 16 hours in 96-well-plates as described in 6.13. As shown in Figure 27, *Escherichia coli* MIVb mutants show an increased fitness, as indicated by extended growth rates, as soon as 25 generations have passed. As indicated with white squares (□), MIVb output strain correlates with MIVb-25-CIP (Δ). MIVb-25-CIP was established after 25 generations, when an aliquot of the culture was plated on LB Agar and LB Agar, supplemented with 128 µg/ml CIP. It was observed that, when comparing both plates, about 3% of the culture was able to grow on LB-agar 128 µg/ml CIP. Colonies of the LB-CIP-plate were designated MIVb-25-CIP. Furthermore, as a reference, the MIVb progenitor strain, MIII (◊) was included in this measurement, with a duplication rate of 35 min (Heisig and Tschorny, 1994).

After determining the growth rates of the individual strains, MIVb strains from 25 to 300 generations, MICs of CIP were determined for each strain. Mutations were identified with next generation sequencing. The results are shown in Table 23.

*Table 23: E. coli variants after 25 to 300 generations with their respective genomic profile and MIC of ciprofloxacin. Mutations are shown in comparison to E. coli WT. Mutations that emerged within this experiment are indicated in bold.*

| Generations passed | Mutations and acquired mutations (bold) | MIC CIP [mg/ml] |
|---|---|---|
| **0** | *gyrA83 gyrA87, parC, yaiO, marR, yccJ, modB, rpoC246, rpoC1227* | 265 |
| **25** | *gyrA83 gyrA87, parC, yaiO, marR, yccJ, modB, rpoC246,* ***rpoC1229, pdeI*** | 32 |
| **100** | *gyrA83 gyrA87, parC, yaiO, marR, yccJ, modB, rpoC246,* ***rpoC1229, pdeI*** | 32 |
| **200** | *gyrA83 gyrA87, parC, yaiO, marR, yccJ, modB, rpoC246,* ***rpoC1229, pdeI, acrA*** | 4 |
| **300** | *gyrA83 gyrA87, parC, yaiO, marR, yccJ, modB, rpoC246,* ***rpoC1229, pdeI*** | 32 |

Here, after 25 generations, mutations within *rpoC* and *pdeI* have been introduced into *Escherichia coli* MIVb. The *rpoC* mutation was introduced into E. coli since MIII, however, after 25 generation of growth in a quinolone free environment, this mutation is replaced with a different mutation at the same position. A triplet-insertion was formerly introduced into MIII, here it is replaced with a single nucleotide polymorphism, a substitutional mutation which leads to an exchange of the amino acid valine to methionine. After 200 generations, a depletion of *acrA* was observed, causing a decrease of MIVb's MIC to CIP from 32 µg/ml to 4 µg/ml at least. However, after 300 generations have passed, the depletion ceases, resulting in an MIC of 32 µg/ml CIP.

# 8. Discussion

## *8.1 Molybdate influx*

In 7.1, CRISPR-Cas9-based mutants of *E. coli* WT, carrying ModB-L106M or ModB-L106M/RpoC-P246Q have been generated. As Sanger sequencing experiments indicate, chromosomal DNA of these strains either contain a cytosine – adenine substitution within *modB* at position 316, or an additional adenine to cytosine substitution at position 737 within *rpoC*.

For of the determination of molybdate incorporation *in vivo*, a *modB*-knockout strain, *Escherichia coli* JW0747-1 and its parent strain *Escherichia coli* BW25113, that was established for the keio collection (Baba et al., 2006), were transformed with the MolyProbe pYN627 plasmid, that encodes a recombinant protein that uses Förster-Resonance energy transfer (FRET) by coupling YFP to CFP for molybdate-sensing (Nakanishi et al., 2013). It could be demonstrated that this system was able to determine molybdate incorporation in different *E. coli* variants. The molybdate levels determined for *E. coli* JW0747-1 and BW25113 differ significantly. The *modB*-knockout mutant shows a FRET/CFP-ratio that was reduced by 17.28% compared to BW25113. The experimental conditions were then used for measurements of molybdate in CRISPR-Cas9-modified *E. coli* WT/ModB-L106M as well as for *E. coli* WT/ModB-L106M/RpoC-P246Q. First experiments showed that FRET-signals generally were much lower in wild-type strains compared to K-12 strains. The FRET-signals, however, increased when the number of cells that were used for the measurement were increased. Thus, FRET-signals of *E. coli* WT could reach the same level as *E. coli* K-12 strains tested previously. During these experiments, a significant decrease in FRET/CFP ratios was observed within *E. coli* WT/ModB-L106M, when compared to *E. coli* WT, however, the decrease in FRET/CFP-ratio was not as drastic as in the *modB*-knockout strain – compared to its progenitor. Also, this effect was reducedafter the *rpoC*-mutation was introduced into *E. coli* WT/ModB-L106M: Its RpoC-P246Q mutant did not show the same FRET/CFP-ratios. However, *E. coli* WT/ModB-L106M/RpoC-P246Q still showed decreased molybdate levels but the high variations within the biological copies did not show a statistical significance for this strain.

## *8.2 Quantification of gene expression using Real-Time PCR*

The results of the FRET measurements of molybdate influx indicate that *E. coli* mutants, carrying the ModB-L106M mutation have lowered levels of molybdate *in vivo*. This effect was diminished, when RpoC-P246Q was introduced into the cells – however the effect was only marginal. But since the introduction of the *modB* mutation into unmodified *modB*-WT background did lead to lower molybdate levels, we hypothesized that this could affect the expression of molybdate-regulated genes. During quinolone selection, ModB-L106M and RpoC-P246Q are concomitantly introduced into the progenitor strain, *E. coli* MIII and designate *E. coli* MIVb. At this state it was not clear, whether these mutations were introduced independently of each other or if they were introduced in a synergistic fashion. In a different experiment it was shown by transcriptomic analysis that in *E. coli* MIVb the expression of many genes differed significantly compared to its parental strain, *E. coli* MIII (data not included in this work). Some of these genes (e.g., *fdnG*) encode enzymes that require molybdate as a cofactor for their enzymatic activity, so we hypothesized that a reduction of molybdate influx bears an energetic advantage for the cell, since molybdate influx is ATP driven and *fdnG* was downregulated in *E. coli* MIVb. To investigate the impact of each mutation on gene expression, four different *E. coli* MIII variants were analyzed by qRT-PCR of molybdate regulated genes: *E. coli* MIII; *E. coli* MIII/ModB-L106M; *E. coli* MIII/RpoC-P246Q and *E. coli* MIVb.

### 8.2.1 Induction of anaerobiosis by increased levels of *dmsA*

As described in 3.11.3, many genes for anaerobic respiration are regulated by molybdate and *modE*. Not only is their expression regulated by molybdate, but also most of these enzymes also require molybdate, bound to its cofactor, for electron transport reactions within the enzyme itself. To assess differentiated expression levels of these molybdate-regulated genes, a multiple quantitative real-time PCR was developed, analyzing the expression of these genes. Many of these genes are involved in the anaerobic respiration pathway. To induce the expression of these genes, *E. coli* strains were cultured under anaerobic conditions, prior to RNA isolation for qRT-PCR. In parallel, these strains were cultured in an aerobic environment to compare their expression levels during anaerobiosis. *dmsA*, which was described in 3.9.1, was included as a control gene, since its expression is highly regulated by anaerobic respiration

and FNR. The expression of *dmsA* was assessed in four different *E. coli* strains alongside with *msrQ, fdnG, soxS, ynfG, torA* and *narV*. As indicated in Figure 21, all four strains expressed at least an about 80-fold higher expression of *dmsA*, when compared to growth in an aerobic environment. The expression in *rpoC* C737A-carrying cells, *E. coli* MIII/RpoC-P246Q and *E. coli* MIVb was even increased 130-fold. These data clearly show the successful induction of the anaerobic respiratory pathway under these experimental conditions.

### 8.2.2 *rpoC* C737A inhibition of *fdnG* induction

FdnG is the periplasmatic $\alpha$-subunit of the formate dehydrogenase-N complex, which catalyzes the reaction of formate to carbon dioxide and transfers the electrons released in this reaction over the $\beta$-subunit (FdnH) to the $\gamma$-subunit (FdnI), which finally transfers the electrons to a menaquinone of the quinone pool. FdnG is the only subunit of this enzyme, that uses a molybdenum cofactor for electron transport (Jormakka et al., 2002). When transcriptomics revealed that *fdnG* is downregulated in *E. coli* MIVb, it was unclear, whether this effect was associated with mutations in either *modB* or *rpoC*. Here, as shown in Figure 22, *fdnG* levels remain unaffected by anaerobic induction in *E. coli* strains that carry RpoC-P246Q as the respective expression levels are almost equal to aerobic levels – in *E. coli* MIII and *E. coli* MIII/ModB-L106M, these levels increase 46-fold and 52-fold. During this experiment it was shown that *fdnG*, that encodes the subunit of a molybdoenzyme for nitrate respiration is clearly unaffected by ModB-L106M and its altered influx.

The expression levels of *msrQ, soxS, ynfG, torA* and *narV* did not differ during anaerobic growth between the strains examined.

### 8.2.3 Expression of molybdate-regulated genes

It was furthermore investigated whether molybdate-regulated genes are affected by lower molybdate incorporation. To investigate this, the gene expression of *modB*, *moaA*, *narL*, *oppA*, *napA*, *hycE* and *deoA* were tested in qRT-PCR for their expression levels within the strains *E. coli* MIII and *E. coli* MIII/ModB-L106M during anaerobic growth. However, none of their expression differed between the tested strains, indicating that a lower molybdate incorporation has no effect on the gene expression. In fact, the expression of these genes seemed to be generally only slightly increased in MIII/ModB-L106M strains demonstrated by

3 independent experiments but without statistical relevance. However, expression of some of these genes require supplemented molybdate during bacterial growth and others are repressed by it. For example, NarL is a transcriptional regulator, that requires molybdate and in turn, regulates other genes (Darwin and Stewart, 1995). The genes *modB* and *moaA*, in contrast, are downregulated by molybdate, which is why supplemental molybdate during this experiment is necessary for future experiments (Anderson et al., 2000; Walkenhorst et al., 1995)

### 8.2.4 Decreased expression of *soxS* in *modB* and *rpoC* mutant strains

When grown aerobically, CRISPR-Cas9-edited variants of *E. coli* MIII - *E. coli* MIII/ModB-L106M and *E. coli* MIII/RpoC-P246Q as well as *E. coli* MIVb all showed an at least 3-fold lower expression of *soxS*, when compared to *E. coli* MIII. As described in 3.10.1, the SoxR/S system regulates genes in response to oxidative stress within the cell. Although it was unclear, how *soxS* is downregulated within these strains by *modB* and *rpoC* mutations, subsequent analysis to determine the effect on SoxS-regulated genes was performed. To underline the effect of SoxS regulated gene expression, a quantitative real-time PCR was performed, after exposing the bacterial strains to oxidative stress, using the ROS-inducing agent paraquat. The results are discussed in chapter 8.2.5.

### 8.2.5 Expression of SoxS regulated genes in *rpoC* C737A variant of *E. coli* MIII

To investigate the effects of downregulated *soxS* expression under aerobic growth, the expression of SoxS regulated genes *acrA*, *nfsA*, *sodA*, *fur*, *oxyR*, *sdhA*, *marA*, *acnB* and *aceB* was quantified in a qRT-PCR experiment for *E. coli* MIII, *E. coli* MIII/ModB-L106M, and *E. coli* MIII/RpoC-P246Q. Increased expression of all these genes, except *acrA* and *nfsA* was detected in the strain MIII/RpoC-P246Q and are discussed in the following chapters.

#### *8.2.5.1 Superoxide dismutase sodA regulation*

In response to oxidative stress, as described in 3.8, Gram-negative bacteria synthesize superoxide dismutases that catalyze the reaction of superoxide anions ($O_2^-$) to hydrogen peroxide, which can further be processed by catalases to form hydroxyl radicals (Touati, 1989). Here, it was shown that *sodA*, the gene that encodes the Mn-containing superoxide dismutase is significantly upregulated in *E. coli* MIII/RpoC-P246Q, where the *rpoC* C737A SNP was

introduced. However, we can already rule out that this effect can be attributed to the RpoC-P246Q mutation alone. As is shown in Figure 25, these effects are diminished, when RpoC-P246Q was introduced into a wild-type background. As mentioned before, *E. coli* MIII/RpoC-P246Q as well as *E. coli* MIVb carry additional mutations, that were introduced during the quinolone selection process. From these findings we can already conclude that RpoC-P246Q has no effect alone, but rather in combination with one or more of the previously introduced mutations.

#### *8.2.5.2 Increased expression of fur*

Cytotoxic effects, promoted by reactive oxygen species are mediated by iron in a large extend. Hydrogen peroxide, which can be generated from superoxide anions, as described in the previous chapter, reacts with iron by catalases to catalyze the reaction of $H_2O_2$ to $H_2O$ and molecular oxygen $O_2$ (Hillar et al., 2000). Fur, the global repressor of genes associated with iron uptake in *Escherichia coli*, is in turn regulated by SoxR/S (Zheng et al., 1999) and regulates the expression of the catalases KatE and KatG (Keseler et al., 2021). As shown in Figure 24, the expression of *fur* is increased in *E. coli* MIII/RpoC-P246Q. We hypothesize, that a long-term FQ treatment promotes the formation of ROS and that quinolone selection results in mutants with decreased quinolone susceptibility with the acquisition of mutations to deplete harmful reactive oxygen species by regulating the expression of e.g., Fur-regulated genes. However, Fur-regulated genes are highly regulated by intracellular iron levels and *fur* expresson itself is regulated by OxyR and SoxR/S. Interestingly, Fur acts as an transcriptional enhancer for succinate dehydrogenase *sdhA*, as a repressor for the outer membrane protein F *ompF*, which mediates the influx of many antibiotics, including quinolones and β-lactams (Sawai, 1992; Zhang et al., 2005), and as a transcriptional enhancer for the catalases KatE and KatG (Hoerter et al., 2005; Kumar and Shimizu, 2011; Zhang et al., 2005), to name a few.

#### *8.2.5.3 Increased expression of oxyR*

The mechanisms on how OxyR regulates gene expression in response to oxidative stress has already been mentioned in 3.10.2. It contains a sensory cysteine residue that is oxidized by $H_2O_2$, which subsequently forms a disulfide bond and reduces its binding affinity to DNA (Åslund et al., 1999; Chiancone and Ceci, 2010). In *Escherichia coli*, the oxidative form of OxyR

promotes the expression of many genes that are involved in the catalyzing of $H_2O_2$ to $H_2O$ and oxygen, like catalases (Hillar et al., 2000; Jacobson et al., 1989).

Furthermore, OxyR regulates the expression of *nsfA* (Keseler et al., 2021), which also has been investigated in this experiment, as well as *fur*, which has been described in the previous chapter (Zheng et al., 1999). By quantitative real-time PCR, a significant raise in *oxyR* expression was observed by introducing RpoC-P246Q into cells with an MIII background. OxyR binds to DNA acting as a transcriptional repressor. When oxidative agents are present, OxyR itself is oxidized resulting in a loss of its binding affinity and is released from DNA, which promotes the transcriptional activation of many genes, involved in ROS detoxification. It has already been discussed that regulation of Fur is mediated by OxyR. When OxyR binds to the promoter region of *fur*, it was shown that *fur* expression was enhanced after hydrogen peroxide treatment (Zheng et al., 1999). This in turn, leads to a signaling cascade to other genes involved in ROS detoxification, as already described.

#### *8.2.5.4 Succinat dehydrogenase A sdhA*

The succinate dehydrogenase, an iron-sulfur cluster protein involved in the tricarboxylic acid (TCA) cycle, was shown to be downregulated in *fur* deficient mutants in *E. coli* (Kumar and Shimizu, 2011; Zhang et al., 2005), indicating that *fur* plays an essential – but not unique role in the regulation of the *sdhCDAB* operon. The findings of this work support these mechanisms since *E. coli* MIII/RpoC-P246Q showed increased expression of both – *fur* and *sdhA*. As in most cases, high iron levels lead to repression of *fur* regulated genes, however, in the case of the *sdhCDAB* operon, iron-free Fur positively regulates the transcription. According to data shown by Rui et al., oxidative stress promotes adjustments in the metabolic pathways in *Escherichia coli*, predominantly by increasing the generation of NADPH while decreasing generation of NADH (see 8.2.5.6) (Rui et al., 2010). Along with *acnB* and *aceB*, these genes are directly involved in the metabolic pathways of *Escherichia coli*.

#### *8.2.5.5 Upregulation of acnB*

*acnB* also belongs to the iron-sulfur cluster proteins. In the case of oxidative stress by $H_2O_2$, iron atoms of this enzyme are oxidized, dissociate and decrease the activity of the enzyme. Many of these enzymes are also involved in the tricarboxylic acid (TCA) cycle (see 8.2.5.6).

Exposure of these enzymes to an oxidative environment lead to the release of free iron, since superoxide is electrostatically attracted to $[4Fe\text{-}4S]^{2+}$ clusters and oxidizes them to the unstable $[4Fe\text{-}4S]^{3+}$ state, which subsequently degrades to $[3Fe\text{-}4S]^{1+}$ while the free iron is released to the cytosol (Varghese et al., 2003). It was also shown, that Aconitase B, as in contrast to Aconitase A, shows higher sensitivity to oxidative stress than aconitase A (Varghese et al., 2003). *acnB* is regulated by RyhB, a small regulatory RNA, which itself is regulated by the *ryhB* Gene. The expression of *ryhB*, however, is regulated by Fur (Benjamin and Massé, 2014). In case of an increased expression of *fur*, the induction of small regulatory RNA RhyB is decreased, which in turn leads to a higher expression of *acnB*. Notably, Aconitase B can shift into an RNA binding state, preventing the expression of its own RNA. In case of iron starvation, however, RNA binding is prevented (Varghese et al., 2003). This mechanism might be the case within this experiment, since *fur* (ferritic uptake regulator) is upregulated in *E. coli* MIII/RpoC-P246Q, and iron uptake is promoted.

#### *8.2.5.6 Upregulation of aceB expression*

The malate synthase A is one of the key enzymes in the glyoxylate pathway. It is encoded by the *aceB* gene, which is transcribed as a part of the *aceBAK* operon. The malate synthase A catalyzes the reaction of acetyl-CoA and glyoxylate to coenzyme A and (S)-malate (Molina et al., 1994). Transcriptome data of a study by Zhang et al. provided insight into the regulation of the *aceBAK* operon. Their results show that the operon is strongly regulated by Crp and Fur. Additional data revealed the presence of Crp and Fur binding sites upstream of the *aceB* gene (Zhang et al., 2005). However, other studies have shown that the *aceBAK* operon is regulated in a complex manner by four other transcription factors (Cozzone, 1998): IclR (Nègre et al., 1992), IHF (Resnik et al., 1996), Cra (formerly known as FruR) (Ramseier et al., 1993) and FadR (Maloy and Nunn, 1982). However, IclR binds to three specific positions downstream of the *aceBAK* operon and two of these sites overlap with the Crp and Fur binding regions, suggesting that "[…] Crp and Fur regulate IclR expression and/or that IclR interacts with Crp and/or Fur as well as with the C-terminal domain of the RNA polymerase alpha-subunit", cited by Zhang (Zhang et al., 2005), who were referring to data by K. Yamamoto and A. Ishihama (Yamamoto and Ishihama, 2003). The findings of this work show in *E. coli* MIII/RpoC-P246Q an upregulation in *aceB*, along with an increased expression of *fur*,

indicating that an upregulation of the *fur* gene indeed promotes the transcription of *aceB* and the involvement of the glyoxylate shunt, supporting the findings of Zhang et al. (Zhang et al., 2005). As data shown by Rui et al., oxidative stress, in their study induced by paraquat, promotes adjustments in the metabolic pathways in *Escherichia coli*, predominantly by increasing NADPH generation and decreased NADH generation, which "[…] reflects a cellular strategy whereby efficiency is traded for survival under stressful conditions." (Rui et al., 2010). Although we can only speculate, which metabolic pathway is decreased, we can clearly observe the higher expression of the *aceB* gene, resulting in higher levels of malate synthase A.

#### *8.2.5.7 Expression of marA and acrA*

MarA is a key regulator of a set of genes including *acrA*, *acrB* and *tolC*, that encode the multidrug efflux pump AcrAB-TolC (Ruiz and Levy, 2010) in order to respond to the presence of antimicrobial agents as mentioned in 3.4.2. By qRT-PCR it was shown that *marA* expression was increased within *E. coli* MIII/RpoC-P246Q. We hypothesized that upregulation of *marA* therefore would also increase the expression of *acrA/B*. As shown in Figure 24, *acrA* expression is also upregulated in *E. coli* MIII/RpoC-P246Q, however, when compared to unmutated *E. coli* MIII, not statistically significant. However, when *E. coli* MIII/RpoC-P246Q is compared to *E. coli* MIII/ModB-L106M, which also does not carry the *rpoC* SNP, the increasing values of *acrA* become clearly visible. MarA is partly activated by SoxS (Keseler et al., 2021). Since we observed a drop in *soxS* rates within CRISPR-Cas9 generated variants of *E. coli*, *E. coli* MIII/ModB-L106M and *E. coli* MIII/RpoC-P246Q, one could assume that this might downregulate the expression of *marA*. However, *E. coli* MIII/ModB-L106M also showed a decreased expression of *soxS* and no increase in *marA.* However, *marA* is also regulated by RhyB, which has already been described in the previous findings on *acnB* expression. It is tempting to speculate that reduced *soxS* expression does not significantly promote an increased expression of *marA*, but rather RhyB.

### 8.2.6 Unaffected expressions of SoxS regulated genes in *E. coli* WT background

After assessing qRT-PCR validations of SoxS regulated genes in *E. coli* MIII and its CRISPR variants, it was aimed to investigate, if these observations are reproducible in *Escherichia coli*,

absent of the MIII background. However, it is clearly visible, that neither *E. coli* WT/ModB-L106M or *E. coli* WT/RpoC-P246Q promotes any of the altered expression patterns that have been alternatively regulated in a MIII background. This strongly suggest, that RpoC-P246Q does have an influence on gene expression, however, only in combination with one or more of the additional mutations of *E. coli* MIII. A promising candidate could be the *rpoC* mutation which has been acquired by MIII affecting position 1227.

## *8.3 Antibiotic-free environment promotes the increasing growth rate by mutational adaptions within highly quinolone resistant E. coli MIVb*

During a cultivation assay of *Escherichia coli* MIVb with a total duration of 300 generations, OCelloScope measurements were assessed to determine the fitness compensation in an antibiotic free environment.

During quinolone selection, which generated *Escherichia coli* MIVb as a successor, this strain acquired many mutational alterations to adapt to a high-FQ environment. However, the increase of its MIC to quinolones resulted in a loss of fitness, shown by the drastic decelerated growth rate, that increased the generation time from 25 minutes (*E. coli* WT) to 120 minutes. For this purpose, *E. coli* MIVb was inoculated in LB broth, in the absence of antibiotic for 300 generations to investigate, if any of the introduced mutations would re-mutate to increase bacterial fitness. We could also see, if there are other mutations that might be introduced to the strain to increase the growth rates of the strain.

During this experiment, after 25 generations, *E. coli* MIVb showed a significant increase in its growth rate, as shown in Figure 27. It was observed that only 3% of colonies of MIVb-25 were detectable on CIP plates, compared to LB Agar plates.

Next-generation sequencing (NGS) was performed by GeneWIZ. The data show a mutational variant in the gene *pdeI*, formerly known as *yliE*. Not much is known about this gene. It is a predicted c-di-CMP-specific phosphodiesterase and overexpression of this gene has shown to reduce biofilm formation (Boehm et al., 2009; Keseler et al., 2021). Interestingly, we have observed a SNP within the gene *yccJ*, already in *Escherichia coli* MIII, which is regulated by CsgD, a key regulator in biofilm formation (Brombacher et al., 2003). However, until now it is very elusive to speculate on the function of these genes, regarding the involvement of quinolones or bacterial fitness. Furthermore, the *rpoC* mutation that was introduced in the

strain MIII, was replaced by another mutation affecting the same position. The previous mutation within *rpoC* is a triplet insertion variant, which is, however, replaced with a substitutional mutation at position 1229, which leads to a change in the amino acid valine to methionine. MIC analysis revealed that the mutations of both, *rpoC* and *pdeI* lead to a decreased MIC of CIP of 32 µg/ml, as opposed to 256 µl/ml in *E. coli* MIVb. This already occured after 25 generations. The OCelloScope data reveal a significant increase in growth rate of this strain, even higher than its parental strain, *E. coli* MIII. *E. coli* MIVb-25 still carries the mutations that led to a high resistance against CIP, however, it seems that the increase of growth rate alone would lead to a significant loss of resistance.

After 200 generations, it was observed that a deletion occurred within the gene *acrA*. As already described in 3.4.2, *acrA* encodes the periplasmatic subunit of the AcrAB/TolC efflux pump in *Escherichia coli*. The deletion comprises 29 nucleotides, resulting in a loss of function of this subunit by a frameshift introduced at pos. 187. Within this strain, ciprofloxacin MIC drops to at least 4 µg/ml (lower concentrations were not assessed). However, after 300 generations the deletion has disappeared, and the mutant MIVb-300 has regained a ciprofloxacin MIC of 32 µg/ml.

Here, without the selective pressure of fluoroquinolones, it was shown that slow growing, highly quinolone resistant *E. coli* acquire increasing fitness with concomitant higher susceptibility to quinolones by the introduction of two mutations, within *rpoC* and *pdeI*. MIVb-300 is denoted with a ciprofloxacin MIC of 32 µg/ml, which may be a three-fold lower MIC than *E. coli* MIVb, however, it's still high enough for clinical relevance (LeBel, 1988) and shows high duplication rates. Although it is not clear, how re-gain of fitness is established through the observed mutations, we show that these adaptions occur quickly.

# 9. Outlook

The aim of this work was to investigate the functions of mutations not previously associated with high-level fluoroquinolone in fitness-reduced highly fluoroquinolone-resistant *E. coli* MIVb and its derivatives. This work provides basic data on the respective functions as well as their relation to mutations associated with quinolone resistance.

It was shown that the mutation in *modB* significantly decreases molybdate levels in *E. coli* wild type, however the reason, why this mutation was acquired by *E. coli* MIVb is still elusive. It

was shown that molybdate levels did not significantly alter the gene expression of molybdate-regulated genes in the *E. coli* MIII strain, that additionally carried the *modB* mutation, however, experimental setup can be modified, to proceed this work. Although gene expression seemed to be increased lightly, statistical significance was not detectable, given the experimental conditions. Standard deviations just seemed to be too high but the cultivation of the cells in molybdate-rich medium seems to be a promising approach to repeat this experiment as already discussed before. Only then, further investigation of the interplay between *modB* and *rpoC* can be assessed.

Although it was shown that the gene product of *rpoC* regulates a vast number of genes that play essential roles during oxidative stress, the exact mechanism, on how RpoC works, is unknown. It was hypothesized that Fur plays a dominant role on regulating these genes, however, exact evidence for that is not provided in this work. For future prospects, qRT-PCR of these genes could be assessed with *fur* deficient mutants of *E. coli*. And although it is known, that RpoC-P246Q in a MIII background promotes a high resistance to quinolones (assessed with MIC) – showing bacteriostatic effects, the role of this mutation on bactericidal effects of quinolones by ROS has not been investigated until now. For this promising experiment, the validations of MICs need to be replaced with bacterial killing assays.

The outcome of the MIVb-300 has shown that bacteria favor the increase of growth-speed at the cost of quinolone resistances. During this process, a deletion occurs in the gene *acrA*, that, surprisingly, reoccurs as generations pass. The mechanism on how *E. coli* could delete and re-insert a DNA sequence of that size is not known. Transposable elements, which promote such mechanisms and occur mostly in plants, have been described in *E. coli* as well, especially in regards of extended spectrum β-lactamases (ESBL) (Poirel et al., 2008). However, a mechanism on *acrA* is not known.

# 10. Literature

Aguilar-Barajas, E., Díaz-Pérez, C., Ramírez-Díaz, M.I., Riveros-Rosas, H., Cervantes, C., 2011. Bacterial transport of sulfate, molybdate, and related oxyanions. BioMetals 24, 687–707. https://doi.org/10.1007/s10534-011-9421-x

Aldred, K.J., Kerns, R.J., Osheroff, N., 2014. Mechanism of Quinolone Action and Resistance. Biochemistry 53, 1565–1574. https://doi.org/10.1021/bi5000564

Aldred, K.J., McPherson, S.A., Turnbough, C.L., Kerns, R.J., Osheroff, N., 2013a. Topoisomerase IV-quinolone interactions are mediated through a water-metal ion bridge: mechanistic basis of quinolone resistance. Nucleic Acids Res. 41, 4628–4639. https://doi.org/10.1093/nar/gkt124

Aldred, K.J., Schwanz, H.A., Li, G., McPherson, S.A., Turnbough, C.L., Kerns, R.J., Osheroff, N., 2013b. Overcoming Target-Mediated Quinolone Resistance in Topoisomerase IV by Introducing Metal-Ion-Independent Drug–Enzyme Interactions. ACS Chem. Biol. 8, 2660–2668. https://doi.org/10.1021/cb400592n

Alekshun, M.N., Levy, S.B., 1999. The mar regulon: multiple resistance to antibiotics and other toxic chemicals. Trends Microbiol. 7, 410–413. https://doi.org/10.1016/S0966-842X(99)01589-9

Allocati, N., Masulli, M., Alexeyev, M., Di Ilio, C., 2013. Escherichia coli in Europe: An Overview. Int. J. Environ. Res. Public. Health 10, 6235–6254. https://doi.org/10.3390/ijerph10126235

Anderson, L.A., McNairn, E., Leubke, T., Pau, R.N., Boxer, D.H., 2000. ModE-Dependent Molybdate Regulation of the Molybdenum Cofactor Operon *moa* in *Escherichia coli*. J. Bacteriol. 182, 7035–7043. https://doi.org/10.1128/JB.182.24.7035-7043.2000

Anderson, V., Osheroff, N., 2001. Type II Topoisomerases as Targets for Quinolone Antibacterials Turning Dr. Jekyll into Mr. Hyde. Curr. Pharm. Des. 7, 337–353. https://doi.org/10.2174/1381612013398013

Andriole, V.T., 2005. The Quinolones: Past, Present, and Future. Clin. Infect. Dis. 41, S113–S119. https://doi.org/10.1086/428051

Åslund, F., Zheng, M., Beckwith, J., Storz, G., 1999. Regulation of the OxyR transcription factor by hydrogen peroxide and the cellular thiol—disulfide status. Proc. Natl. Acad. Sci. 96, 6161–6165. https://doi.org/10.1073/pnas.96.11.6161

Baba, T., Ara, T., Hasegawa, M., Takai, Y., Okumura, Y., Baba, M., Datsenko, K.A., Tomita, M., Wanner, B.L., Mori, H., 2006. Construction of *Escherichia coli* K-12 in-frame, single-gene knockout mutants: the Keio collection. Mol. Syst. Biol. 2. https://doi.org/10.1038/msb4100050

Bader, M., Muse, W., Ballou, D.P., Gassner, C., Bardwell, J.C.A., 1999. Oxidative Protein Folding Is Driven by the Electron Transport System. Cell 98, 217–227. https://doi.org/10.1016/S0092-8674(00)81016-8

Bardwell, J.C.A., McGovern, K., Beckwith, J., 1991. Identification of a protein required for disulfide bond formation in vivo. Cell 67, 581–589. https://doi.org/10.1016/0092-8674(91)90532-4

Basu, R.S., Warner, B.A., Molodtsov, V., Pupov, D., Esyunina, D., Fernández-Tornero, C., Kulbachinskiy, A., Murakami, K.S., 2014. Structural Basis of Transcription Initiation by Bacterial RNA Polymerase Holoenzyme. J. Biol. Chem. 289, 24549–24559. https://doi.org/10.1074/jbc.M114.584037

Benjamin, J.-A.M., Massé, E., 2014. The iron-sensing aconitase B binds its own mRNA to prevent sRNA-induced mRNA cleavage. Nucleic Acids Res. 42, 10023–10036. https://doi.org/10.1093/nar/gku649

Berg, B.L., Stewart, V., 1990. Structural genes for nitrate-inducible formate dehydrogenase in Escherichia coli K-12. Genetics 125, 691–702. https://doi.org/10.1093/genetics/125.4.691

Berks, B.C., 1996. A common export pathway for proteins binding complex redox cofactors? Mol. Microbiol. 22, 393–404. https://doi.org/10.1046/j.1365-2958.1996.00114.x

Berks, B.C., Palmer, T., Sargent, F., 2005. Protein targeting by the bacterial twin-arginine translocation (Tat) pathway. Curr. Opin. Microbiol. 8, 174–181. https://doi.org/10.1016/j.mib.2005.02.010

Birnboim, H.C., Doly, J., 1979. A rapid alkaline extraction procedure for screening recombinant plasmid DNA. Nucleic Acids Res. 7, 1513–1523. https://doi.org/10.1093/nar/7.6.1513

Boehm, A., Steiner, S., Zaehringer, F., Casanova, A., Hamburger, F., Ritz, D., Keck, W., Ackermann, M., Schirmer, T., Jenal, U., 2009. Second messenger signalling governs *Escherichia coli* biofilm induction upon ribosomal stress. Mol. Microbiol. 72, 1500–1516. https://doi.org/10.1111/j.1365-2958.2009.06739.x

Bonnefoy, V., Demoss, J.A., 1994. Nitrate reductases inEscherichia coli. Antonie Van Leeuwenhoek 66, 47–56. https://doi.org/10.1007/BF00871632

Bowater, R., Doherty, A.J., 2006. Making Ends Meet: Repairing Breaks in Bacterial DNA by Non-Homologous End-Joining. PLoS Genet. 2, e8. https://doi.org/10.1371/journal.pgen.0020008

Brokx, S.J., Rothery, R.A., Zhang, G., Ng, D.P., Weiner, J.H., 2005. Characterization of an *Escherichia coli* Sulfite Oxidase Homologue Reveals the Role of a Conserved Active Site Cysteine in Assembly and Function. Biochemistry 44, 10339–10348. https://doi.org/10.1021/bi050621a

Brombacher, E., Dorel, C., Zehnder, A.J.B., Landini, P., 2003. The curli biosynthesis regulator CsgD co-ordinates the expression of both positive and negative determinants for biofilm formation in Escherichia coli. Microbiology 149, 2847–2857. https://doi.org/10.1099/mic.0.26306-0

Bush, N.G., Diez-Santos, I., Abbott, L.R., Maxwell, A., 2020. Quinolones: Mechanism, Lethality and Their Contributions to Antibiotic Resistance. Molecules 25, 5662. https://doi.org/10.3390/molecules25235662

Cassels, F., Wolf, M., 1995. Colonization factors of diarrheagenicE. coli and their intestinal receptors. J. Ind. Microbiol. 15, 214–226. https://doi.org/10.1007/BF01569828

Cattoir, V., Poirel, L., Nordmann, P., 2008. Plasmid-Mediated Quinolone Resistance Pump QepA2 in an *Escherichia coli* Isolate from France. Antimicrob. Agents Chemother. 52, 3801–3804. https://doi.org/10.1128/AAC.00638-08

Champoux, J.J., 2001. DNA Topoisomerases: Structure, Function, and Mechanism. Annu. Rev. Biochem. 70, 369–413. https://doi.org/10.1146/annurev.biochem.70.1.369

Chiancone, E., Ceci, P., 2010. The multifaceted capacity of Dps proteins to combat bacterial stress conditions: Detoxification of iron and hydrogen peroxide and DNA binding. Biochim. Biophys. Acta BBA - Gen. Subj. 1800, 798–805. https://doi.org/10.1016/j.bbagen.2010.01.013

Chiang, S.M., Schellhorn, H.E., 2012. Regulators of oxidative stress response genes in Escherichia coli and their functional conservation in bacteria. Arch. Biochem. Biophys. 525, 161–169. https://doi.org/10.1016/j.abb.2012.02.007

Chow, R.T., Dougherty, T.J., Fraimow, H.S., Bellin, E.Y., Miller, M.H., 1988a. Association between early inhibition of DNA synthesis and the MICs and MBCs of carboxyquinolone antimicrobial agents for wild-type and mutant [gyrA nfxB(ompF) acrA] Escherichia coli K-12. Antimicrob. Agents Chemother. 32, 1113–1118. https://doi.org/10.1128/AAC.32.8.1113

Chow, R.T., Dougherty, T.J., Fraimow, H.S., Bellin, E.Y., Miller, M.H., 1988b. Association between early inhibition of DNA synthesis and the MICs and MBCs of carboxyquinolone antimicrobial agents for wild-type and mutant [gyrA nfxB(ompF) acrA] Escherichia coli K-12. Antimicrob. Agents Chemother. 32, 1113–1118. https://doi.org/10.1128/AAC.32.8.1113

Clark, D., 1989. The fermentation pathways of Escherichia coli. FEMS Microbiol. Rev. 63, 223–234. https://doi.org/10.1016/0168-6445(89)90033-8

Correia, S., Poeta, P., Hébraud, M., Capelo, J.L., Igrejas, G., 2017. Mechanisms of quinolone action and resistance: where do we stand? J. Med. Microbiol. 66, 551–559. https://doi.org/10.1099/jmm.0.000475

Courcelle, J., Khodursky, A., Peter, B., Brown, P.O., Hanawalt, P.C., 2001. Comparative Gene Expression Profiles Following UV Exposure in Wild-Type and SOS-Deficient *Escherichia coli*. Genetics 158, 41–64. https://doi.org/10.1093/genetics/158.1.41

Cozzone, A.J., 1998. REGULATION OF ACETATE METABOLISM BY PROTEIN PHOSPHORYLATION IN ENTERIC BACTERIA. Annu. Rev. Microbiol. 52, 127–164. https://doi.org/10.1146/annurev.micro.52.1.127

Darwin, A.J., Stewart, V., 1995. Expression of the narX, narL, narP, and narQ genes of Escherichia coli K-12: regulation of the regulators. J. Bacteriol. 177, 3865–3869. https://doi.org/10.1128/jb.177.13.3865-3869.1995

Davies, J., Wright, G.D., 1997. Bacterial resistance to aminoglycoside antibiotics. Trends Microbiol. 5, 234–240. https://doi.org/10.1016/S0966-842X(97)01033-0

Deibler, R.W., Rahmati, S., Zechiedrich, E.L., 2001. Topoisomerase IV, alone, unknots DNA in *E. coli*. Genes Dev. 15, 748–761. https://doi.org/10.1101/gad.872301

Depuydt, M., Leonard, S.E., Vertommen, D., Denoncin, K., Morsomme, P., Wahni, K., Messens, J., Carroll, K.S., Collet, J.-F., 2009. A Periplasmic Reducing System Protects Single Cysteine Residues from Oxidation. Science 326, 1109–1111. https://doi.org/10.1126/science.1179557

Deweese, J.E., Osheroff, N., 2010. The use of divalent metal ions by type II topoisomerases. Metallomics 2, 450. https://doi.org/10.1039/c003759a

Doi, Y., Wachino, J., Arakawa, Y., 2016. Aminoglycoside Resistance. Infect. Dis. Clin. North Am. 30, 523–537. https://doi.org/10.1016/j.idc.2016.02.011

Drlica, K., Hiasa, H., Kerns, R., Malik, M., Mustaev, A., Zhao, X., 2009. Quinolones: Action and Resistance Updated. Curr. Top. Med. Chem. 9, 981–998. https://doi.org/10.2174/156802609789630947

Dutton, R.J., Boyd, D., Berkmen, M., Beckwith, J., 2008. Bacterial species exhibit diversity in their mechanisms and capacity for protein disulfide bond formation. Proc. Natl. Acad. Sci. 105, 11933–11938. https://doi.org/10.1073/pnas.0804621105

Emmerson, A.M., 2003. The quinolones: decades of development and use. J. Antimicrob. Chemother. 51, 13–20. https://doi.org/10.1093/jac/dkg208

Ezraty, B., Gennaris, A., Barras, F., Collet, J.-F., 2017. Oxidative stress, protein damage and repair in bacteria. Nat. Rev. Microbiol. 15, 385–396. https://doi.org/10.1038/nrmicro.2017.26

Fàbrega, A., Madurga, S., Giralt, E., Vila, J., 2009. Mechanism of action of and resistance to quinolones: Mechanism of action of and resistance to quinolones. Microb. Biotechnol. 2, 40–61. https://doi.org/10.1111/j.1751-7915.2008.00063.x

Fernández de Henestrosa, A.R., Ogi, T., Aoyagi, S., Chafin, D., Hayes, J.J., Ohmori, H., Woodgate, R., 2002. Identification of additional genes belonging to the LexA regulon in Escherichia coli: Novel LexA-regulated genes in E. coli. Mol. Microbiol. 35, 1560–1572. https://doi.org/10.1046/j.1365-2958.2000.01826.x

Forterre, P., Gadelle, D., 2009. Phylogenomics of DNA topoisomerases: their origin and putative roles in the emergence of modern organisms. Nucleic Acids Res. 37, 679–692. https://doi.org/10.1093/nar/gkp032

Forterre, P., Gribaldo, S., Gadelle, D., Serre, M.-C., 2007. Origin and evolution of DNA topoisomerases. Biochimie 89, 427–446. https://doi.org/10.1016/j.biochi.2006.12.009

Foti, J.J., Devadoss, B., Winkler, J.A., Collins, J.J., Walker, G.C., 2012. Oxidation of the Guanine Nucleotide Pool Underlies Cell Death by Bactericidal Antibiotics. Science 336, 315–319. https://doi.org/10.1126/science.1219192

Fourmy, D., Yoshizawa, S., Puglisi, J.D., 1998. Paromomycin binding induces a local conformational change in the A-site of 16 s rRNA. J. Mol. Biol. 277, 333–345. https://doi.org/10.1006/jmbi.1997.1551

Gellert, M., Mizuuchi, K., O'Dea, M.H., Itoh, T., Tomizawa, J.-I., 1977. Nalidixic acid resistance: A second genetic character involved in DNA gyrase activity. Proc. Natl. Acad. Sci. 74, 4772–4776. https://doi.org/10.1073/pnas.74.11.4772

Gennaris, A., Ezraty, B., Henry, C., Agrebi, R., Vergnes, A., Oheix, E., Bos, J., Leverrier, P., Espinosa, L., Szewczyk, J., Vertommen, D., Iranzo, O., Collet, J.-F., Barras, F., 2015. Repairing oxidized proteins in the bacterial envelope using respiratory chain electrons. Nature 528, 409–412. https://doi.org/10.1038/nature15764

Griffey, R.H., Hofstadler, S.A., Sannes-Lowery, K.A., Ecker, D.J., Crooke, S.T., 1999. Determinants of aminoglycoside-binding specificity for rRNA by using mass spectrometry. Proc. Natl. Acad. Sci. 96, 10129–10133. https://doi.org/10.1073/pnas.96.18.10129

Grunden, A.M., Ray, R.M., Rosentel, J.K., Healy, F.G., Shanmugam, K.T., 1996. Repression of the Escherichia coli modABCD (molybdate transport) operon by ModE. J. Bacteriol. 178, 735–744. https://doi.org/10.1128/jb.178.3.735-744.1996

Guillard, T., Cambau, E., Chau, F., Massias, L., de Champs, C., Fantin, B., 2013. Ciprofloxacin Treatment Failure in a Murine Model of Pyelonephritis Due to an AAC(6′)-Ib-cr-Producing Escherichia coli Strain Susceptible to Ciprofloxacin *In Vitro*. Antimicrob. Agents Chemother. 57, 5830–5835. https://doi.org/10.1128/AAC.01489-13

Hasona, A., Self, W.T., Ray, R.M., Shanmugam, K.T., 1998. Molybdate-dependent transcription of *hyc* and *nar* operons of *Escherichia coli* requires MoeA protein and ModE-molybdate. FEMS Microbiol. Lett. 169, 111–116. https://doi.org/10.1111/j.1574-6968.1998.tb13306.x

Heisig, P., Tschorny, R., 1994. Characterization of fluoroquinolone-resistant mutants of escherichia coli selected in vitro. Antimicrob. Agents Chemother. 38, 1284–1291. https://doi.org/10.1128/AAC.38.6.1284

Helling, R.B., Goodman, H.M., Boyer, H.W., 1974. Analysis of Endonuclease R· *Eco* RI Fragments of DNA from Lambdoid Bacteriophages and Other Viruses by Agarose-Gel Electrophoresis. J. Virol. 14, 1235–1244. https://doi.org/10.1128/jvi.14.5.1235-1244.1974

Higuchi, K., Katayama, T., Iwai, S., Hidaka, M., Horiuchi, T., Maki, H., 2003. Fate of DNA replication fork encountering a single DNA lesion during *oriC* plasmid DNA replication *in vitro*: Fork stall in oriC plasmid replication *in vitro*. Genes Cells 8, 437–449. https://doi.org/10.1046/j.1365-2443.2003.00646.x

Hillar, A., Peters, B., Pauls, R., Loboda, A., Zhang, H., Mauk, A.G., Loewen, P.C., 2000. Modulation of the Activities of Catalase−Peroxidase HPI of *Escherichia coli* by Site-Directed Mutagenesis. Biochemistry 39, 5868–5875. https://doi.org/10.1021/bi0000059

Hille, R., 1996. The Mononuclear Molybdenum Enzymes. Chem. Rev. 96, 2757–2816. https://doi.org/10.1021/cr950061t

Hoerter, J.D., Arnold, A.A., Ward, C.S., Sauer, M., Johnson, S., Fleming, T., Eisenstark, A., 2005. Reduced hydroperoxidase (HPI and HPII) activity in the Δfur mutant contributes to increased sensitivity to UVA radiation in Escherichia coli. J. Photochem. Photobiol. B 79, 151–157. https://doi.org/10.1016/j.jphotobiol.2005.01.003

Hong, Y., Li, Q., Gao, Q., Xie, J., Huang, H., Drlica, K., Zhao, X., 2020. Reactive oxygen species play a dominant role in all pathways of rapid quinolone-mediated killing. J. Antimicrob. Chemother. 75, 576–585. https://doi.org/10.1093/jac/dkz485

Hooper, D.C., 2001. Mechanisms of Action of Antimicrobials: Focus on Fluoroquinolones. Clin. Infect. Dis. 32, S9–S15. https://doi.org/10.1086/319370

Hooper, D.C., 1999. Mode of Action of Fluoroquinolones: Drugs 58, 6–10. https://doi.org/10.2165/00003495-199958002-00002

Imlay, J.A., 2015. Transcription Factors That Defend Bacteria Against Reactive Oxygen Species. Annu. Rev. Microbiol. 69, 93–108. https://doi.org/10.1146/annurev-micro-091014-104322

Imlay, J.A., 2013. The molecular mechanisms and physiological consequences of oxidative stress: lessons from a model bacterium. Nat. Rev. Microbiol. 11, 443–454. https://doi.org/10.1038/nrmicro3032

Imlay, J.A., 2003. Pathways of Oxidative Damage. Annu. Rev. Microbiol. 57, 395–418. https://doi.org/10.1146/annurev.micro.57.030502.090938

Iobbi-Nivol, C., Leimkühler, S., 2013. Molybdenum enzymes, their maturation and molybdenum cofactor biosynthesis in Escherichia coli. Biochim. Biophys. Acta BBA - Bioenerg. 1827, 1086–1101. https://doi.org/10.1016/j.bbabio.2012.11.007

Jacobson, F.S., Morgan, R.W., Christman, M.F., Ames, B.N., 1989. An Alkyl Hydroperoxide Reductase from Salmonella typhimurium Involved in the Defense of DNA against Oxidative Damage. J. Biol. Chem. 264, 1488–1496. https://doi.org/10.1016/S0021-9258(18)94214-6

Jinek, M., Chylinski, K., Fonfara, I., Hauer, M., Doudna, J.A., Charpentier, E., 2012. A Programmable Dual-RNA–Guided DNA Endonuclease in Adaptive Bacterial Immunity. Science 337, 816–821. https://doi.org/10.1126/science.1225829

Jormakka, M., Törnroth, S., Byrne, B., Iwata, S., 2002. Molecular Basis of Proton Motive Force Generation: Structure of Formate Dehydrogenase-N. Science 295, 1863–1868. https://doi.org/10.1126/science.1068186

Jozefczuk, J., Adjaye, J., 2011. Quantitative Real-Time PCR-Based Analysis of Gene Expression, in: Methods in Enzymology. Elsevier, pp. 99–109. https://doi.org/10.1016/B978-0-12-385118-5.00006-2

Kadokura, H., Beckwith, J., 2009. Detecting Folding Intermediates of a Protein as It Passes through the Bacterial Translocation Channel. Cell 138, 1164–1173. https://doi.org/10.1016/j.cell.2009.07.030

Kaper, J.B., Nataro, J.P., Mobley, H.L.T., 2004. Pathogenic Escherichia coli. Nat. Rev. Microbiol. 2, 123–140. https://doi.org/10.1038/nrmicro818

Keseler, I.M., Gama-Castro, S., Mackie, A., Billington, R., Bonavides-Martínez, C., Caspi, R., Kothari, A., Krummenacker, M., Midford, P.E., Muñiz-Rascado, L., Ong, W.K., Paley, S., Santos-Zavaleta, A., Subhraveti, P., Tierrafría, V.H., Wolfe, A.J., Collado-Vides, J., Paulsen, I.T., Karp, P.D., 2021. The EcoCyc Database in 2021. Front. Microbiol. 12, 711077. https://doi.org/10.3389/fmicb.2021.711077

Kobayashi, K., Fujikawa, M., Kozawa, T., 2014. Oxidative stress sensing by the iron–sulfur cluster in the transcription factor, SoxR. J. Inorg. Biochem. 133, 87–91. https://doi.org/10.1016/j.jinorgbio.2013.11.008

Kumar, R., Shimizu, K., 2011. Transcriptional regulation of main metabolic pathways of cyoA, cydB, fnr, and fur gene knockout Escherichia coli in C-limited and N-limited aerobic continuous cultures. Microb. Cell Factories 10, 3. https://doi.org/10.1186/1475-2859-10-3

Lamberg, K.E., Kiley, P.J., 2000. FNR-dependent activation of the class II dmsA and narG promoters of Escherichia coli requires FNR-activating regions 1 and 3. Mol. Microbiol. 38, 817–827. https://doi.org/10.1046/j.1365-2958.2000.02172.x

LeBel, M., 1988. Ciprofloxacin: Chemistry, Mechanism of Action, Resistance, Antimicrobial Spectrum, Pharmacokinetics, Clinical Trials, and Adverse Reactions. Pharmacother. J. Hum. Pharmacol. Drug Ther. 8, 3–30. https://doi.org/10.1002/j.1875-9114.1988.tb04058.x

Lesher, G.Y., Froelich, E.J., Gruett, M.D., Bailey, J.Hays., Brundage, R.Pauline., 1962. 1,8-Naphthyridine Derivatives. A New Class of Chemotherapeutic Agents. J. Med. Pharm. Chem. 5, 1063–1065. https://doi.org/10.1021/jm01240a021

Levine, C., Hiasa, H., Marians, K.J., 1998. DNA gyrase and topoisomerase IV: biochemical activities, physiological roles during chromosome replication, and drug sensitivities. Biochim. Biophys. Acta BBA - Gene Struct. Expr. 1400, 29–43. https://doi.org/10.1016/S0167-4781(98)00126-2

Lindsey, R.H., Pendleton, M., Ashley, R.E., Mercer, S.L., Deweese, J.E., Osheroff, N., 2014. Catalytic Core of Human Topoisomerase II$\alpha$: Insights into Enzyme–DNA Interactions and Drug Mechanism. Biochemistry 53, 6595–6602. https://doi.org/10.1021/bi5010816

Little, J.W., 1991. Mechanism of specific LexA cleavage: Autodigestion and the role of RecA coprotease. Biochimie 73, 411–421. https://doi.org/10.1016/0300-9084(91)90108-D

Little, J.W., Mount, D.W., 1982. The SOS regulatory system of Escherichia coli. Cell 29, 11–22. https://doi.org/10.1016/0092-8674(82)90085-X

Little, S., 1995. Amplification-Refractory Mutation System ( ARMS ) Analysis of Point Mutations. Curr. Protoc. Hum. Genet. 7. https://doi.org/10.1002/0471142905.hg0908s07

Llano-Sotelo, B., Hickerson, R.P., Lancaster, L., Noller, H.F., Mankin, A.S., 2009. Fluorescently labeled ribosomes as a tool for analyzing antibiotic binding. RNA 15, 1597–1604. https://doi.org/10.1261/rna.1681609

Lu, C., Bentley, W.E., Rao, G., 2003. Comparisons of oxidative stress response genes in aerobicEscherichia coli fermentations. Biotechnol. Bioeng. 83, 864–870. https://doi.org/10.1002/bit.10732

Luo, Y., Pfuetzner, R.A., Mosimann, S., Paetzel, M., Frey, E.A., Cherney, M., Kim, B., Little, J.W., Strynadka, N.C.J., 2001. Crystal Structure of LexA. Cell 106, 585–594. https://doi.org/10.1016/S0092-8674(01)00479-2

Ma, D., Alberti, M., Lynch, C., Nikaido, H., Hearst, J.E., 1996. The local repressor AcrR plays a modulating role in the regulation of acrAB genes of Escherichia coli by global stress signals. Mol. Microbiol. 19, 101–112. https://doi.org/10.1046/j.1365-2958.1996.357881.x

Magalon, A., Fedor, J.G., Walburger, A., Weiner, J.H., 2011. Molybdenum enzymes in bacteria and their maturation. Coord. Chem. Rev. 255, 1159–1178. https://doi.org/10.1016/j.ccr.2010.12.031

Maloy, S.R., Nunn, W.D., 1982. Genetic regulation of the glyoxylate shunt in Escherichia coli K-12. J. Bacteriol. 149, 173–180. https://doi.org/10.1128/jb.149.1.173-180.1982

Martinez-Martinez, L., 2003. Interaction of plasmid and host quinolone resistance. J. Antimicrob. Chemother. 51, 1037–1039. https://doi.org/10.1093/jac/dkg157

Maslowska, K.H., Makiela-Dzbenska, K., Fijalkowska, I.J., 2019. The SOS system: A complex and tightly regulated response to DNA damage. Environ. Mol. Mutagen. 60, 368–384. https://doi.org/10.1002/em.22267

McNicholas, P.M., Chiang, R.C., Gunsalus, R.P., 1998. Anaerobic regulation of the *Escherichia coli dmsABC* operon requires the molybdate-responsive regulator ModE. Mol. Microbiol. 27, 197–208. https://doi.org/10.1046/j.1365-2958.1998.00675.x

McNicholas, P.M., Gunsalus, R.P., 2002. The Molybdate-Responsive *Escherichia coli* ModE Transcriptional Regulator Coordinates Periplasmic Nitrate Reductase *(napFDAGHBC)* Operon Expression with Nitrate and Molybdate Availability. J. Bacteriol. 184, 3253–3259. https://doi.org/10.1128/JB.184.12.3253-3259.2002

McNicholas, P.M., Rech, S.A., Gunsalus, R.P., 1997. Characterization of the ModE DNA-binding sites in the control regions of modABCD and moaABCDE of Escherichia coli. Mol. Microbiol. 23, 515–524. https://doi.org/10.1046/j.1365-2958.1997.d01-1864.x

Mettert, E.L., Kiley, P.J., 2015. Fe–S proteins that regulate gene expression. Biochim. Biophys. Acta BBA - Mol. Cell Res. 1853, 1284–1293. https://doi.org/10.1016/j.bbamcr.2014.11.018

Mitscher, L.A., 2005. Bacterial Topoisomerase Inhibitors: Quinolone and Pyridone Antibacterial Agents. Chem. Rev. 105, 559–592. https://doi.org/10.1021/cr030101q

Molina, I., Pellicer, M.-T., Badia, J., Aguilar, J., Baldoma, L., 1994. Molecular Characterization of Escherichia coli Malate Synthase G. Differentiation with the Malate Synthase A Isoenzyme. Eur. J. Biochem. 224, 541–548. https://doi.org/10.1111/j.1432-1033.1994.00541.x

Mukherjee, K., Nagai, H., Shimamoto, N., Chatterji, D., 1999. GroEL is involved in activation of Escherichia coli RNA polymerase devoid of the omega subunit in vivo. Eur. J. Biochem. 266, 228–235. https://doi.org/10.1046/j.1432-1327.1999.00848.x

Nakanishi, Y., Iida, S., Ueoka-Nakanishi, H., Niimi, T., Tomioka, R., Maeshima, M., 2013. Exploring Dynamics of Molybdate in Living Animal Cells by a Genetically Encoded FRET Nanosensor. PLoS ONE 8, e58175. https://doi.org/10.1371/journal.pone.0058175

Nataro, J.P., Kaper, J.B., 1998. Diarrheagenic *Escherichia coli*. Clin. Microbiol. Rev. 11, 142–201. https://doi.org/10.1128/CMR.11.1.142

Nègre, D., Cortay, J.-C., Galinier, A., Sauve, P., Cozzone, A.J., 1992. Specific interactions between the IclR repressor of the acetate operon of Escherichia coli and its operator. J. Mol. Biol. 228, 23–29. https://doi.org/10.1016/0022-2836(92)90488-6

Neher, S.B., Flynn, J.M., Sauer, R.T., Baker, T.A., 2003. Latent ClpX-recognition signals ensure LexA destruction after DNA damage. Genes Dev. 17, 1084–1089. https://doi.org/10.1101/gad.1078003

Pagès, V., Fuchs, R.P., 2003. Uncoupling of Leading- and Lagging-Strand DNA Replication During Lesion Bypass in Vivo. Science 300, 1300–1303. https://doi.org/10.1126/science.1083964

Paterson, E.S., Boucher, S.E., Lambert, I.B., 2002. Regulation of the *nfsA* Gene in *Escherichia coli* by SoxS. J. Bacteriol. 184, 51–58. https://doi.org/10.1128/JB.184.1.51-58.2002

Pitts, S.L., Liou, G.F., Mitchenall, L.A., Burgin, A.B., Maxwell, A., Neuman, K.C., Osheroff, N., 2011. Use of divalent metal ions in the DNA cleavage reaction of topoisomerase IV. Nucleic Acids Res. 39, 4808–4817. https://doi.org/10.1093/nar/gkr018

Poirel, L., Madec, J.-Y., Lupo, A., Schink, A.-K., Kieffer, N., Nordmann, P., Schwarz, S., 2018. Antimicrobial Resistance in *Escherichia coli*. Microbiol. Spectr. 6, 6.4.14. https://doi.org/10.1128/microbiolspec.ARBA-0026-2017

Poirel, L., Naas, T., Nordmann, P., 2008. Genetic support of extended-spectrum β-lactamases. Clin. Microbiol. Infect. 14, 75–81. https://doi.org/10.1111/j.1469-0691.2007.01865.x

Pommier, Y., Leo, E., Zhang, H., Marchand, C., 2010. DNA Topoisomerases and Their Poisoning by Anticancer and Antibacterial Drugs. Chem. Biol. 17, 421–433. https://doi.org/10.1016/j.chembiol.2010.04.012

Poole, K., 2007. Efflux pumps as antimicrobial resistance mechanisms. Ann. Med. 39, 162–176. https://doi.org/10.1080/07853890701195262

Pribis, J.P., García-Villada, L., Zhai, Y., Lewin-Epstein, O., Wang, A.Z., Liu, J., Xia, J., Mei, Q., Fitzgerald, D.M., Bos, J., Austin, R.H., Herman, C., Bates, D., Hadany, L., Hastings, P.J., Rosenberg, S.M., 2019. Gamblers: An Antibiotic-Induced Evolvable Cell Subpopulation Differentiated by Reactive-Oxygen-Induced General Stress Response. Mol. Cell 74, 785-800.e7. https://doi.org/10.1016/j.molcel.2019.02.037

Puzari, M., Chetia, P., 2017. RND efflux pump mediated antibiotic resistance in Gram-negative bacteria Escherichia coli and Pseudomonas aeruginosa: a major issue worldwide. World J. Microbiol. Biotechnol. 33, 24. https://doi.org/10.1007/s11274-016-2190-5

Pyne, M.E., Moo-Young, M., Chung, D.A., Chou, C.P., 2015. Coupling the CRISPR/Cas9 System with Lambda Red Recombineering Enables Simplified Chromosomal Gene

Replacement in Escherichia coli. Appl. Environ. Microbiol. 81, 5103–5114. https://doi.org/10.1128/AEM.01248-15

Quillardet, P., Rouffaud, M.-A., Bouige, P., 2003. DNA array analysis of gene expression in response to UV irradiation in Escherichia coli. Res. Microbiol. 154, 559–572. https://doi.org/10.1016/S0923-2508(03)00149-9

Ramseier, T.M., Nègre, D., Cortay, J.-C., Scarabel, M., Cozzone, A.J., Saier, M.H., 1993. In Vitro Binding of the Pleiotropic Transcriptional Regulatory Protein, FruR, to the fru, pps, ace, pts and icd Operons of Escherichia coli and Salmonella typhimurium. J. Mol. Biol. 234, 28–44. https://doi.org/10.1006/jmbi.1993.1561

Reisch, C.R., Prather, K.L.J., 2015. The no-SCAR (Scarless Cas9 Assisted Recombineering) system for genome editing in Escherichia coli. Sci. Rep. 5, 15096. https://doi.org/10.1038/srep15096

Resnik, E., Pan, B., Ramani, N., Freundlich, M., LaPorte, D.C., 1996. Integration host factor amplifies the induction of the aceBAK operon of Escherichia coli by relieving IclR repression. J. Bacteriol. 178, 2715–2717. https://doi.org/10.1128/jb.178.9.2715-2717.1996

Robicsek, A., Jacoby, G.A., Hooper, D.C., 2006a. The worldwide emergence of plasmid-mediated quinolone resistance. Lancet Infect. Dis. 6, 629–640. https://doi.org/10.1016/S1473-3099(06)70599-0

Robicsek, A., Strahilevitz, J., Jacoby, G.A., Macielag, M., Abbanat, D., Hye Park, C., Bush, K., Hooper, D.C., 2006b. Fluoroquinolone-modifying enzyme: a new adaptation of a common aminoglycoside acetyltransferase. Nat. Med. 12, 83–88. https://doi.org/10.1038/nm1347

Rodríguez-Martínez, J.M., Machuca, J., Cano, M.E., Calvo, J., Martínez-Martínez, L., Pascual, A., 2016. Plasmid-mediated quinolone resistance: Two decades on. Drug Resist. Updat. 29, 13–29. https://doi.org/10.1016/j.drup.2016.09.001

Rui, B., Shen, T., Zhou, H., Liu, J., Chen, J., Pan, X., Liu, H., Wu, J., Zheng, H., Shi, Y., 2010. A systematic investigation of Escherichia coli central carbon metabolism in response to superoxide stress. BMC Syst. Biol. 4, 122. https://doi.org/10.1186/1752-0509-4-122

Ruiz, C., Levy, S.B., 2010. Many Chromosomal Genes Modulate MarA-Mediated Multidrug Resistance in *Escherichia coli*. Antimicrob. Agents Chemother. 54, 2125–2134. https://doi.org/10.1128/AAC.01420-09

Sawai, T., 1992. OmpF channel permeability of quinolones and their comparison with β-lactams. FEMS Microbiol. Lett. 95, 105–108. https://doi.org/10.1016/0378-1097(92)90744-9

Schaechter, M., The View From Here Group, 2001. *Escherichia coli* and *Salmonella* 2000: the View From Here. Microbiol. Mol. Biol. Rev. 65, 119–130. https://doi.org/10.1128/MMBR.65.1.119-130.2001

Schmidt, B.H., Burgin, A.B., Deweese, J.E., Osheroff, N., Berger, J.M., 2010. A novel and unified two-metal mechanism for DNA cleavage by type II and IA topoisomerases. Nature 465, 641–644. https://doi.org/10.1038/nature08974

Self, W.T., Grunden, A.M., Hasona, A., Shanmugam, K.T., 2001. Molybdate transport. Res. Microbiol. 152, 311–321. https://doi.org/10.1016/S0923-2508(01)01202-5

Shevchik, V.E., Condemine, G., Robert-Baudouy, J., 1994. Characterization of DsbC, a periplasmic protein of Erwinia chrysanthemi and Escherichia coli with disulfide isomerase activity. EMBO J. 13, 2007–2012. https://doi.org/10.1002/j.1460-2075.1994.tb06470.x

Smith, J.T., 1986. Wirkmechanismus der Chinolone. Infection 14, S3–S15. https://doi.org/10.1007/BF01645191

Snyder, M., Drlica, K., 1979. DNA gyrase on the bacterial chromosome: DNA cleavage induced by oxolinic acid. J. Mol. Biol. 131, 287–302. https://doi.org/10.1016/0022-2836(79)90077-9

Spiro, S., Guest, J.R., 1990. FNR and its role in oxygen-regulated gene expression in *Escherichia coli*. FEMS Microbiol. Lett. 75, 399–428. https://doi.org/10.1111/j.1574-6968.1990.tb04109.x

Stein, G.E., 1988. The 4-Quinolone Antibiotics: Past, Present, and Future. Pharmacother. J. Hum. Pharmacol. Drug Ther. 8, 301–314. https://doi.org/10.1002/j.1875-9114.1988.tb04088.x

Stewart, V., 1988. Nitrate respiration in relation to facultative metabolism in enterobacteria. Microbiol. Rev. 52, 190–232. https://doi.org/10.1128/mr.52.2.190-232.1988

Strahilevitz, J., Jacoby, G.A., Hooper, D.C., Robicsek, A., 2009. Plasmid-Mediated Quinolone Resistance: a Multifaceted Threat. Clin. Microbiol. Rev. 22, 664–689. https://doi.org/10.1128/CMR.00016-09

Sugino, A., Peebles, C.L., Kreuzer, K.N., Cozzarelli, N.R., 1977. Mechanism of action of nalidixic acid: Purification of *Escherichia coli nalA* gene product and its relationship to DNA gyrase and a novel nicking-closing enzyme. Proc. Natl. Acad. Sci. 74, 4767–4771. https://doi.org/10.1073/pnas.74.11.4767

Sun, H.I., Jeong, D.U., Lee, J.H., Wu, X., Park, K.S., Lee, J.J., Jeong, B.C., Lee, S.H., 2010. A novel family (QnrAS) of plasmid-mediated quinolone resistance determinant. Int. J. Antimicrob. Agents 36, 578–579. https://doi.org/10.1016/j.ijantimicag.2010.08.009

Sutherland, C., Murakami, K.S., 2018. An Introduction to the Structure and Function of the Catalytic Core Enzyme of *Escherichia coli* RNA Polymerase. EcoSal Plus 8, ecosalplus.ESP-0004-2018. https://doi.org/10.1128/ecosalplus.ESP-0004-2018

Tooke, C.L., Hinchliffe, P., Bragginton, E.C., Colenso, C.K., Hirvonen, V.H.A., Takebayashi, Y., Spencer, J., 2019. β-Lactamases and β-Lactamase Inhibitors in the 21st Century. J. Mol. Biol. 431, 3472–3500. https://doi.org/10.1016/j.jmb.2019.04.002

Touati, D., 1989. The Molecular Genetics of Superoxide Dismutase in *E. Coli* . An Approach to Understanding the Biological Role and Regulation of Sods in Relation to Other Elements of the Defence System Against Oxygen Toxicity. Free Radic. Res. Commun. 8, 1–9. https://doi.org/10.3109/10715768909087967

Tran, J.H., Jacoby, G.A., 2002. Mechanism of plasmid-mediated quinolone resistance. Proc. Natl. Acad. Sci. 99, 5638–5642. https://doi.org/10.1073/pnas.082092899

Tran, J.H., Jacoby, G.A., Hooper, D.C., 2005a. Interaction of the Plasmid-Encoded Quinolone Resistance Protein Qnr with *Escherichia coli* DNA Gyrase. Antimicrob. Agents Chemother. 49, 118–125. https://doi.org/10.1128/AAC.49.1.118-125.2005

Tran, J.H., Jacoby, G.A., Hooper, D.C., 2005b. Interaction of the Plasmid-Encoded Quinolone Resistance Protein QnrA with *Escherichia coli* Topoisomerase IV. Antimicrob. Agents Chemother. 49, 3050–3052. https://doi.org/10.1128/AAC.49.7.3050-3052.2005

Varghese, S., Tang, Y., Imlay, J.A., 2003. Contrasting Sensitivities of *Escherichia coli* Aconitases A and B to Oxidation and Iron Depletion. J. Bacteriol. 185, 221–230. https://doi.org/10.1128/JB.185.1.221-230.2003

Walkenhorst, H.M., Hemschemeier, S.K., Eichenlaub, R., 1995. Molecular analysis of the molybdate uptake operon, modABCD, of Escherichia coli and modR, a regulatory gene. Microbiol. Res. 150, 347–361. https://doi.org/10.1016/S0944-5013(11)80016-9

Walker, G.C., 1984. Mutagenesis and inducible responses to deoxyribonucleic acid damage in Escherichia coli. Microbiol. Rev. 48, 60–93. https://doi.org/10.1128/mr.48.1.60-93.1984

Wohlkonig, A., Chan, P.F., Fosberry, A.P., Homes, P., Huang, J., Kranz, M., Leydon, V.R., Miles, T.J., Pearson, N.D., Perera, R.L., Shillings, A.J., Gwynn, M.N., Bax, B.D., 2010.

Structural basis of quinolone inhibition of type IIA topoisomerases and target-mediated resistance. Nat. Struct. Mol. Biol. 17, 1152–1153. https://doi.org/10.1038/nsmb.1892

Xiong, X., Bromley, E.H.C., Oelschlaeger, P., Woolfson, D.N., Spencer, J., 2011. Structural insights into quinolone antibiotic resistance mediated by pentapeptide repeat proteins: conserved surface loops direct the activity of a Qnr protein from a Gram-negative bacterium. Nucleic Acids Res. 39, 3917–3927. https://doi.org/10.1093/nar/gkq1296

Yamamoto, K., Ishihama, A., 2003. Two different modes of transcription repression of the Escherichia coli acetate operon by IclR. Mol. Microbiol. 47, 183–194. https://doi.org/10.1046/j.1365-2958.2003.03287.x

Yamane, K., Wachino, J., Suzuki, S., Kimura, K., Shibata, N., Kato, H., Shibayama, K., Konda, T., Arakawa, Y., 2007. New Plasmid-Mediated Fluoroquinolone Efflux Pump, QepA, Found in an *Escherichia coli* Clinical Isolate. Antimicrob. Agents Chemother. 51, 3354–3360. https://doi.org/10.1128/AAC.00339-07

Yoon, S.-J., Park, J.-E., Yang, J.-H., Park, J.-W., 2002. OxyR Regulon Controls Lipid Peroxidation-mediated Oxidative Stress in Escherichia coli. BMB Rep. 35, 297–301. https://doi.org/10.5483/BMBRep.2002.35.3.297

Zechiedrich, E.L., Khodursky, A.B., Bachellier, S., Schneider, R., Chen, D., Lilley, D.M.J., Cozzarelli, N.R., 2000. Roles of Topoisomerases in Maintaining Steady-state DNA Supercoiling in Escherichia coli. J. Biol. Chem. 275, 8103–8113. https://doi.org/10.1074/jbc.275.11.8103

Zhang, A.P.P., Pigli, Y.Z., Rice, P.A., 2010. Structure of the LexA–DNA complex and implications for SOS box measurement. Nature 466, 883–886. https://doi.org/10.1038/nature09200

Zhang, Z., Gosset, G., Barabote, R., Gonzalez, C.S., Cuevas, W.A., Saier, M.H., 2005. Functional Interactions between the Carbon and Iron Utilization Regulators, Crp and Fur, in *Escherichia coli*. J. Bacteriol. 187, 980–990. https://doi.org/10.1128/JB.187.3.980-990.2005

Zheng, M., Åslund, F., Storz, G., 1998. Activation of the OxyR Transcription Factor by Reversible Disulfide Bond Formation. Science 279, 1718–1722. https://doi.org/10.1126/science.279.5357.1718

Zheng, M., Doan, B., Schneider, T.D., Storz, G., 1999. OxyR and SoxRS Regulation of *fur*. J. Bacteriol. 181, 4639–4643. https://doi.org/10.1128/JB.181.15.4639-4643.1999

Zheng, M., Wang, X., Templeton, L.J., Smulski, D.R., LaRossa, R.A., Storz, G., 2001. DNA Microarray-Mediated Transcriptional Profiling of the *Escherichia coli* Response to Hydrogen Peroxide. J. Bacteriol. 183, 4562–4570. https://doi.org/10.1128/JB.183.15.4562-4570.2001

Zupok, A., Iobbi-Nivol, C., Méjean, V., Leimkühler, S., 2019. The regulation of Moco biosynthesis and molybdoenzyme gene expression by molybdenum and iron in bacteria. Metallomics 11, 1602–1624. https://doi.org/10.1039/c9mt00186g

# 11. Hazardous materials/Gefahrenstoffe

| Name | GHS Pictogram | Hazard statements | Precautionary statements |
|---|---|---|---|
| Ammonium chloride |  | H302<br>H319 | P305+P351+P338 |
| Ampicillin-Na-salt |  | H317<br>H334 | P261<br>P280<br>P342 + P311 |
| Calcium chloride-dihydrate |  | H319 | P305+P351+P338 |
| Chloramphenicol |  | H350 | P201<br>P308 + P313 |
| Dodecylsulfate-Na salt (SDS) | 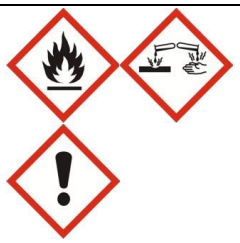 | H228<br>H302 + H332<br>H315<br>H318<br>H335<br>H412 | P210<br>P261<br>P273<br>P280<br>P305 + P351 + P338 |
| Ethanol |  | H225<br>H319 | P210<br>P305 + P351 + P338<br>P370 + P378<br>P403 + P235 |

| | | | |
|---|---|---|---|
| Ethidium bromide |  | H302<br>H330<br>H341 | P260<br>P281<br>P284<br>P310 |
| Ethylenediamine-tetraacetate (EDTA) |  | H319 | P305 + P351 + P338 |
| Glacial acetic acid |  | P280<br>P305+P351+P338<br>P310 | H226, H314 |
| Hydrogen chloride |  | P261<br>P280<br>P305+P351+P338<br>P310<br>P410+P403 | H280<br>H314<br>H331 |
| Methyl viologen dichloride hydrate (Paraquat) | 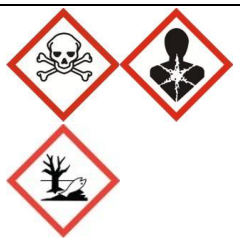 | P260, P273, P280, P284,<br>P301+P310,<br>P305+P351+P338 | H301, H311, H315,<br>H319, H330, H335,<br>H372, H410 |
| Monopotassium phosphate |  | P264, P280,<br>P305+P351+P338<br>P321, P332+P313<br>P337+P313 | H315, H319 |
| Sodium hydroxide |  | P280,<br>P305+P351+P338<br>P310 | H290, H314 |
| Spectinomycine sulfate |  | P202, P280 P301+P312<br>P308+P313 | H302-H361d |

## 12. CMR substances/KMR Stoffe

| | | | |
|---|---|---|---|
| Ethidium bromide |  | H302<br>H330<br>H341 | P260<br>P281<br>P284<br>P310 |

## 13. Eidesstattliche Versicherung

Hiermit versichere ich an Eides statt, die vorliegende Dissertation selbst verfasst und keine anderen als die angegebenen Hilfsmittel benutzt zu haben. Die eingereichte schriftliche Fassung entspricht der auf dem elektronischen Speichermedium. Ich versichere, dass diese Dissertation nicht in einem früheren Promotionsverfahren eingereicht wurde.

Hamburg, den 20.10.22

Philip Bienert